Mechanical Behaviour and Long-Term Performance of Steel Fibre Reinforced Rubberised Concrete

A thesis presented for the degree of

Doctor of Philosophy in Civil and Structural Engineering

at The University of Sheffield

By

Abdulaziz Alsaif

Sheffield

May 2019

To my parents for their sacrifices and prayers,

To my brothers and sisters for always being there,

To my wife and daughter for their support, patience and love.

Abstract

Large quantities of post-consumer tyres are discarded worldwide every year (1.5 billion units/year) causing several health risks and polluting the environment. Tyres are made of high quality, highly durable, flexible and strong materials, the properties of which are suitable for construction applications. Rigid concrete pavements, although they flexurally strong, lack the flexibility of asphalt pavements, which is necessary to accommodate subgrade movements and settlements resulting from poor compaction during construction, or induced by moisture, temperature and freeze-thaw movements. Incorporating waste tyre materials (rubber and steel fibres) into concrete (Steel Fibre Reinforced Rubberised Concrete -SFRRuC) can impart unique properties and make it an ideal material for pavement systems with a flexibility similar to flexible pavements and flexural strength similar to rigid concrete pavements. However, SFRRuC pavements are expected to be susceptible to several deteriorating processes including fatigue due to cyclic traffic loading, corrosion of steel fibres as a result of chemical attack by chloride, thermal movements due to heat of hydration, shrinkage/expansion due to moisture movement and freeze-thaw. This research aims to investigate the fresh, mechanical, transport/pore-structure related properties and long-term behaviour of SFRRuC so as to assess its potential for use in pavement construction.

Initial study investigated the influence on both fresh and mechanical properties of concrete made by partially replacing coarse and fine mineral aggregates by different grades and percentages of tyre rubber particles. The effect of reinforcing the rubberised concrete (RuC) with Recycle Tyre Steel Fibres (RTSF) or blends of Manufactured Steel Fibres (MSF) and RTSF to enhance the flexural performance was also examined. The addition of fibres in RuC mixes was found to substantially mitigate loss in flexural strength due to the rubber addition (from 50% to 9.6% loss, compared to conventional concrete). The use of fibres in RuC enhanced strain capacity (from 0.04 mm for conventional concrete to 1.32 mm for SFRRuC produced with 60% rubber content and 40 kg/m^3 of blended fibres) and post-peak energy absorption behaviour.

Subsequent studies examined experimentally the transport/pore-structure related properties and long-term behaviour of SFRRuC including corrosion, freeze-thaw and flexural fatigue. It was found that due to the presence of fibres, the increase in water permeability (e.g. volume of permeable, sorptivity and chloride penetration and diffusion) as a result of adding rubber is minor, generally within the range of highly durable concrete mixes. No visual signs of deterioration or cracking (except superficial rust) were observed on the surface of the concrete specimens subjected to 150 or 300 days of accelerated chloride corrosion exposure. SFRRuC was able to withstand 56 freeze-thaw cycles with acceptable scaling and no internal damage or degradation in mechanical performance. The replacement of mineral aggregates with rubber particles improved the ductility and flexibility of SFRRuC, but reduced its fatigue resistance.

A probabilistic analysis of the fatigue life data provided the level of appropriate design stresses and confirmed that SFRRuC can be used for flexible pavements. A modified design approach based on Concrete Society (TR34) is proposed for SFRRuC pavements. Finite element analyses confirm that flexible SFRRuC pavements can accommodate large subgrade movements and settlements.

Acknowledgments

First, I would like to express my deepest gratitude to my supervisors Dr. Kypros Pilakoutas and Dr. Maurizio Guadagnini for their precious time, continuous support, patience, motivation, and immense knowledge that greatly helped in completion of this work. It would have not been possible without their invaluable support and endless enthusiasm.

I would like also to thank Dr. Susan Bernal for her supervision throughout the durability topics of the research, especially by instigating discussions and raising important questions.

I acknowledge the financial support provided by King Saud University/ Ministry of Education throughout the period of this research.

I am thankful to the technicians in concrete and heavy structures laboratories, for their continuous and excellent quality help, and to all members in Concrete and Earthquake Engineering (CEE) group for their technical and numerical support.

I am grateful to my colleagues and friends in Rooms E110 and E110A, for their encouragement and continuous support. My special gratitude goes to Dr. Panos Papastergiou and Dr. Reyes Garcia for their restless and endless supervision during the whole thesis.

I am deeply indebt to my parents and my brothers and sisters for their love and being close to me regardless of the distance which have been separating us for the duration of this study. Without them these work would not have been possible

And, last but not least, special thanks to my wife, Abrar Almushayqih, for her love, patience and encouragement during my study, and then, of course, my little daughter, Reem, for her motive beautiful smiles.

Table of Contents

List of Figures

List of Tables

List of Abbreviations

A	Absorption
CA	Coarse aggregates
CDP	Concrete damaged plasticity
CMOD	Crack mouth opening displacement
CR	Coarse rubber
CRCP	Continuously reinforced concrete pavement
CTE	Coefficient of thermal expansion
DFs	Durability factors
EC2	Eurocode 2
ETRA	European tyre recycling association
FA	Fine aggregates
FE	Finite element
fib	Fédération internationale du béton
FR	Fine rubber
F-T	Freeze-thaw
ITZ	Interfacial transition zone
JPCP	Jointed plain concrete pavement
LVDT	Linear variable differential transformer
MSF	Manufactured steel fibres
NA or N	Natural aggregates
PFA	Pulverised fuel ash
RA or R	Rubber aggregates
RCC	Roller compacted concrete
RDM	Relative dynamic modulus of elasticity
RH	Relative humidity
RTSF	Recycled tyre steel fibres
RuC	Rubberised concrete
SCC	Self-compacted concrete
SCRuC	Self-compacting rubberised concrete
SF	Silica fume
SFRC	Steel fibre reinforced concrete
SFRRuC	Steel fibre reinforced rubberised concrete
SG	Specific gravity

ULS	Ultimate limit state
UPTT	Ultrasonic pulse transit time
USFD	The University of Sheffield
VPV	Volume of permeable voids
WTR	Waste tyre rubber

List of Symbols

A	*S*hape parameter (or Weibull slope)
a, b, c	Experimental coefficients
$AgNO_3$	Silver nitrate
B	Width of the specimen
CPE8R	8-node quadrilateral plane strain reduced integration elements
C_s	Total chloride concentration at the surface
CV	Coefficient of variation
C_x	Total chloride concentration at the colour change boundary
D_{app}	Apparent chloride diffusion coefficients
Ec_{ontrol}	Modulus of elasticity of control concrete
E_{RuC}	Modulus of elasticity of rubberised concrete
E_s	Static flexural elastic modulus
$f_{cm,cube}$	Mean cube compressive strength
$f_{ctk,fl}$	Characteristic flexural strength
$f_{ctm,fl}$	Mean static flexural strength
f_{Ri}	Residual flexural strength
$f_{Ri,c}$	Characteristic residual flexural strength
h	Height of the specimen (chapter 4)
h	Thickness of the rigid concrete pavement (chapter 5)
i	Failure order number of specimens
I	Radius of the relative stiffness of the slab
j	Rank of the specimen
K	Intrinsic permeability (Chapter 3)
K	Number of specimens tested at given stress ratio (Chapter 5)
L	Span length of the tested specimen
M_0	Mass of specimens after curing and before testing
M_{28}	Mass of scaled materials after 28 cycles
M_{56}	Mass of scaled materials after 56 cycles
$M_{d,n}$	Mass of the oven dried scaled material collected after cycle *n*
M_k	Modulus of elastic subgrade reaction
M_n	The moment capacity along the hogging yield lines
M_p	Flexural moment at the bottom of the slab and along the sagging yield lines
n	Number of freeze-thaw cycles

N	Fatigue life
NaCl	Sodium chloride solution
N_e	Estimated fatigue Life
P_f	Probability of failure
P_s	Probability of survival
R	Correlation coefficient
S	Stress ratio
S_e	Estimated stress ratio
$S_{e,ave}$	The average estimated stress ratio
T	Time
U	Scaling parameter (or characteristic life)
u_w	Average values of u
V	Poisson's ratio
W	Standard axle load
W_e	Evaporable moisture concentrations
X	Maximum average distance of colour change boundary from the concrete surface
Z	Equivalent contact radios of tyre
α^*	Maximum-likelihood estimators for α and ϑ
α_w	Average values of α
δ_f	Deflection
δ_{fmax}	Strain capacity
θ^*	Maximum-likelihood estimators for ϑ
M	Mean fatigue life of the tested specimens
σ_{max}	Maximum tensile stress of the slab
Γ()	Gamma function
β	Curve intercept point

This page is intentionally left blank

Chapter 1

Introduction

This chapter introduces the research motivation and background and presents the aims, objectives, methodology and the layout of this thesis.

This PhD thesis comprises four peer-reviewed published journal papers [1-4], focusing on the structural and durability performance of Steel Fibre Reinforced Rubberised Concrete (SFRRuC) pavements using recycled rubber granules and steel fibres (extracted from post-consumer tyres) as reinforcement. Rubber particles are incorporated into concrete pavements to replace conventional aggregates and enhance flexibility, a property that is essential to enable pavements to accommodate subgrade induced movement and settlements. In addition to recycled rubber, recycled steel fibres are also used in this innovative pavement to improve its mechanical behaviour and durability and significantly mitigate the negative effects of rubber aggregates.

This chapter initially introduces the environmental aspects of post-consumer tyre disposal and recycling. It then explains the scientific motivation behind this study and briefly presents a literature review on the use of steel fibres/rubber particles in concrete. The sections to follow, present the research aim and main objectives as well as significance and additionality.

1.1 Research motivation

1.1.1 Recycling post-consumer tyres in construction

The consumer attitude of our society, along with a rapidly increasing population, have led to a remarkable increase in waste production, which is resulting in profound changes to our environment. Hence, in the last few decades, humanity is focusing on waste recycling and reducing the environmental impact of used products. Although recycling has been already part of life for most households in Europe (plastics, glass, paper), there are still many end-of-life products that can be recycled, or used in other applications after some processing, to recover the constituent materials and energy spent to produce them.

Although the construction industry is a major producer of waste, as the largest user of materials with a large variety of properties, it can also potentially absorb large amounts of appropriately processed waste materials of similar properties. One of these products is post-consumer tyres (from cars or trucks), which are accumulating in large quantities worldwide every year. Tyres are made of high quality, highly durable, flexible and strong materials, the properties of which are invaluable in construction.

According to ETRA [5], it is estimated that the global tyre production ranges between 1-1.5 billion tyres per year. It is inevitable that for each tyre placed in the market, another one reaches its on-road life and takes the disposal route. Most post-consumer tyres in developing countries

are accumulated in stockpiles or are landfilled, causing several health risks (e.g. by providing breeding ground for rats, mice, vermin and mosquitos [6, 7]) and polluting the environment. Tyres are made of extremely flammable materials, hence tyre stockpiles are considered as high-risk fire hazards. In 1991, the EU identified these risks and the Landfill Directive 1991/31/EC [8] was introduced, which resulted in a major reduction of post-consumer tyres going to landfill (from 62% in 1992 to 10% in 2010). A decade ago, the European Directive 2008/98/EC [9] set a disposal waste tyre strategy that aimed to encourage the sustainable management of waste tyres and support the development of novel applications to utilise their constitutive components. Tyres consist of highly engineered materials, which have remarkable mechanical properties. The three main by-products obtained from end-of-life tyre recycling are: a) rubber granules, b) steel fibres and c) polymer fibres (Figure 1.1).

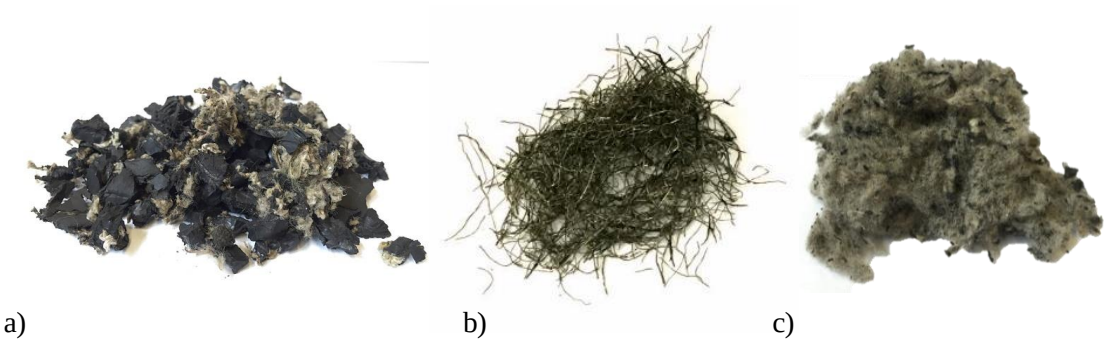

Figure 1.1: Raw materials obtained from post-consumer tyres recycling: a) rubber granules, b) steel fibres, c) polymer fibres

These three products are extracted from post-consumer tyres by mechanical shredding techniques. The tyres are shredded into large chunks and then fed to a rotational granulator that can produce rubber particles in various sizes (see Figure 1.2). The steel fibres are separated by using electromagnets and screening whilst the lightweight polymer material is obtained by passing the tyre-shredded material through air streams and vacuum chamber.

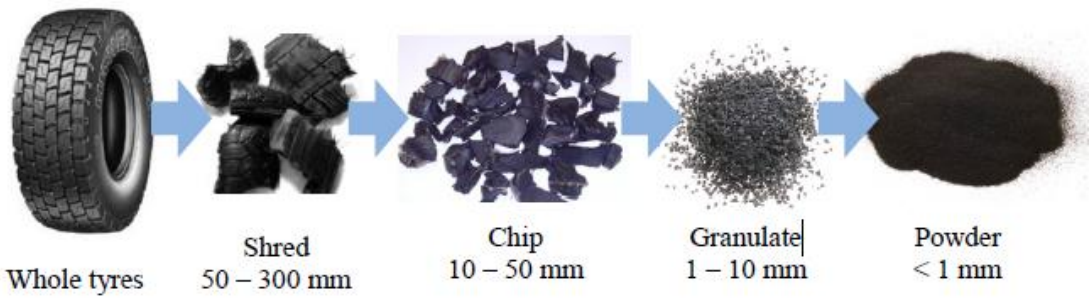

Figure 1.2: Range of rubber granules after [10]

1.1.1.1 Waste Tyre Rubber (WTR) from post-consumer tyres

Currently there are two main routes for the management of WTR:

Incineration: post-consumer tyres can be incinerated as fuel in cement kilns or to produce energy in the form of steam or electricity [6, 11]. This approach is not desirable since only a fraction (less than a third) of the initial embodied energy is recovered and emissions that are harmful for the environment are generated during the incineration process.

Applications: After mechanical shredding and screening, WTR is graded according to size (similarly to mineral aggregates) and can be used in making artificial reefs, impact-absorbing protective walls used for car racing, sound proof panels and rubberised asphalt [12]. WTR can be mixed with polymer binders to provide soft impact-vibration absorbing underlays in playgrounds/sports fields or protective underlining systems for underground and buried infrastructure [13, 14]. Although the "applications" approach leads to a more sustainable/desirable waste management, the volume of post-consumer tyre by-products used in manufacturing new products is still quite low.

Since concrete is one of the most produced construction materials in the world [15, 16], the potential of using WTR in concrete applications can be high. WTR can be used in structural concrete application to partially replace conventional aggregates when there is a need to increase its deformability and energy dissipation. It is debatable if the incorporation of virgin rubber particles in concrete can offer better performance than WTR as the load and environmental exposure on the latter do not appear to significantly affect its engineering properties. The vast majority of experimental studies on RuC have utilised WTR since it is much less expensive (and also contributes to the circular economy) than virgin rubber and available in large quantities.

1.1.1.2 Recycled Steel Fibre extracted from post-consumer tyres (RTSF)

In the past, the majority of the tyre recycling plants used to send steel fibres extracted from post-consumer tyres to landfill as they were too contaminated (with rubber) to be used for remelting in the steel mill industry (Figure 1.3a). However, in 2006, the EC [8] legislation banned any form of waste tyre disposal in landfill and forced the tyre recycling plants to start developing methodologies to clean the steel fibres more efficiently (residual rubber contamination <15% by mass) so that they can be sent to steel mills for re-melting [17]. Since scrap steel price varies with demand and sometimes it barely covers the cost of processing, small recyclers stockpile processed steel fibres awaiting for a more profitable solution to be developed (Figure 1.3b).

a) b)

Figure 1.3: a) Typical contaminated RTSF sample and b) stockpiled RTSF [17]

In early 2000, The University of Sheffield (USFD) started investigating the use of RTSF (extracted from post-consumer tyres using the mechanical shredding process) as reinforcement in structural concrete applications (such as industrial flooring) and a patent was filed for the use of processed steel fibres from tyres in concrete [18]. In 2010, a spin-out company was established (Twincon Ltd) with a sole purpose to form a route-to-market strategy for the commercialisation of RTSF. The company developed a methodology to clean and screen sorted RTSF with minimal rubber contamination (<2% residual rubber) and exclude long fibres, which can cause agglomeration. For CE marking purposes, a quality control process was developed, which includes automated fibre scanning equipment using photogrammetry techniques and can provide accurate RTSF length distributions for each production batch. Past research on the use of RTSF as reinforcement in concrete has shown that RTSF can enhance the flexural performance of concrete and can partially substitute manufactured steel fibres [16, 19, 20]. Although most of these experimental laboratory studies manually integrated the RTSF into concrete, the integration of RTSF in real construction projects can be easily achieved on site by first placing the fibres into a rotating perforated drum (for fibre dispersal) and then dispersing them into the concrete truck mixer using a blower.

1.1.2 Road pavements

Durable materials are essential for paving road surfaces in modern transport infrastructure. Road pavements mainly sustain automobile and pedestrian traffic loads, but also provide comfort as well as good frictional resistance for tyres in all weathers. Road construction is governed by two main paving systems:

a. flexible pavements: made of several well-compacted natural soil layers finished with a top asphalt layer (using bitumen binder)

b. rigid pavements: using plain conventional concrete (cement binder) or reinforced with steel mesh/rebars.

Selecting the appropriate paving system depends on various factors including traffic loading, environmental conditions, subgrade status, cost and construction materials availability [21].

Flexible pavement is the most common paving system mainly due to its lower cost and faster implementation compared to rigid concrete pavement system [22]. It can provide good riding quality due to the absence of joints and offer enough flexibility to accommodate subgrade induced movements and settlements, a factor that rigid concrete pavements truly lack. Flexible pavements consist of several layers so that load is distributed evenly through the component layers (see Figure 1.4a).

Rigid pavements have higher flexural strength, longer life span and lower maintenance costs compared to flexible pavements [23]. The American Concrete Pavement Association [24] reported that well-designed rigid concrete pavements can offer up to 2.5 times longer service life, up to 21% lower lifetime cost and up to 21% better benefit/cost ratio over flexible pavements. Concrete pavements consist of a strong and rigid concrete structural layer so that load is distributed over a relative wide area of the subgrade (see Figure 1.4b).

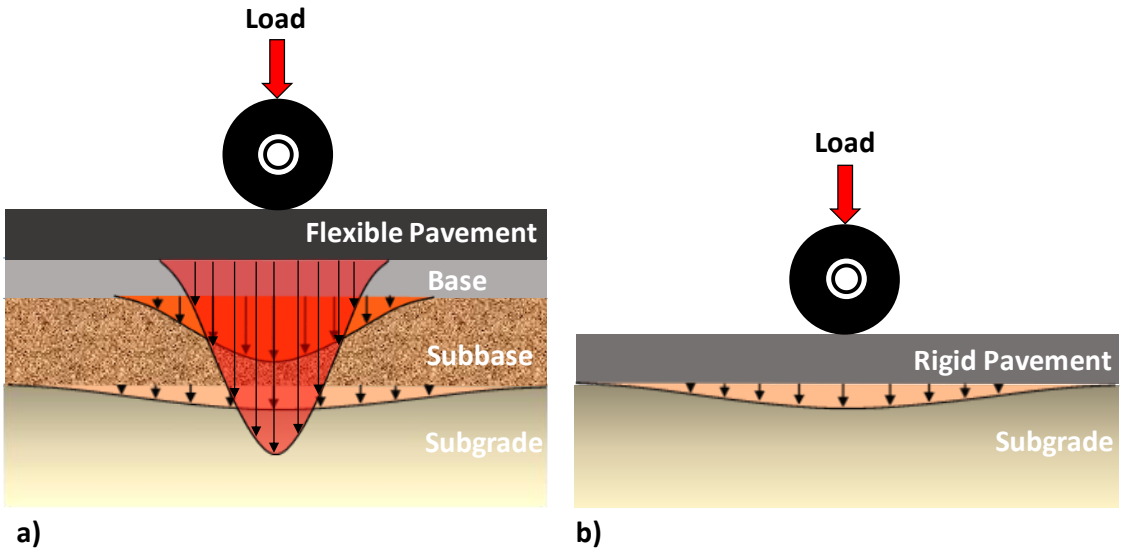

Figure 1.4: Stresses at various layers a) Flexible asphalt pavement and (b) rigid concrete pavement

The most popular types of rigid pavements are the Continuously Reinforced Concrete Pavement (CRCP) and Jointed Plain Concrete Pavement (JPCP). In CRCP, conventional steel rebars are used to resist flexural tensile stresses, whilst in JPCP, the flexural tensile stresses are resisted by concrete through thicker slabs and higher concrete strength. For JPCP, transverse joints are

required at regular intervals to accommodate displacements due to concrete shrinkage and thermal movements. For both CRCP and JPCP, the manufacture cost is higher than flexible pavements since placing steel rebars/mesh or making joints is costly and labour intensive.

Rigid concrete pavements lack flexibility and hence attract higher stress in the concrete, which may cause fatigue cracking due to repeated loading. This also limits the ability of rigid concrete pavements to accommodate subgrade movements and settlements resulting from poor compaction during construction, or induced by moisture, temperature and freeze-thaw (see Figure 1.5a). Abaza and Hussein [25] reported that large temperature changes can produce additional tensile stresses, which could lead to concrete pavement cracks. Ice lenses can also form beneath the concrete surface as a result of uneven frost action on the subgrade and can potentially create unsupported or poorly supported regions in the pavement structure and cause additional flexural stresses [26]. De-icing salts, used to melt ice and snow, contain high volumes of sodium and/or magnesium chloride that can cause steel reinforcement corrosion and surface spalling in CRCP. Therefore, the ideal pavement system requires a degree of flexibility similar to flexible pavements but a higher flexural strength similar to rigid concrete pavements at a reasonable cost, fast construction and minimal labour effort.

1.1.2.1 Using WTR and steel fibres in concrete pavements

This thesis develops and examines the materials for a novel pavement system based on a flexible concrete pavement approach utilising Waste Tyre Rubber (chips and crumbs) to partially replace mineral aggregates (up to 60% by volume) in concrete. The hypothesis is that flexible Rubberised Concrete (RuC) pavements can have stiffnesses similar to flexible pavements, thus become capable of accommodating subgrade induced movements and settlements whilst having significant flexural strength (see Figure 1.5b). The rubber particles can also act to balance internal stresses and behave like absorbers for temperature-related stresses and freeze-thaw phenomena [25]. Furthermore, the addition of appropriate amount of rubber particles may also enhance durability as they increase the amount of closed pores in the cement paste matrix and the Interfacial Transition Zone (ITZ) between the cement paste and aggregates creating a pressure release system for freeze-thaw stresses [27]. The incorporation of rubber can also enhance the strain capacity of the concrete pavement and resist shrinkage cracking, especially when shrinkage is restrained by the subgrade.

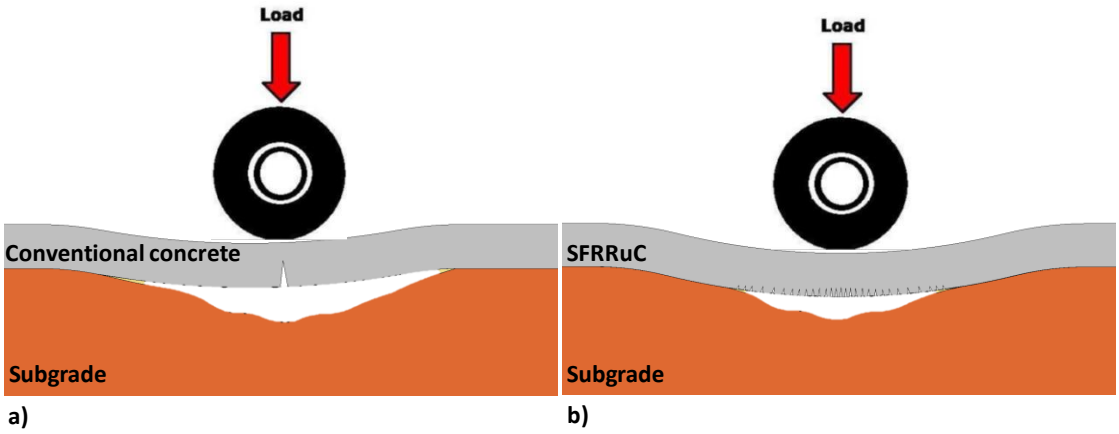

Figure 1.5: Ability of different pavement solutions to accommodate settlements a) conventional rigid concrete pavement and (b) flexible SFRRuC pavement

It is well known, however, that the addition of large quantities of rubber particles in concrete deteriorates significantly its mechanical and durability properties [13, 14, 28-32]. To address this issue, the authors adopt the use of steel fibres (manufactured and/or recycled tyre steel fibres) in RuC, leading to a composite called Steel Fibre Reinforced Rubberised Concrete (SFRRuC). Previous work at USFD found that reinforcing plain concrete pavement with steel fibres can considerably enhance its mechanical and long term performance because the fibres help in maintaining integrity by restraining the development of micro-cracks [33].

SFRRuC pavements are expected to be susceptible to several deteriorating processes including fatigue due to cyclic traffic loading, corrosion of steel fibres as a result of chemical attack by chloride, thermal movements due to heat of hydration, shrinkage/expansion due to moisture movement and freeze-thaw. These deteriorating processes are mainly dominated by the rate of transport of aggressive agents and the degree of saturation [17].

1.2 Brief literature review on steel fibre reinforced concrete (SFRC)

Various types of steel fibres have been developed for various applications and uses. Depending on the manufacturing process, they differ in geometry and mechanical properties. Studies have shown that the mechanical properties of SFRC are affected by the fibre characteristics (type, quantity, aspect ratio, geometry and distribution in concrete), concrete properties (strength and nominal maximum size of aggregate), specimen size and geometry, loading rate and casting method [34, 35]. When steel fibres are added into concrete, they enhance the flexural strength, toughness, impact strength and ductility. While smaller and thinner fibres (micro-fibres) tend to "sew" micro-cracks, longer and thicker fibres (macro-fibres) tend to limit the propagation of

cracks by bridging wider cracks [36, 37]. Figure 1.6 shows the sewing and bridging actions of micro and macro fibres [38]. The addition of steel fibres has also proven to be beneficial to durability and shrinkage cracks [39, 40].

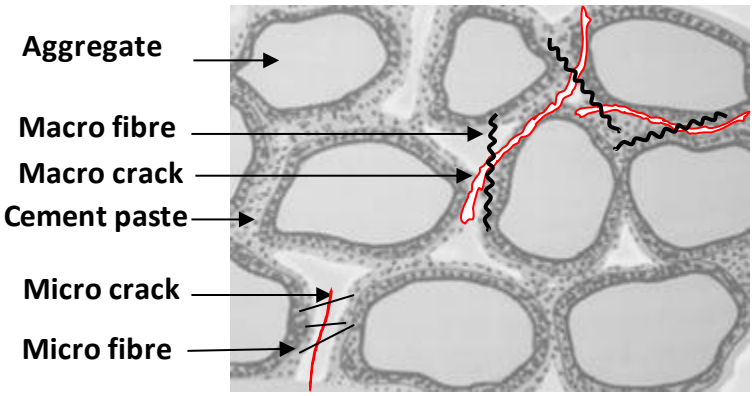

Figure 1.6: Schematic drawing of sewing and bridging actions of micro and macro fibres

Many studies have focused on the use of Recycled Tyre Steel Fibres (RTSF) as reinforcement in concrete to replace Manufactured Steel Fibres (MSF) [20, 41-43]. Most of these studies demonstrated that RTSF reinforced concrete can have comparable performance to MSF reinforced concrete similar fibre dosages. Graeff [10] examined the feasibility of using RTSF and MSF as reinforcement in SFRC and Roller Compacted Concrete (RCC) pavements. The main deterioration processes of the pavements were investigated and the study showed that RTSF concrete reacted well against accelerated corrosion and freeze-thaw. In fatigue, it was found that the RTSF concrete specimens sustained higher stress levels than plain concrete or exhibited longer endurance life at the same stress level. RTSF delayed the propagation of micro-cracks into meso-cracks whilst MSF were found to control macro-cracks more efficiently. The use of steel fibres was found to improve the fatigue resistance and, as a result, the thickness of SFRC pavements was reduced by up to 26%.

Many studies examined hybrid steel fibre reinforced concrete aiming to get better performance by combining the advantages of different types of fibres. For example, Hu et al. [20] examined the mechanical performance of various crimped type MSF and sorted RTSF blends and concluded that, at the same total fibre dosage, blended mixes exhibited the best overall performance compared to concrete mixes reinforced with only one fibre type. Additionally, Younis et al. [66] observed that blended mixes of crimped type MSF and sorted RTSF exhibited higher flexural strength and toughness than MSF-only mixes. Both studies used crimped MSF since their deformed shape improves bonding [67] and pull-out resistance [68]. Crimped steel fibres were also reported to be the most efficient in providing shrinkage restraint, compared to melt extract and hooked steel fibres [69].

1.3 Brief literature review on rubberised concrete (RuC)

1.3.1 Mechanical properties of RuC

The low stiffness of rubber makes it a suitable aggregate candidate, since it can improve some of the mechanical properties of concrete such as ductility, energy absorption, toughness and brittleness [7, 44-47]. This may be attributed to the ability of rubber to deform and fill internal voids in concrete under load and absorb the deformation energy of expanding cracks [48]. These properties, along with the material reduced unit weight [49], better impact and fatigue loading resistance [50], skid resistance [6], sound absorption [51], thermal and electric isolation [52] and its significant environmental and economic benefits, have made RuC an attractive option for industrial and academic research. However, researchers have found that when rubber aggregates replace mineral aggregates, there is a significant loss in compressive/flexural strength and stiffness. The main causes of the reduction in mechanical properties are:

a. rubber is nearly incompressible and has a higher Poisson's ratio compared to the other constituent materials in RuC; under compression, rubber particles expand laterally and increase stress concentrations and micro-cracks in the cement paste, leading to compressive strength reduction [7, 29, 53-55].
b. The weak bond between the cement paste and rubber aggregates causes rubber particles (of low stiffness) to act like voids, leading to a poor Interfacial Transitional Zone (ITZ) and further loss in strength and stiffness [29, 53, 55, 56].
c. The rough and non-polar surfaces of rubber particles tend to repel water and increase the amount of entrapped air in the mix, thus increasing air content and decreasing strength [7, 29, 57-60].
d. When casting and vibrating RuC in moulds, rubber particles may move upwards due to their lower specific gravity and the weak bond with the wet cement paste [55]. This could lead to a high concentration of rubber particles at the top and a non-uniform stiffness and strength distribution [55].

Researchers have also observed that RuC is less workable than conventional concrete [29, 58, 61] due to the specific surface texture of the rubber particles which develop higher friction with the mix constituents [15, 32, 62, 63]. In addition, the workability of RuC might be affected by other parameters related to the production technique used to process WTR (e.g. mechanical shredding and cryogenic), the tendency of rubber particles to interlock, and the presence of other contaminants in the rubber particles (e.g. dust, textile and steel fibres) [58, 62].

1.3.2 Durability and transport properties of RuC

Extensive research has investigated the durability properties of rubberised concrete. However, there is little consensus regarding the RuC freeze/thaw resistance and its water transport properties. According to Richardson et al. [60], the addition of a small amount of crumb rubber (0.6% by weight of concrete) increases the porosity of the cement matrix and this enhances the freeze/thaw resistance. Crumb rubber can act like a shock absorber and balance the internal stress in the concrete matrix caused by hydrostatic pressure of freeze/thaw [27]. Other studies, however, observed a reduction in the freeze/thaw resistance of RuC when excessive rubber content (> 30% as volume replacement of sand) is used [28, 64]. This reduction was attributed to the combined effect of the volume of air content and rubber particles in the mix. Kardos and Durham [28] showed that the permeability (chloride ion penetration) increases with up to 40% volume replacement of sand by crumb rubber. Oikonomou and Mavridou [49] reported a considerable reduction in water absorption and chloride ion penetration in concrete when crumb rubber particles were included (up to 12.5% as volume replacement of sand). Ganjian et al. [55] concluded that while fine rubber particles (up to 10% as volume replacement of cement) decrease the concrete porosity, its permeability increases due to poor rubber-cement paste bond, which allows for the pressurised water to flow through capillaries within the concrete. Most durability work has been done on relatively small amounts of rubber replacement (< 20% of the total aggregate volume) and more work is required to enable the use of larger amounts of rubber.

1.4 Brief literature review on steel fibre reinforced RUC (SFRRuC)

Very limited studies have dealt with the behaviour of SFRRuC and most of these studies focused on the mechanical behaviour of cementitious mortars in which rubber crumb partially replaced fine aggregates [44, 65]. For instance, Turatsinze et al. [44] studied the effect of incorporating both steel fibres and rubber particles on the mechanical behaviour of the cement-based mortar. The sand was replaced with different volumes of rubber crumbs at 30% and 40% and MSF were added at 20 or 40 kg/m^3. It was observed that the synergy from both materials significantly improved the flexural post-cracking behaviour as well as the strain capacity. Nguyen et al. [65] assessed experimentally the effect of blending rubber and steel fibres in cement-based mortars. The results showed that the addition of rubber reduced the compressive strength and elastic modulus, whilst the steel fibres did not affect these properties. It was also observed that the steel fibre reinforcement partly counterbalanced the detrimental effect of rubber addition on the tensile strength. Little information exists on the mechanical behaviour of SFRRuC where both

fine and coarse rubber particles replace conventional fine and coarse aggregates in large quantities (>20% by volume). Furthermore, the literature lacks studies on durability and transport properties as well as long-term performance of SFRRuC.

1.5 Research aim and objectives

The aim of this research was to investigate the fresh, mechanical, transport/pore-structure related properties and long-term behaviour of Steel Fibre Reinforced Rubberised Concrete (SFRRuC) pavements, as an alternative for flexible pavements. The coarse and fine mineral aggregates are partially replaced by different grades and percentages of tyre rubber particles and concrete is reinforced with RTSF or a blended of MSF and RTSF. The following objectives were employed to achieve the above aim:

Obj. 1 Provide a comprehensive literature review on the fresh properties, mechanical behaviour and long-term performance of a) RuC, b) SFRC and c) SFRRuC.

Obj. 2 Implement a pilot study to identify the fresh properties, compressive and flexural behaviour and shrinkage cracking control of SFRRuC using MSF and/or RTSF.

Obj. 3 Conduct a parametric experimental study to investigate the transport and pore structure-related properties of SFRRuC such as volume of permeable voids, gas permeability, sorptivity, chloride penetrability and diffusivity.

Obj. 4 Evaluate the resistance of SFRRuC specimens against corrosion to wet-dry cycles.

Obj. 5 Investigate the effect of accelerated freeze-thaw cycles in SFRRuC.

Obj. 6 Examine the fatigue behaviour of SFRRuC and apply available probabilistic analysis approaches to estimate the design fatigue stress ratios.

Obj. 7 Modify available rigid concrete pavement design approaches to account for the fatigue resistance as well as the flexibility and ductility of SFRRuC.

Obj. 8 Conduct finite element analyses to demonstrate the capability of flexible SFRRuC to accommodate subgrade movements and settlements.

Figure 1.7 shows a diagram of the experimental and analytical work undertaken to investigate the performance of SFRRuC.

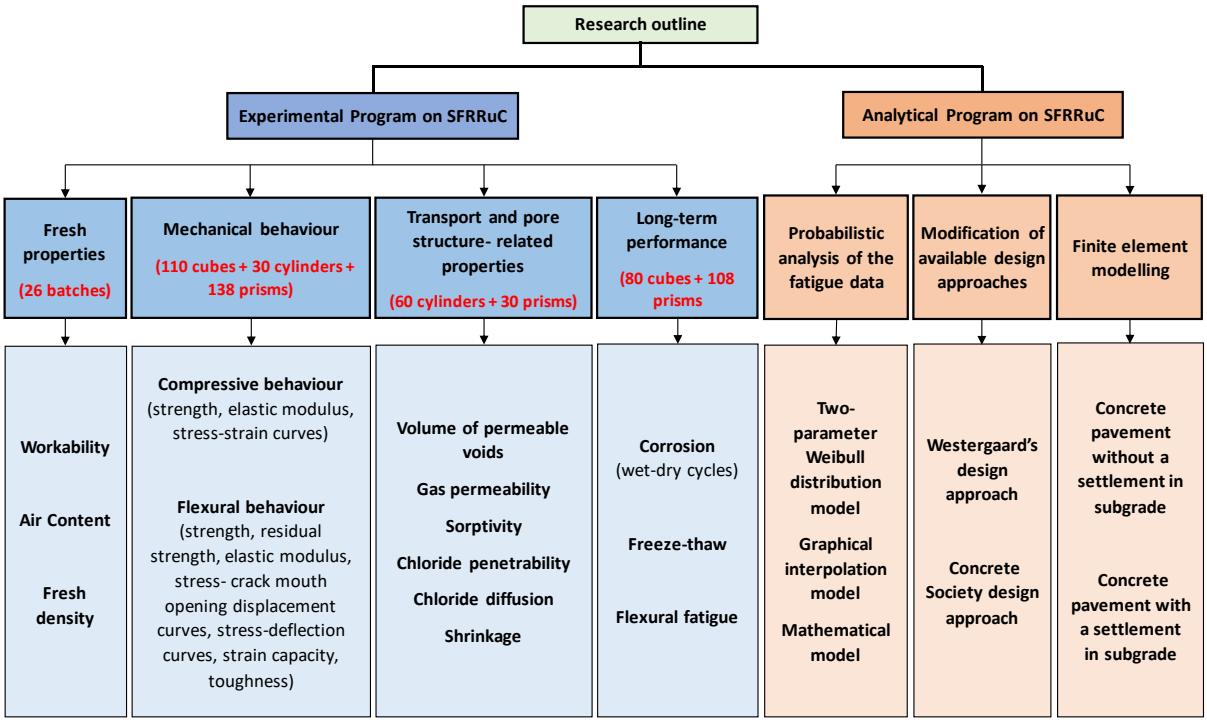

Figure 1.7: Diagram of the research outline and main expected output results

1.6 Research significance and additionality

The development of flexible SFRRuC pavement would address critical challenges ranging from technological barriers and environmental concerns (described in section 1.1.1) to economic aspects. The addition of steel fibres into RuC enhances significantly its mechanical properties such as the compressive/flexural strength, post-cracking behaviour, ductility, toughness, flexibility, energy dissipation and some of durability's characteristics. In full-scale applications, it is also expected that the proposed concrete pavements will lead to the following advantages:

a. Accommodate subgrade movements and settlements and enhance resistance to wearing.
b. Enable a better load distribution owing to the high flexural strength and excellent post-peak behaviour.
c. Increased life span.
d. Avoid/reduce the need of expansion joints.
e. Eliminate the need of a subbase and extra materials.
f. Be less dependent on the strength of subgrade.

Replacing conventional aggregates with WTR particles in concrete also contributes to the natural resource preservation and environment protection, and can be considered as an innovative way of managing the end-of-life tyre disposal business in a more sustainable manner. The

development of sustainable concrete pavements using tyre by-products can offer economically and structurally sound alternatives.

1.7 Thesis layout

This thesis consists of six chapters, including four published peer-reviewed journal papers, and four appendices with further results and details.

Chapter 2 comprises paper [4] [A. Alsaif, L. Koutas, S.A. Bernal, M. Guadagnini, and K. Pilakoutas, *Mechanical performance of steel fibre reinforced rubberised concrete for flexible concrete pavements*, Construction and Building Materials 172 (2018) 533-543] and addresses objectives 1 and 2. This study evaluates the effects of incorporating rubber and steel fibres on the fresh and mechanical properties of SFRRuC with the aim of producing SFRRuC for flexible pavements. Ten concrete batches were cast with 0%, 20%, 40% and 60% of WTR (by volume) replacing both fine and coarse aggregates. Various dosages and blends of steel fibres [(0), (20 kg/m^3 MSF + 20 kg/m^3 RTSF) and (40 kg/m^3 RTSF)] were used. The fresh properties for each mix were evaluated using the slump test, density test and air content test. 30 cubes (150 mm) and 30 cylinders (100 x 200 mm) were tested to evaluate the uniaxial compressive behaviour (strength, elastic modulus and stress-strain behaviour). In addition, 30 notched prisms (100 x 100 x 500 mm) were also produced to assess the flexural behaviour (strength, elastic modulus, stress-deflection curves, residual strength and strain capacity) as well as the free/autogenous/dry shrinkage.

Chapter 3 is based on paper [1] [A. Alsaif, S.A. Bernal, M. Guadagnini, and K. Pilakoutas, *Durability of steel fibre reinforced rubberised concrete exposed to chlorides*, Construction and Building Materials 188 (2018) 130-142] and addresses objectives 1, 3 and 4. This study investigates the durability, transport and pore-structure related properties of the SFRRuC mixes examined in chapter 2. A plain concrete mix as well as three SFRRuC mixes were cast using various rubber replacement levels (0, 30 and 60% by volume) and reinforced with a blend of 20 kg/m^3 MSF and 20 kg/m^3 RTSF. Different curing conditions (mist room or 3% NaCl) and ages of testing (28, 90, 150 or 300 days) were also examined. The following parameters were investigated: 1) fresh properties (slump, air content and unit weight), 2) mechanical behaviour [compressive and flexural (3-point bending) behaviour] and 3) transport properties (volume of permeable voids, gas permeability, sorptivity and chloride penetrability and diffusivity). The chloride corrosion effects due to exposure to a simulated accelerated marine environment (intermittent wet-dry cycles in 3% NaCl solution) were also evaluated.

Chapter 4 presents paper [3] [A. Alsaif, S.A. Bernal, M. Guadagnini, and K. Pilakoutas, Freeze-thaw resistance of steel fibre reinforced rubberised concrete, Construction and Building Materials 195 (2019) 450-458] and addresses objectives 1 and 5. This study assesses the freeze-thaw performance of SFRRuC for flexible concrete pavements. The experimental program comprised a plain concrete mix and three SFRRuC mixes using 100 mm cubes and 100 x 100 x 500 mm prisms, which were fully immersed into 3% NaCl solution and placed in a freeze-thaw chamber to apply temperature cycles ranging from -15 ^{o}C to 20 ^{o}C. The freeze-thaw performance was assessed through visual inspection, mass loss, coefficient of thermal expansion (CTE), internal damage based on the changes in relative dynamic modulus of elasticity (RDM) and residual mechanical properties including compressive strength, flexural strength, modulus of elasticity and toughness.

Chapter 5 comprises paper [2] [A. Alsaif, R. Garcia, F.P. Figueiredo, K. Neocleous, A. Christofe, M. Guadagnini, and K. Pilakoutas, *Fatigue performance of flexible steel fibre reinforced rubberised concrete pavement*, Engineering Structures 193 (2019) 170-183] and addresses objectives 1, 6, 7 and 8. This study examines experimentally and analytically the mechanical and fatigue performance of SFRRuC. A total of 12 cubes (100 mm) and 48 prisms (100 x 100 x 500 mm) were cast to assess the uniaxial compressive strength and flexural performance (4-point testing). Prisms were subjected to flexural fatigue tests using four-point-bending cyclic load (f=15 Hz) at stress ratios of 0.5, 0.7 and 0.9. Three different probabilistic approaches implemented to estimate the design stress ratios for the tested mixes. Possible design implications of using SFRRuC as a new flexible pavement alternative are also discussed by means of a practical example. A modification to the Concrete Society (TR34) design equation is also proposed to account for fatigue as well as flexibility and ductility of SFRRuC. Finite element analyses are undertaken to assess the ability of the flexible SFRRuC pavements to accommodate large subgrade movements and settlements.

Chapter 6 summarises the main conclusions derived from Chapters 2-5 and provides recommendations for future work.

1.8 References

[1] A. Alsaif, S.A. Bernal, M. Guadagnini, and K. Pilakoutas, *Durability of steel fibre reinforced rubberised concrete exposed to chlorides,* Construction and Building Materials 188 (2018) 130-142.

[2] A. Alsaif, R. Garciaa, F.P. Figueiredoa, K. Neocleousb, A. Christofeb, M. Guadagnini, and K. Pilakoutas, *Fatigue performance of flexible steel fibre reinforced rubberised concrete pavement,* Engineering Structures 193 (2019) 170-183.

[3] A. Alsaif, S.A. Bernal, M. Guadagnini, and K. Pilakoutas, *Freeze-thaw resistance of steel fibre reinforced rubberised concrete*, Construction and Building Materials 159 (2019) 450-458.

[4] A. Alsaif, L. Koutas, S.A. Bernal, M. Guadagnini, and K. Pilakoutas, *Mechanical performance of steel fibre reinforced rubberised concrete for flexible concrete pavements,* Construction and Building Materials 172 (2018) 533-543.

[5] ETRA, *The European Tyre Recycling Association,* 2016, Available at: http://www.etra-eu.org [Last accessed: 02/01/2018].

[6] R. Siddique and T.R. Naik, *Properties of concrete containing scrap-tire rubber–an overview,* Waste Management 24 (6) (2004) 563-569.

[7] A.R. Khaloo, M. Dehestani, and P. Rahmatabadi, *Mechanical properties of concrete containing a high volume of tire–rubber particles,* Waste Management 28 (12) (2008) 2472-2482.

[8] Council of the European Union, *Council Directive 1999/31/EC of 26 April 1999 on the landfill of waste*, 1999.

[9] Council of the European Union, *Council Directive 2008/98/EC on waste (Waste Framework Directive)*, 2008.

[10] A. Graeff, *Long term performance of recycled steel fibre reinforced concrete for pavement applications*, in *Department of Civil and Structural Engineering*, 2011, The University of Sheffield, Sheffield.

[11] D. Fedroff, S. Ahmad, and B. Savas, *Mechanical properties of concrete with ground waste tire rubber,* Transportation Research Record, Journal of the Transportation Research Board 1532 (1996) 66-72.

[12] N. Fattuhi and L. Clark, *Cement-based materials containing shredded scrap truck tyre rubber,* Construction and Building Materials 10 (4) (1996) 229-236.

[13] M. Bravo and J. de Brito, *Concrete made with used tyre aggregate: durability-related performance,* Journal of Cleaner Production 25 (2012) 42-50.

[14] B.S. Thomas and R.C. Gupta, *A comprehensive review on the applications of waste tire rubber in cement concrete,* Renewable and Sustainable Energy Reviews 54 (2016) 1323-1333.

[15] S. Raffoul, R. Garcia, K. Pilakoutas, M. Guadagnini, and N.F. Medina, *Optimisation of rubberised concrete with high rubber content: An experimental investigation,* Construction and Building Materials 124 (2016) 391-404.

[16] K. Pilakoutas, K. Neocleous, and H. Tlemat, *Reuse of tyre steel fibres as concrete reinforcement,* Proceedings of the ICE-Engineering Sustainability 157 (3) (2004) 131-138.

[17] H. Angelakopoulos, *D1.2 - State of the art on FRC, SFRC and fibre blend RC*, in *Innovative Reuse of all Tyre Components in Concrete*, 2014, anagennisi.

[18] USFD. *Thin wire reinforcement for concrete.* B.P. Application (2001), Editor, UK.

[19] K. Neocleous, H. Angelakopoulos, K. Pilakoutas, and M. Guadagnini, *Fibre-reinforced roller-compacted concrete transport pavements,* Proceedings of the ICE-Transport 164 (TR2) (2011) 97-109.

[20] H. Hu, P. Papastergiou, H. Angelakopoulos, M. Guadagnini, and K. Pilakoutas, *Mechanical properties of SFRC using blended manufactured and recycled tyre steel fibres,* Construction and Building Materials 163 (2018) 376-389.

[21] D. Wum, *The semi-rigid pavement with higher performances for roads and parking aprons*, CAFEO 29, Sustainable Urbanization-Engineering Challenges and Opportunities (2011) 27-30.

[22] D. Thomas, *Choosing between asphalt and concrete pavement,* Public Works Magazine, 2006.

[23] E. Sullivan, *Update: paving, new realities,* Flash report–breaking analysis of the economy, construction and cement industries (2009), Washington DC, USA.

[24] ACPA, *A Comparison of pavement performance and costs,* American Concrete Pavement Association (2000) Washington, USA.

[25] O.A. Abaza and Z.S. Hussein, *Flexural behavior of steel fiber-reinforced rubberized concrete,* Journal of Materials In Civil Engineering 28 (1) (2015) 04015076.

[26] A. Vaitkus, J. Gražulytė, E. Skrodenis, and I. Kravcovas, *Design of frost resistant pavement structure based on road weather stations (RWSs) Data,* Sustainability 8 (12) (2016) 1328.

[27] G. Skripkiūnas, A. Grinys, and E. Janavičius, *Porosity and durability of rubberized concrete*, in *The Second International Conference on Sustainable Construction Materials and Technologies* (2010).

[28] A.J. Kardos and S.A. Durham, *Strength, durability, and environmental properties of concrete utilizing recycled tire particles for pavement applications,* Construction and Building Materials 98 (2015) 832-845.

[29] Z. Khatib and F. Bayomy, *Rubberized portland cement concrete,* Journal of Materials in Civil Engineering 11 (3) (1999) 206-213.

[30] K.B. Najim and M.R. Hall, *A review of the fresh/hardened properties and applications for plain- (PRC) and self-compacting rubberised concrete (SCRC),* Construction and Building Materials 24 (11) (2010) 2043-2051.

[31] N.F. Medina, D.F. Medina, F. Hernández-Olivares, and M. Navacerrada, *Mechanical and thermal properties of concrete incorporating rubber and fibres from tyre recycling,* Construction and Building Materials 144 (2017) 563-573.

[32] D. Flores-Medina, N.F. Medina, and F. Hernández-Olivares, *Static mechanical properties of waste rests of recycled rubber and high quality recycled rubber from crumbed tyres used as aggregate in dry consistency concretes,* Materials and Structures 47 (7) (2014) 1185-1193.

[33] A.G. Graeff, *Long-term performance of recycled steel fibre reinforced concrete for pavement applications*, 2011, University of Sheffield.

[34] D.A. Fanella and A.E. Naaman, *Stress-strain properties of fiber reinforced mortar in compression*, in *ACI Journal proceedings* (1985), ACI.

[35] A. Bentur and S. Mindess, *Fibre reinforced cementitious composites*, (2006), CRC Press.

[36] P.K. Mehta and P.J. Monteiro, *Concrete: microstructure, properties, and materials*, 3 (2006), McGraw-Hill New York.

[37] P. Rossi and E. Parant, *Damage mechanisms analysis of a multi-scale fibre reinforced cement-based composite subjected to impact and fatigue loading conditions,* Cement And Concrete Research 38 (3) (2008) 413-421.

[38] Y. Mo and R.H. Roberts, *Carbon Nanofiber Concrete for Damage Detection of Infrastructure*, (2013), InTech.

[39] K. Hossain, M. Lachemi, M. Sammour, and M. Sonebi, *Strength and fracture energy characteristics of self-consolidating concrete incorporating polyvinyl alcohol, steel and hybrid fibres,* Construction and Building Materials 45 (2013) 20-29.

[40] N. Ganesan, P. Indira, and M. Sabeena, *tensionsStiffening and cracking of hybrid fiber-reinforced concrete,* ACI Materials Journal 110 (6) (2013).

[41] M.A. Aiello, F. Leuzzi, G. Centonze, and A. Maffezzoli, *Use of steel fibres recovered from waste tyres as reinforcement in concrete: Pull-out behaviour, compressive and flexural strength,* Waste Management 29 (6) (2009) 1960-1970.

[42] K. Pilakoutas, K. Neocleous, and H. Tlemat, *Reuse of tyre steel fibres as concrete reinforcement,* Proceedings of the ICE-Engineering Sustainability 157 (3) (2004) 131-138, ISSN 1478-4629.

[43] H. Tlemat, *Steel fibres from waste tyres to concrete: testing, modelling and design*, 2004, The University of Sheffield.

[44] A. Turatsinze, J.L. Granju, and S. Bonnet, *Positive synergy between steel-fibres and rubber aggregates: Effect on the resistance of cement-based mortars to shrinkage cracking,* Cement and Concrete Research 36 (9) (2006) 1692-1697.

[45] A. Benazzouk, O. Douzane, K. Mezreb, B. Laidoudi, and M. Queneudec. *Thermal conductivity of cement composites containing rubber waste particles: Experimental study and modelling.* Construction and Building Materials 22(4) (2008) 573-579.

[46] K.S. Son, I. Hajirasouliha, and K. Pilakoutas, *Strength and deformability of waste tyre rubber-filled reinforced concrete columns,* Construction and Building Mateials 25 (1) (2011) 218-226.

[47] A.C. Ho, A. Turatsinze, R. Hameed, and D.C. Vu, *Effects of rubber aggregates from grinded used tyres on the concrete resistance to cracking,* Journal of Cleaner Production 23 (1) (2012) 209-215.

[48] F. Liu, W. Zheng, L. Li, W. Feng, and G. Ning, *Mechanical and fatigue performance of rubber concrete,* Construction and Building Materials 47 (2013) 711-719.

[49] N. Oikonomou and S. Mavridou, *Improvement of chloride ion penetration resistance in cement mortars modified with rubber from worn automobile tires,* Cemement and Concrcrete Composite 31 (6) (2009) 403-407.

[50] F. Hernández-Olivares, G. Barluenga, M. Bollati, and B. Witoszek, *Static and dynamic behaviour of recycled tyre rubber-filled concrete,* Cement and Concrete Research 32 (10) (2002) 1587-1596.

[51] P. Sukontasukkul, *Use of crumb rubber to improve thermal and sound properties of pre-cast concrete panel,* Construction and Building Materials 23 (2) (2009) 1084-1092.

[52] C.A. Issa and G. Salem, *Utilization of recycled crumb rubber as fine aggregates in concrete mix design,* Construction and Building Materials 42 (2013) 48-52.

[53] G. Li, M.A. Stubblefield, G. Garrick, J. Eggers, C. Abadie, and B. Huang, *Development of waste tire modified concrete,* Cement and Concrete Research 34 (12) (2004) 2283-2289.

[54] A. El-Dieb, M. Abd El-Wahab, and M. Abdel-Hameed, *Mechanical, fracture, and microstructural investigations of rubber concrete,* Journal of Materials in Civil Engineering 20 (10) (2008) 640-649.

[55] E. Ganjian, M. Khorami, and A.A. Maghsoudi, *Scrap-tyre-rubber replacement for aggregate and filler in concrete,* Construction and Building Materials 23 (5) (2009) 1828-1836.

[56] M.C. Bignozzi and F. Sandrolini, *Tyre rubber waste recycling in self-compacting concrete,* Cement and Concrete Research 36 (4) (2006) 735-739.

[57] F. Hernández-Olivares and G. Barluenga, *Fire performance of recycled rubber-filled high-strength concrete,* Cement and Concrete Research 34 (1) (2004) 109-117.

[58] E. Güneyisi, M. Gesoğlu, and T. Özturan, *Properties of rubberized concretes containing silica fume,* Cement and Concrete Research 34 (12) (2004) 2309-2317.

[59] C. Albano, N. Camacho, J. Reyes, J.L. Feliu, and M. Hernández, *Influence of scrap rubber addition to Portland I concrete composites: Destructive and non-destructive testing,* Composite Structures 71 (3) (2005) 439-446.

[60] A.E. Richardson, K. Coventry, and G. Ward, *Freeze/thaw protection of concrete with optimum rubber crumb content,* Journal of Cleaner Production 23 (1) (2012) 96-103.

[61] M. Gesoglu and E. Guneyisi, *Strength development and chloride penetration in rubberized concretes with and without silica fume,* Materials and Structures 40 (9) (2007) 953-964.

[62] N.N. Eldin and A.B. Senouci, *Measurement and prediction of the strength of rubberized concrete,* Cement and Concrete Composites 16 (4) (1994) 287-298.

[63] E. Güneyisi, M. Gesoglu, N. Naji, and S. İpek, *Evaluation of the rheological behavior of fresh self-compacting rubberized concrete by using the Herschel–Bulkley and modified Bingham models,* Archives of Civil and Mechanical Engineering 16 (1) (2016) 9-19.

[64] X. Zhu, C. Miao, J. Liu, and J. Hong, *Influence of crumb rubber on frost resistance of concrete and effect mechanism,* Procedia Engineering 27 (2012) 206-213.

[65] T. Nguyen, A. Toumi, and A. Turatsinze, *Mechanical properties of steel fibre reinforced and rubberised cement-based mortars,* Materials and Design 31 (1) (2010) 641-647.

[66] K.H. Younis, K. Pilakoutas, M. Guadagnini, and H. Angelakopoulos, Feasibility of Using Recycled Steel Fibres To Enhance the Behaviour of Recycled Aggregate Concrete, International Workshop – Fibre Reinforced Concrete: From Design to Structural Applications (2014) 598–608.

[67] N. Jafarifar, Shrinkage behaviour of steel-fibre-reinforced-concrete pavements, in Civil and Structural Engineering. 2012, University of Sheffield.

[68] A. Lukasenoks, A. Macanovskis, and A. Krasnikovs, Matrix strength influence on composite fibre reinforced concrete behaviour in flexure and single fibre pull-out, in In proceedings of the international scientific conference. [Latvijas Lauksaimniecības universitāte]. 2018.

[69] P.S. Mangat and M.M. Azari, Shrinkage of steel fibre reinforced cement composites, Materials and structures 21(3) (1988) 163-171.

This page is intentionally left blank

Chapter 2

Mechanical Performance of Steel Fibre Reinforced Rubberised Concrete (SFRRuC) for Flexible Concrete Pavements

A. Alsaif, L. Koutas, S.A. Bernal, M. Guadagnini, and K. Pilakoutas, Mechanical performance of steel fibre reinforced rubberised concrete for flexible concrete pavements, Construction and Building Materials 172 (2018) 533-543.

Author contribution statement

Dr Koutas, Dr Bernal, Dr Guadagnini and Prof. Pilakoutas supervised the PhD study of the first author. All authors discussed the results and commented on the manuscript.

This study aims to develop materials for flexible concrete pavements as an alternative to asphalt concrete or polymer-bound rubber surfaces and presents a study on steel fibre reinforced rubberised concrete (SFRRuC). The main objective of this study is to investigate the effect of steel fibres (manufactured and/or recycled fibres) on the fresh and mechanical properties of rubberised concrete (RuC) comprising waste tyre rubber (WTR). Free shrinkage is also examined. The main parameters investigated through ten different mixes are WTR and fibre contents. The results show that the addition of fibres in RuC mixes with WTR replacement substantially mitigates the loss in flexural strength due to the rubber content (from 50% to 9.6% loss, compared to conventional concrete). The use of fibres in RuC can also enable the development of sufficient flexural strength and enhance strain capacity and post-peak energy absorption behaviour, thus making SFRRuC an ideal alternative construction material for flexible pavements.

This chapter consists of a "stand alone" journal paper and contains a relevant bibliography at the end of the chapter. Appendix A provides additional information and further test results.

2.1 Introduction and Background

Road pavements and slabs on grade are constructed either with flexible asphalt or rigid concrete. Flexible pavements can better accommodate local deformations, but lack the durability of concrete which is by nature much stiffer. A flexible concrete pavement could combine the advantages of both types of pavements, however, requires a radical change in how it is constructed. Rubberised concrete which can be design to have stiffness values similar to that of asphalt, can be used as an alternative construction material for flexible pavements. It is well known, however, that the use of rubber in substantial enough quantities can also adversely affect all of the other mechanical properties of Portland-based concrete. Furthermore, virgin rubber aggregates are significantly more expensive than natural aggregates. To address these issues, this study aims to use recycled materials derived from waste tyre rubber (WTR) not only to provide economically and structurally sound alternatives, but also to enable the development of a sustainable flexible concrete pavement solution.

2.1.1 Waste tyre materials

According to The European Tyre Recycling Association [1], approximately 1.5 billion tyres are produced worldwide each year and a quarter of this amount is arisen in EU countries. It is also estimated that for every tyre brought to the market, another tyre reaches its service life and becomes waste. The European Directive 1991/31/EC [2] introduced a set of strict regulations to prevent the disposal of waste tyres in landfills as a means of preventing environmental pollution and mitigating health and fire hazard [3-5]. As a result, in the EU any type of waste tyre disposal in the natural environment has been banned since 2006. The European Directive 2008/98/EC [6] has also established a disposal hierarchy leading to a serious effort for effective waste tyre management, minimising energy consumption.

Typical car or truck tyres comprise 75-90% rubber, 5-15% high-strength corded steel wire and 5-20% polymer textile. WTR is currently used as fuel, in particular in cement kilns. It is also used in applications, such as synthetic turf fields, artificial reefs, sound proof panels, playground surfaces and protective lining systems for underground infrastructure [7, 8]. While these applications make a positive contribution to recycling WTR, demand with respect to the volume of waste tyres is still small. Since cement-based materials constitute the largest portion of construction materials worldwide, recycling WTR in concrete is a positive way to respond to the environmental challenge and to the significant redundant volumes of waste materials.

2.1.2 Rubberised concrete

In the past two decades, several studies have investigated the addition of WTR in concrete, but only recently for structural applications [9-12]. Concretes containing rubber particles present high ductility and strain capacity, increased toughness and energy dissipation [11, 13, 14]. These properties, along with the material's high impact and skid resistance, sound absorption, thermal and electrical insulation [5, 15-17] make rubberised concretes (RuC) a very attractive building material for non-structural applications.

Despite the good mechanical properties of rubber, production of RuC has several important drawbacks: (a) reduction in workability associated with the surface texture of the rubber particles [3, 11, 18, 19], (b) increased air content as the rough and non-polar surface of rubber particles tend to repel water and increase the amount of entrapped air [20-22], and (c) reduction in the compressive strength (up to approximately 90% reduction with 100% replacement of natural aggregates), tensile strength and stiffness [11, 23]. The reduction in mechanical properties is mainly attributed to the lower stiffness and higher Poisson's ratio of rubber (nearly 0.5) compared to the other materials in the mixture, and the weak bond between cement paste and rubber particles [21, 24, 25]. One of the potential alternatives to enhance the mechanical performance of RuC is the addition of fibres.

2.1.3 Steel fibre reinforced concrete using recycled fibres

The steel cord used as tyre reinforcement is a very high strength cord of fine wires (0.1- 0.3 mm). The same cord is currently being used in limited volumes to reinforce concrete in high value security applications, such as vaults and safe rooms. At the same time when extracted from tyres, the cord is either discarded or at best re-melted. Commercially available steel fibre reinforcement for concrete comprises thin fibres with a diameter ranging from 0.3 to 1 mm and has a sizable market mainly in tunnel and slabs on grade applications. Hence, it is natural to consider tyre wire for concrete applications [26], as using recycled tyre steel fibres (RTSF) from waste tyres, instead of manufactured steel fibres (MSF), can reduce costs and positively contribute to sustainability by reducing the emissions of CO_2 generated from manufacturing steel fibres [27, 28]. Recently, many studies have examined the use of recycled steel fibres in concrete [27, 29-32]. By assessing mechanical properties, most of these studies confirm the ability of classified RTSF to reinforce concrete.

2.1.4 Steel fibre reinforced rubberised concrete

Despite the fact that there are many studies on RuC and SFRC, there are very few studies examining the effect of using steel fibres and rubber particles together in concrete, and most of these focus on cement-based mortars or self-compacted concrete (SCC) [33-37]. Turatsinze et al. [33] investigated the synergistic effect of MSF and rubber particles, in particular replacing sand in cement-mortars. They observed that the addition of steel fibres improved the flexural post-cracking behaviour, while the addition of rubber (up to 30% by volume of sand) significantly increased the deflection at peak load. Ganesan et al. [35] studied the influence of incorporating crumb rubber and MSF in SCC. Compared to conventional SCC, they reported a 35% increase in flexural strength when 15% of sand (by volume) was replaced with crumb rubber and 0.75% (by volume) fraction of steel fibres was added. Xie et al. [36] conducted an experimental study on the compressive and flexural behaviour of MSF reinforced recycled aggregate concrete with crumb rubber. They found that as the amount of rubber content was increased, the reduction in the compressive strength was smaller compared to other studies, and they attributed this behaviour to the inclusion of steel fibres. They also concluded that steel fibres played a significant role in enhancing the residual flexural strength, which was slightly affected by the increase in rubber content. Finally, Medina et al. [37] examined the mechanical properties of concrete incorporating crumb rubber and steel or plastic fibres coated with rubber. They observed that concrete with rubber and fibres presents better compressive and flexural behaviour as well as impact energy absorption than plain rubberised concrete.

To the best of the authors' knowledge only limited information is available on the mechanical behaviour of steel fibre reinforced rubberised concrete (SFRRuC) where both fine and coarse aggregates are replaced with rubber particles in significant volumes (exceeding 20% by volume of total aggregates) and further studies are needed to understand its performance where much larger rubber volumes are used. Large volumes of rubber are necessary to achieve more flexible concrete pavements. In addition, the behaviour of SFRRuC in which RTSF are used alone or in a blend with MSF, has not been studied yet.

This study investigates the fresh properties as well as the compressive and flexural behaviour of several SFRRuC mixes with the aim of developing optimized mixes suitable for pavement applications. Coarse and fine aggregates are partially replaced by different sizes and percentages of tyre rubber particles and various dosages and blends of steel fibres, MSF and/or RTSF, are used as fibre reinforcement. Details of the experimental programme and the main experimental results are presented and discussed in the following sections. This study contributes to the

objectives of the EU-funded collaborative project Anagennisi (http://www.anagennisi.org/) that aims to develop innovative solutions to reuse all waste tyre components.

2.2 Experimental Programme

2.2.1 Parameters under investigation

The parameters assessed in this study were: (i) the rubber content used as partial replacement of both fine and coarse aggregates (0%, 20%, 40% or 60% replacement by volume), and (ii) steel fibre content (0 or 20 kg/m^3 MSF + 20 kg/m^3 RTSF, or 40 kg/m^3 RTSF). A total of 10 different concrete mixes were prepared for this study aiming to identify the effect of rubber content as well as the effect of the type and content of steel fibre reinforcement on the fresh and mechanical properties of SFRRuC mixes. For each mix, three cubes (150 mm-size), three cylinders (100 mm-diameter and 200 mm-length), and three prisms (100x100 mm-cross section and 500 mm-length) were cast. The cubes and cylinders were used to obtain the uniaxial compressive strength and the compressive stress-strain curve, respectively, whereas the prisms were cured in different conditions to evaluate free shrinkage strain (autogenous and drying) and then subjected to three-point bending. Table 2.1 summarises the different mix characteristics and the ID assigned to the mixes. The mix ID follows the format NX, where N denotes the amount of rubber content used as partial replacement of both fine and coarse aggregates (0, 20, 40 or 60%), while X represents the type of steel fibre reinforcement and can be either P, BF or RF (Plain, Blend of Fibres or Recycled Fibres, respectively**)**. For instance, *60BF* is the rubberised concrete mix that contains 60% of rubber particles as conventional aggregate replacement and consists of blend fibres (20 kg/m^3 MSF and 20 kg/m^3 RTSF).

Table 2.1 Concrete mix ID, and quantities of rubber and steel fibres added in each mix

Mix No.	Mix ID	% Rubber replacing aggregates by volume		Fine rubber (kg/m^3)	Coarse rubber (kg/m^3)	MSF (kg/m^3)	RTSF (kg/m^3)
		Fine	Coarse				
1	*0P*	0	0	0	0	0	0
2	*0BF*	0	0	0	0	20	20
3	*0RF*	0	0	0	0	0	40
4	*20P*	20	20	49.5	60.4	0	0
5	*20BF*	20	20	49.5	60.4	20	20
6	*40P*	40	40	99	120.9	0	0
7	*40BF*	40	40	99	120.9	20	20
8	*60P*	60	60	148.5	181.3	0	0
9	*60BF*	60	60	148.5	181.3	20	20
10	*60RF*	60	60	148.5	181.3	0	40

2.2.2 Materials and mix preparation

2.2.2.1 Materials

A high strength commercial Portland Lime Cement CEM II-52.5 N containing around 10–15% Limestone in compliance with BS EN 197-1 [38] was used as binder. The coarse aggregates used comprised natural round river washed gravel with particle sizes of 5-10 mm and 10-20 mm [specific gravity (SG)=2.65, absorption (A) =1.2%]. The fine aggregates used comprised medium grade river washed sand with particle sizes of 0-5 mm (SG=2.65, A=0.5%). Pulverised fuel ash (PFA) and silica fume (SF) were used as partial replacement of cement (10% by weight for each) to enhance the fresh and mechanical properties of the mixes. Plasticiser and superplasticiser were also added to improve cohesion and mechanical properties (mix details are given in Section 2.2.2.2).

The rubber particles used in this study were recovered through the shredding process of waste tyres at ambient temperature and where obtained from two different sources. As depicted in Figure 2.1a, the fine rubber particles were provided in the ranges of 0-0.5 mm, 0.5-0.8 mm, 1-2.5 mm and 2-4 mm and were used in the concrete mix in the ratio 12:12:32:44 of the total added fine rubber content, while the course rubber particles were supplied in the ranges of 4-10 mm and 10-20 mm and were utilized in the concrete mix in the ratio 50:50 of the total added course rubber content. Figure 2.2 presents the particle size distribution of the natural aggregates (NA) and rubber particles used, obtained according to ASTM-C136 [39]. To limit the influence of rubber size on concrete particle packing, conventional aggregates were replaced with rubber particles of roughly similar size distribution to minimise the impact on the packing of the concrete mix constituents. A relative density of 0.8 was used to calculate the mass of rubber replacing natural aggregates, as determined using a large rubber sample that was accurately cut and measured. However, as shown in Figure 2.2, the curve that combines 60% rubber aggregate + 40% NA is below than that of 100% NA, indicating that rubber aggregates have a slightly different size distribution than natural aggregates with less fines in the fine aggregate region (i.e. 0-5 mm). This is necessary due to their irregular shape, rough texture, contamination, excessive friction and interlock among rubber particles, which has an impact on workability.

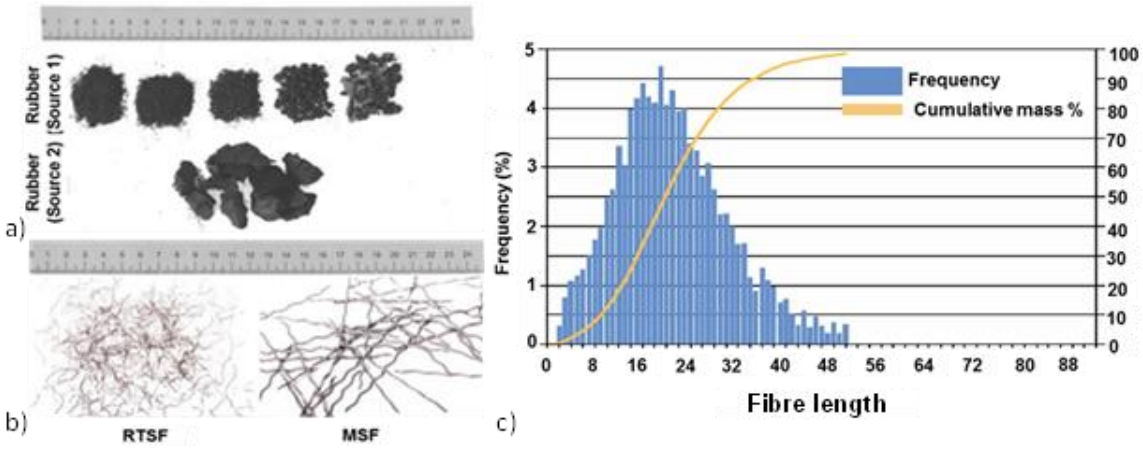

Figure 2.1: a) Rubber particles, b) MSF and RTSF used in this study and c) length distribution analysis of RTSF

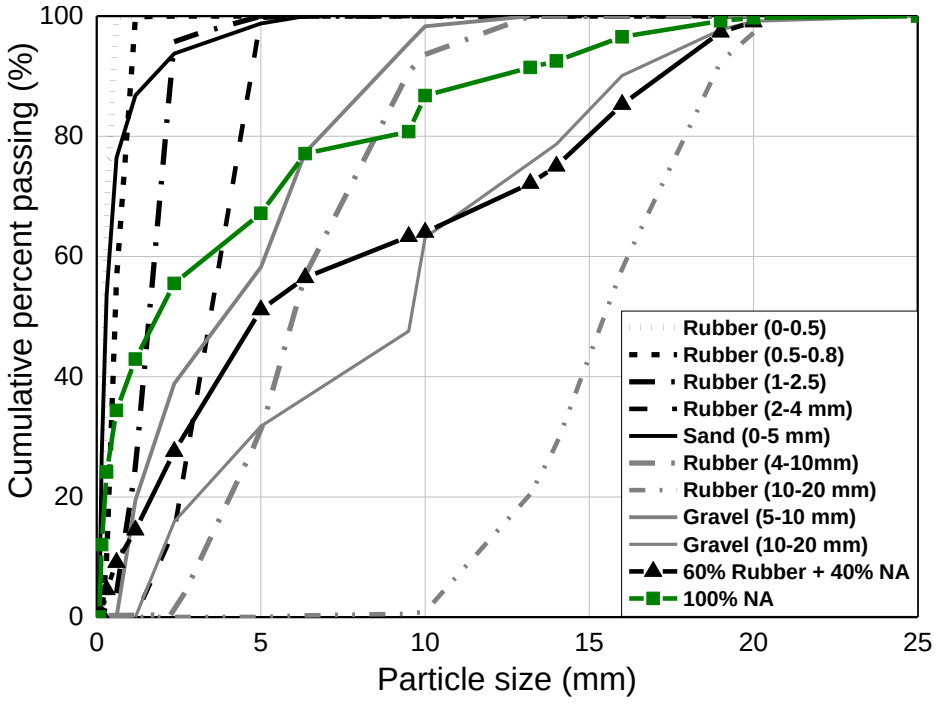

Figure 2.2: Particle size distribution for conventional aggregates and rubber

Table 2.2 reports the physical properties of the coarse aggregates (5-20 mm) and the coarse rubber particles (4-20 mm), obtained through a series of tests: (a) particle density and water absorption according to EN 1097-6 [40], (b) loose bulk density according to EN 1097-3 [41], and (c) particle shape-flakiness index according to EN 933-3 [42]. The physical properties of the fine aggregates and fine rubber particles were not evaluated due to difficulties in performing the tests on fine rubber particles as they floated when submerged in water.

As it was not possible to complete the flakiness tests for all particle sizes, in the end this information was not used directly in the mix design. It should be noted though that the higher

flakiness influenced the optimisation of the mix design and more fines and supplementary materials were necessary, as reported in [11].

Table 2.2 Physical properties of coarse aggregates and coarse rubber particles

Physical properties/Type of rubber	Rubber - Source 1 4-10 mm	Rubber - Source 2 10-20 mm	Natural aggregates 5-10 mm	Natural aggregates 10-20 mm
Apparent particle density, kg/m^3	1136	1103	2685	2685
Oven-dried density, kg/m^3	1032	1090	2599	2599
Saturated and surface-dried particle density, kg/m^3	1123	1101	2631	2631
Water absorption after 24h, %	5.3-8.8	0.8-1.3	1.2	1.2
Bulk specific gravity	1.1	1.1	2.6	2.6
Bulk density, kg/m^3	454	485	1511	1583
Flakiness index	6.64	17.48	7.05	9.7

The MSF were crimped type steel fibres with a length of 55 mm, diameter of 0.8 mm and tensile strength of 1100 MPa. The RTSF were cleaned and screened fibres (typically containing < 2% of residual rubber) and had lengths in the range of 15-45 mm (at least 60% by mass), diameters <0.3 mm and tensile strength of 2000 MPa. Figure 2.1b presents both types of fibres (MSF and RTSF) used in this study and Figure 2.1c illustrates the length distribution of the RTSF based on a digital optical correlation method that combines photogrammetry and advanced pattern recognition to determine the length of individual fibre from high speed image of free falling dispersed fibres [43].

2.2.2.2 Mix design

The mix design used in this experimental study (adopted from Raffoul et al. [11]) was optimised to be used for typical concrete bridge piers targeting a compressive strength of 60 MPa (cylinder), and suited the replacement of 0%, 20%, 40% and 60% of WTR without excessive degradation in fresh and mechanical properties. The optimised mix proportions for 0% rubber content (conventional concrete), are shown in Table 2.3.

Table 2.3 Concrete mix proportions (without rubber content)

Material	Quantity
CEM II – 52.5 MPa	340 kg/m^3
Silica fume (SF)	42.5 kg/m^3
Pulverised fuel ash (PFA)	42.5 kg/m^3
Natural fine aggregates 0-5 mm	820 kg/m^3
Natural coarse aggregates 5-10 mm	364 kg/m^3
Natural coarse aggregates 10-20 mm	637 kg/m^3
Water	150 l/m^3
Plasticiser	2.5 l/m^3*
Superplasticiser	5.1 l/m^3

*It was increased at higher amounts of rubber and fibres were added to the concrete (2.5-4.75 l/m^3).

2.2.2.3 Mixing, casting and curing procedure

A 200 litre pan mixer was used for all mixes. The procedure used for mixing the concrete started with conventional aggregates dry mixed for 30 seconds together with the rubber particles. Subsequently, half of the total amount of water was added and mixed for about 1 minute. The mix was allowed to rest for 3 minutes allowing the conventional aggregates to get saturated. After that, the cementitious materials (Portland cement, silica fume and fly ash) were added, followed by the remaining water and the chemical admixtures. The fresh concrete was finally mixed for another 3 minutes. For those concrete mixes with steel fibres, fibres were manually integrated into the concrete during mixing at the last mixing stage.

The concrete fresh properties including slump, air content and fresh density, were then assessed for each mix according to the standardised methods described in EN 12350-2 [44], EN 12350-7 [45], and EN 12350-6 [46], respectively. The concrete specimens were cast in plastic cube (150 mm) and cylinder moulds (100x200 mm), and prismatic steel moulds (100x100x500 mm) according to EN 12390-2 [47] and EN 14651 [48]. The specimens were cast in two layers and vibrated (25s per layer) on a vibrating table. After casting, specimens were covered with plastic sheets to prevent moisture loss, and left under standard laboratory conditions for 48h until demoulding. The specimens were then kept in a mist room (21 $^{\circ}$C $\pm$ 2 and 95 $\pm$ 5% relative humidity (RH)) for 28 days, except for the prisms used for shrinkage measurements that were left in the mist room for 7 days and then stored in a control room (24 $^{\circ}$C $\pm$ 2 and 42 $\pm$ 5 RH) for 50 days. After the curing period, the specimens were kept under standard laboratory conditions (20 $^{\circ}$C $\pm$ 2 and 50 $\pm$ 5 RH) until testing.

2.3 Test set-up and procedure

2.3.1 Compression testing

Prior to testing, the top faces of the cylinders were cut and ground according to EN 12390-3 [49]. For the RuC cylinders, extra measures were taken to prevent local failure during testing by confining their two ends with high-ductility post-tensioned straps, as proposed by Garcia et al. [50]. Axial compression tests were performed on concrete cubes and cylinders according to EN 12390-3 [49] under monotonic loading until failure. For all tested cylinders, the compression tests were performed using a servo-hydraulic universal testing machine with a load capacity of 1000 kN. The load was applied on the cylinders at a displacement rate of 0.3 mm/min. The local axial strain was measured using two diagonally opposite strain gauges at mid-height. The global axial strain was measured using three laser sensors, with an accuracy of 40με, placed radially around the specimens (120^{o} apart) using two metallic rings. The metallic rings were attached to the specimens using four clamp screws, covering the middle zone of the cylinder and resulting in 100 mm gauge length. The tests on cubes were carried out using a standard compression machine with a load capacity of 3000 kN at a loading rate of 0.4 MPa/s.

2.3.2 Three-point bending tests

The flexural behaviour of the concrete specimens was assessed by performing three-point bending tests using an electromagnetic universal testing machine with a load capacity of 300 kN. A detailed schematic of the test setup is provided in Figure 2.3. The loading point allowed for both the in-plane and out-of-plane rotation of the prism. Two LVDTs were mounted at the middle of a yoke (one on each side) as suggested by the JCI [51] to measure the net deflection at mid-span.

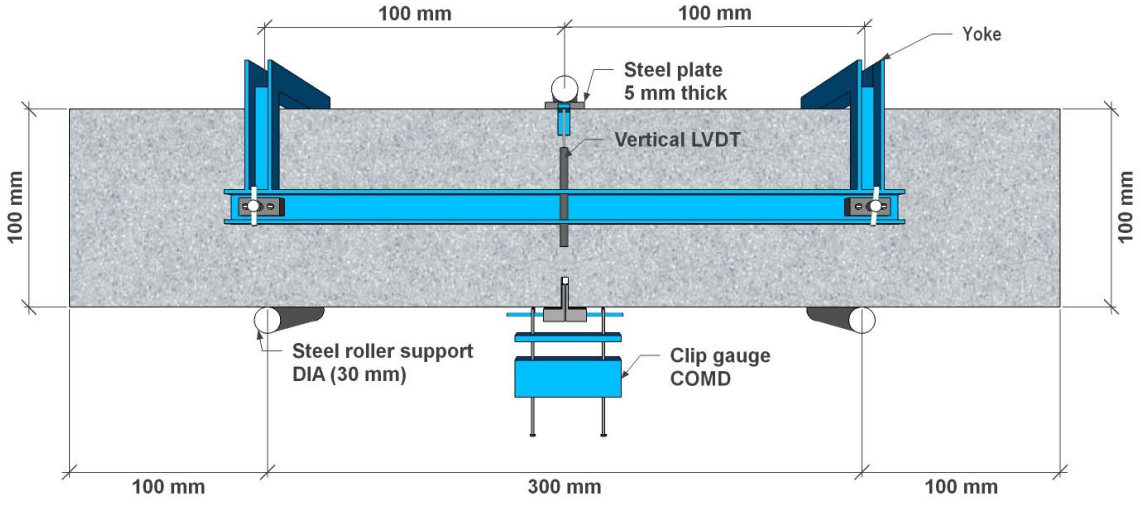

Figure 2.3: Schematic representation of the flexural test set-up

A clip gauge of 12.5 mm-length was fixed at the middle of the bottom side of the prism, where a 5 mm-wide and 15 mm-deep notch had been sawn. The clip gauge measurement (crack mouth opening displacement -CMOD) was used to control the loading rate as suggested by RILEM [52]. All tests were performed under a rate of 50 µm/min for CMOD ranging from 0 to 0.1 mm, 200 µm/min for CMOD ranging from 0.1 to 4 mm, and 8000 µm/min for CMOD higher than 4 mm.

2.3.3 Free-shrinkage

The autogenous and drying shrinkage tests were performed according to EN-126174 [53]. However, to avoid issues of fibre alignment along the mould boundaries, the size of the prismatic specimens was increased from 40x40x160 mm (as suggested by the standard) to 100x100x500 mm. Specimens were demoulded two days after casting and fitted with steel "Demec" points (locating discs) using plastic padding. Two Demec points were fixed 300 mm apart on each of the vertical (as cast) sides of the prism.

The first strain measurement was recorded after 30 minutes to allow for the hardening of the adhesive. For autogenous shrinkage, the specimens were kept in a mist room with controlled temperature and humidity conditions (21 ^{o}C $\pm$ 2 and 95 $\pm$ 5% RH) and measurements were taken at the ages of 1, 2, 3 and 7 days after demoulding. For drying shrinkage, specimens were stored in a chamber with controlled temperature and humidity conditions (24 ^{o}C $\pm$ 2 and 40 $\pm$ 5 RH) and measurements were taken at the ages of 10, 14, and 28 and 56 days after demoulding.

2.4 Experimental Results and Discussion

2.4.1 Fresh state properties

2.4.1.1 Workability

To assess the workability of rubberised concrete, most researchers (including the authors of this paper) use the slump test which appears to be a consistent and easy-to-apply method in practice [3, 7, 10, 11, 19]. Table 2.4 shows the slump results of all mixes as well as their corresponding slump classes, all of which fulfil the consistency requirements as described in pavement design standard BS EN 13877-1[54] and the normative reference BS EN 206-1 [55] either for fixed-form or slip-form (class S1) paving . The desired slump class was targeted to be at least S3 (slump ≥ 90 mm), by modifying the plasticiser dosage which was increased proportionally to the amount of rubber and steel fibres in each mix. All mixes achieved the targeted slump, however, the workability for mixes *60BF* and *60RF* was quite low (40 and 35 mm, respectively) although high amounts of plasticiser and superplasticiser were added (4 per m^3 and 5.1 per m^3 of concrete,

respectively). Nevertheless, this low workability did not raise any issues during handling, placing or finishing of the mixes due to the high rubber dosage (60%). No signs of segregation, bleeding or excessive "balling" were observed in any of the mixes.

Table 2.4 Fresh concrete properties for all concrete mixes

Mix No.	Mix ID	Extra plasticiser added L/m^3	Slump (mm)	Slump class	Air content %	Bulk density (kg/m^3)	Theoretical density (kg/m^3)
1	*0P*	0	240	S5	1.35	2406	2426
2	*0BF*	0	195	S4	1.5	2452	2454
3	*0RF*	0	195	S4	1.15	2447	2454
4	*20P*	0.25	200	S4	1.9	2258	2211
5	*20BF*	0.5	170	S4	3	2269	2239
6	*40P*	0.5	170	S4	3.15	2046	1996
7	*40BF*	1	130	S3	3.35	2086	2025
8	*60P*	1	150	S3	2.35	1869	1780
9	*60BF*	1.5	40	S1	3.35	1889	1811
10	*60RF*	1.5	35	S1	4.15	1884	1811

The results show that slump decreases with the addition of steel fibres, and further decreases with the inclusion of rubber, even though the amount of plasticiser was increased proportionally. By comparing the slump values of the control mix with the SFRC mixes without rubber (*0BF* and *0RF*), it can be seen that fibres caused a slump drop of 18.8% for both SFRC mixes. This decrease may be caused by increased friction between the RTSF, which have a large specific surface area, and the concrete constituents during mixing. Additionally, the tendency of steel fibres to agglomerate also has an adverse effect on workability.

The slump of the RuC mixes without steel fibres, *20P, 40P* and *60P*, also decreased by 16.6%, 29.1% and 37.5%, respectively, in comparison to the control mix. The surface shape and texture of rubber appear to have increased friction compared to conventional aggregates. Furthermore, fine impurities (i.e. rubber dust and fluff) on the rubber particles may also have reduced the free water in the fresh concrete mix.

The combined effects of both steel fibres and rubber on reducing the workability can be clearly seen from the slump values of SFRRuC mixes, *20BF, 40BF, 60BF* and *60RF,* where the slump significantly dropped by 29.1%, 45.8%, 83.3% and 85.4%, respectively, in comparison to the control mix.

2.4.1.2 Air content and unit weight

Air content has been shown to increase with the addition of fibres and/or rubber in concrete [56, 57] and a similar trend is observed in this study. As indicated in Table 2.4, the air content (entrapped air) in the concrete in general rises when increasing the rubber content, and further increases with the addition of fibres (except for mixes *0RF* and *60P* which can be considered outliers). The increase in the air content is possibly due to the rough and non-polar surface of rubber particles which tend to repel water and increase the amount of entrapped air in the mix. The large specific surface area of the fibres and their tendency to occasionally agglomerate can also contribute to increase air entrapment.

It was expected that the air content of the concrete mix with a blend of fibres (MSF and RTSF) would be less than the air content of the concrete mix with RTSF alone as the blend fibres mix has lower amount of fibres, hence lower specific surface area of fibres. However, as shown in Table 2.4, there is no clear trend in this respect and more work is needed before firm conclusions can be made.

From Table 2.4, it is clear that, as expected, the measured density of the concretes assessed significantly decreases with increasing rubber content. Although this was mainly due to the lower specific gravity of rubber particles (0.8) compared to the specific gravity of fine and coarse aggregates (2.65), density was also slightly affected by the increase in air content. On the other hand, the addition of steel fibres resulted in a marginal increase in the density (in both conventional and RuC) due to the higher specific gravity of steel fibres (7.8). The last column in Table 2.4 presents the theoretical density of each mix, assuming that there is no air content. A good correlation between the theoretical and experimental values is observed. The measured density values dropped by 148-215 kg/m^3 for each 20% addition of rubber replacement, whereas the theoretical decline was 215 kg/m^3. The difference between these two is attributed to air content and the assumed specific gravity value used for rubber (0.8), which might not be accurate for all rubber particles used, as tyres arise from various sources.

2.4.2 Compressive behaviour

The mean (average from three cubes and three cylinders, respectively) compressive strength and elastic modulus values are shown in Table 2.5. The modulus of elasticity values were obtained by using the secant modulus of the stress-strain curves (from 0 to 30% of the peak stress) similar to fib 2010 model code [58]. Standard deviation values are given in brackets below the mean values.

Table 2.5 Mechanical properties of all concrete mixes tested under compression

Mix ID	*0P*	*0BF*	*0RF*	*20P*	*20BF*	*40P*	*40BF*	*60P*	*60BF*	*60RF*
Age of testing (days)	30	30	31	31	32	32	33	33	34	34
Cube strength (MPa)	78.2 (4.5)	93.7 (3.5)	101.5 (2.9)	51.1 (1.5)	52.0 (3.0)	23.3 (0.2)	25.1 (1.6)	10.6 (0.5)	11.7 (1.4)	11.9 (0.2)
Cylinder strength (MPa)	68.9 (20.7)	78.8 (5.0)	94.8 (7.0)	33.1 (5.1)	33.9 (4.4)	10.8 (0.4)	16.5 (1.4)	7.6 (1.0)	8.2 (1.4)	7.8 (0.3)
Modulus of elasticity (GPa)	44.3 (4.0)	43.0 (1.2)	45.7 (1.2)	30.7 (5.1)	20.0 (0.0)	22.0 (5.3)	17.3 (1.5)	8.0 (0.0)	8.3 (1.5)	4.7 (1.2)

2.4.2.1 Cube strength

It can be observed that the addition of steel fibres in conventional concrete increases the compressive strength by 20% when a blend of MSF and RTSF (20 kg/m^3 and 20 kg/m^3) is used, and by 30% when only RTSF is used (40 kg/m^3). Steel fibres enhanced the compressive strength by controlling the tensile transverse strains developed, due to the Poisson effect during axial loading, thus delaying micro-crack coalescence and eventually unstable propagation that causes compression failure. RTSF are particularly effective in this respect, possibly due to their random geometry and better distribution in the mix due to their small diameters.

The replacement of fine and coarse aggregates with rubber particles had, as expected, a significant adverse effect on the compressive strength. The drop in the compressive strength, with respect to the control mix, was around 35%, 70% and 86% for mixes with 20%, 40% and 60% aggregate replacement, respectively. The reduction in compressive strength can be mainly attributed to the lower stiffness and higher Poisson ratio of rubber compared to conventional aggregates, and the weak bond between cement paste and rubber [20, 21]. Under axial load, rubber particles develop large lateral deformations (due to Poisson effect) which cause lateral tensile stresses and micro-cracks in the cement paste, thus accelerating the unstable propagation of cracks and causing failure at a lower load compared to conventional concrete. The differences in elastic characteristics and possibly poor bonding conditions between cement paste and rubber particles may also lead to uneven stress distribution in the concrete.

The addition of fibres into the RuC mixes did not have a significant effect on the compressive strength. Compared to the RuC mixes that had the same amount of rubber and did not contain fibres, the increase in the compressive strength as a result of the addition of MSF and/or RTSF

was 1.7% for *20BF*, 7.6% for *40BF*, 10% for *60BF* and 12% for *60RF*. This indicates that the compressive strength of the SFRRuC is dominated by the amount of rubber, while sensitivity to steel fibre content is very low.

2.4.2.2 Stress-strain characteristics

Figure 2.4 shows representative axial stress-strain curves (up to the peak stress) for selected tested cylinders. As there are considerable local strain variations and global bending issues, the cylinders that displayed better agreement between global and local axial strains and lower level of bending during loading were chosen. As pointed out by other researchers [11, 25], there is a very high variability in the recorded results, mainly due to large accidental bending, resulting from uneven bearing surfaces and/or due to the non-uniform distribution of the rubber particles in the concrete mass.

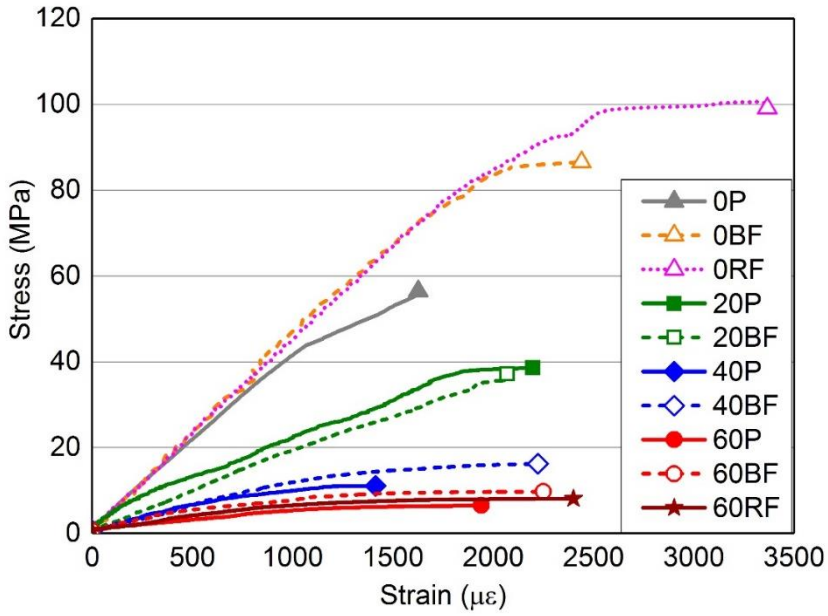

Figure 2.4: Stress-strain curves of the concrete assessed

It can be seen from Table 2.5 and Figure 2.4 that as the rubber content increases, the peak stress and the initial slope of the stress-strain curves substantially decreases. For the applications considered in this study (i.e. concrete pavements and slabs on grade), the loss in compression strength is not as important as the increase in deformability, provided that sufficient flexural strength is maintained.

Figure 2.5 shows that the modulus of elasticity of rubberised concretes (E_{RuC}) without fibre addition, normalised with respect to the control concrete mix (Ec_{ontrol}), reduces with an increased rubber content. Such reduction in stiffness can be attributed to the lower stiffness of

rubber particles (compared to conventional aggregates) and to the higher air content, as confirmed in section 2.4.1.2. An exponential curve is also shown to provide an equation for the estimation of modulus of elasticity. The reduction in elastic stiffness may be undesirable in some structural applications, but it can help develop new structural solutions, in particular at the soil structure interaction level.

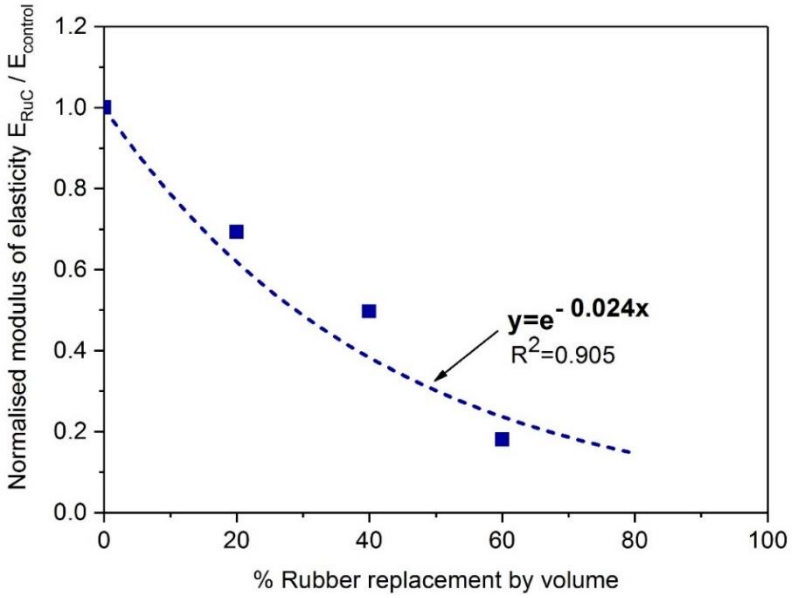

Figure 2.5: Correlation between the normalized modulus of elasticity of rubberised concretes as a function of rubber aggregate content

As shown in Table 2.5, the effect of steel fibres on compressive stiffness is not conclusive. However, steel fibres overall tend to increase the peak stress and corresponding strain (apart from mix *20BF*). This enhancement is expected due to the steel fibre ability to control the development of transverse deformations.

The addition of rubber and steel fibres had a more significant effect on the failure mode (Figure 2.6). Whilst the plain concrete specimens failed in a sudden and brittle manner, the RuC specimens failed in a much more ductile manner. This can be attributed to the relatively low elastic modulus of the rubber particles, which increases the deformation capacity before cracking, but also to the tensile resistance of rubber aggregates. The RuC specimens with steel fibres exhibited more (and thinner) vertical cracks at failure, compared to the ones without fibres. This suggests that ductility was also improved somewhat by adding fibres.

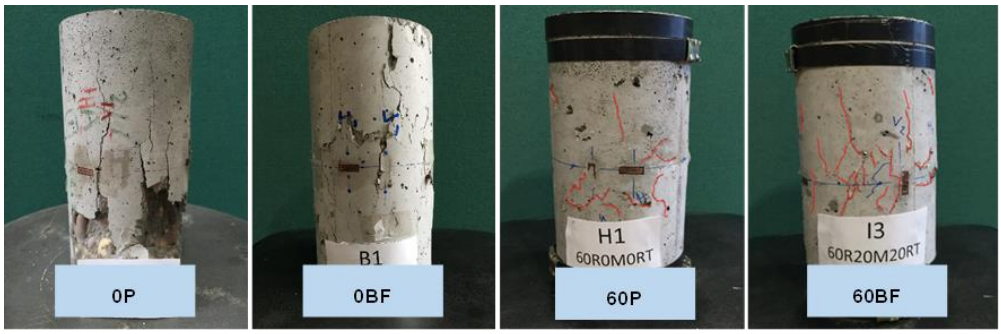

Figure 2.6: Typical compression failure of tested concrete cylinders

2.4.3 Flexural behaviour

The failure mode was the same for all specimens and a typical example is shown in Figure 2.7; a single crack initiated at the notch of the mid-span section and propagated vertically towards the compression zone.

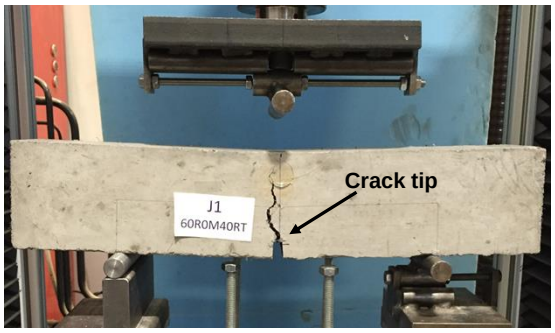

Figure 2.7: Photograph showing a typical flexural failure of the tested concrete prisms

The mean values (average of three prisms) of strain capacity, flexural strength and elastic modulus are shown in Table 2.6. The elastic theory was used to determine the flexural modulus of elasticity by using the secant modulus of the load-deflection curves (from 0 to 30% of the peak load).

Table 2.6 Mechanical properties of all concrete mixes tested in flexural

Mix ID	*0P*	*0BF*	*0RF*	*20P*	*20BF*	*40P*	*40BF*	*60P*	*60BF*	*60RF*
Age of testing (days)	60	60	61	61	62	62	63	63	64	64
Flexural strength (MPa)	7.3 (0.2)	9.2 (0.8)	9.5 (0.7)	5.6 (0.1)	6.9 (0.9)	3.7 (0.4)	6.6 (0.4)	2.6 (0.2)	5.5 (0.1)	4.2 (0.3)
Modulus of elasticity (GPa)	46.8 (2.1)	47.5 (1.0)	48.3 (3.34)	29.3 (2.31)	34.0 (3.1)	18.3 (2.6)	23.5 (5.9)	8.1 (1.6)	8.3 (1.1)	10.1 (2.5)
Strain capacity, δ_{fmax} (mm)	0.04 (0.01)	0.06 (0.02)	0.22 (0.07)	0.05 (0.01)	0.26 (0.32)	0.06 (0.01)	1.34 (0.21)	0.14 (0.03)	1.32 (0.74)	0.55 (0.36)

2.4.3.1 Flexural Strength

Flexural strength values are compared in Figure 2.8. The addition of steel fibres enhanced the flexural strength by 26% for *0BF* and 30% for *0RF*, with respect to the control mix. This improvement was anticipated as the steel fibres act as flexural reinforcement.

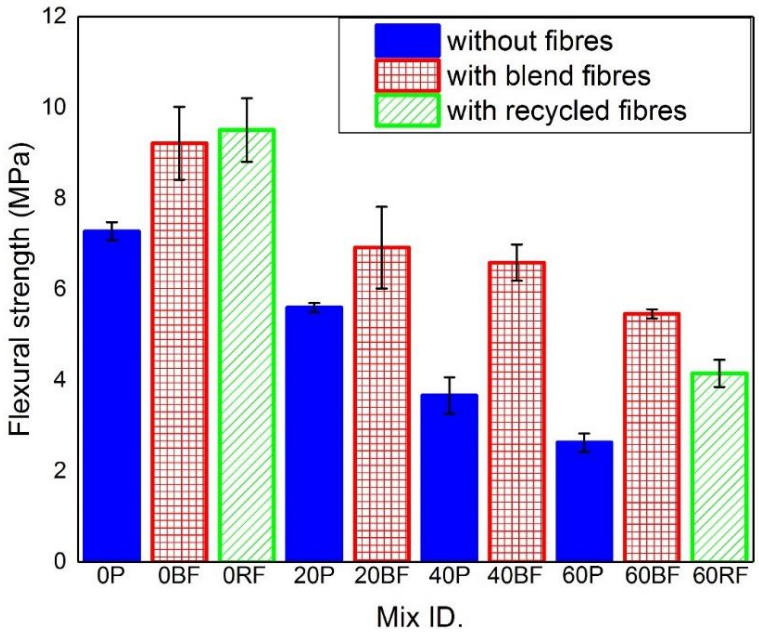

Figure 2.8: Flexural strength of the tested concrete mixes

Consistent with the reported by other authors [25, 36, 59], replacing the fine and coarse aggregates with rubber particles had an adverse effect on flexural strength. The flexural strength of the RuC mixes without fibres, *20P, 40P* and *60P,* was 23%, 49% and 64% lower than that of the conventional concrete, respectively. As for the compressive strength, the reduction in flexural strength may be attributed to the lack of good bonding conditions between the rubber particles and the cement paste, as well as the low stiffness and higher Poisson's ratio of rubber (nearly 0.5) compared to conventional aggregates [20, 21]. The high Poisson's ratio means that the rubber once in tension will contract faster than concrete in the lateral direction, facilitating loss of bond. The low stiffness also means that the rubber contributes very little in tension at the low strain at which the cement matrix cracks.

The addition of steel fibres in the RuC resulted in a substantial enhancement of its flexural strength, therefore mitigating the adverse effect of partially replaced natural aggregates by recycled rubber particles. By comparing the flexural strength of the SFRRuC mixes, *20BF, 40BF, 60BF* and *60RF,* with the flexural strength of the RuC mixes without fibres, *20P, 40P* and *60P*, it is noted that the flexural strength was increased by 23%, 78%, 111.5% and 61.5%, respectively.

Although the flexural strength gain of the *60RF* mix is not as high as the *60BF* mix, it still provides sufficient flexural strength for SFRRuC pavements and slabs on grade and can potentially lead to more sustainable solutions by eliminating the need for virgin materials.

Figure 2.9 shows the normalised compressive and flexural strength for all mixes, with respect to the control mix (concrete without fibres and/or rubber). It is clear that the loss in compressive strength as a result of the addition of rubber is more pronounced than the flexural strength loss. Even without the fibres, the loss in flexural resistance of the RuC is less than the loss in compressive strength; this indicates that the rubber is making a modest contribution to the tensile capacity of the concrete in tension. When fibres are added, the tensile resistance is further enhanced and hence, considerable flexural resistance is developed even when large volumes of rubber are present.

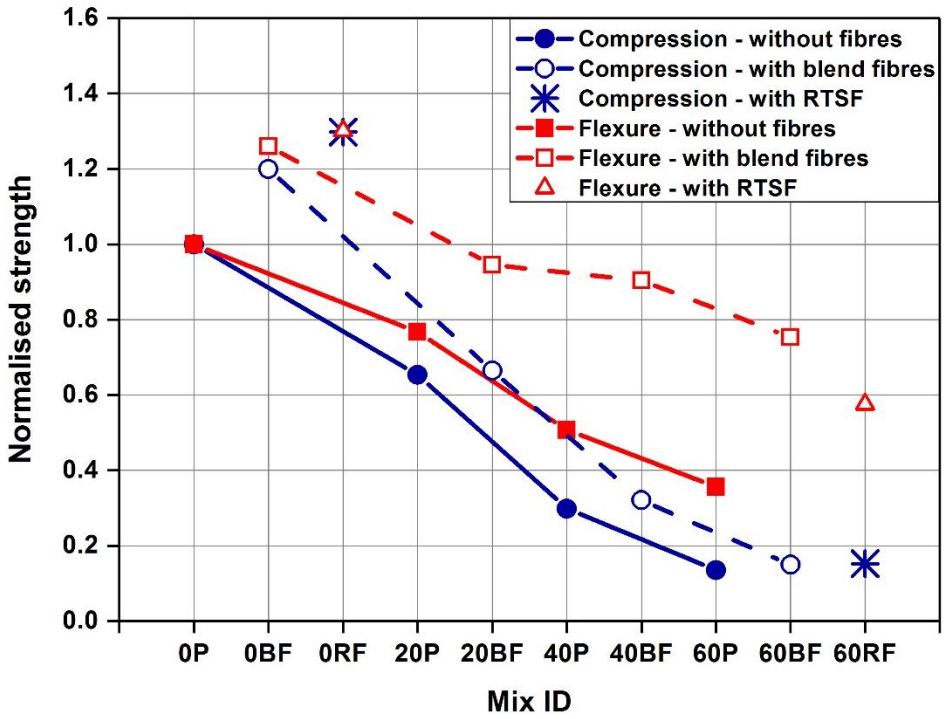

Figure 2.9: Normalised strength as a function of rubber volume in the concrete

2.4.3.2 Modulus of elasticity

The values obtained from the flexural tests are in general similar to those from the compressive tests. As expected, there is a small increase (up to 3%) in the elastic modulus when fibres are added. A significant reduction in the elastic modulus is also found for the RuC mixes, with the decrease being almost proportional to the amount of rubber content. In particular, the modulus of elasticity of the RuC mixes without fibres, *20P, 40P* and *60P*, was 37.4%, 60.9% and 82.7% lower than that of the control mix, respectively. The addition of steel fibres into RuC mixes recovered only marginally part of the modulus of elasticity loss. This confirms that, within the

elastic domain, the inclusion of rubber particles plays a dominant role on flexural stiffness, whereas the steel fibres make a minimal contribution.

2.4.3.3 Strain capacity

The flexural strain capacity was assessed by examining the stress-deflection curves. The deflection δ_{fmax} corresponding to the peak stress, fmax, is taken as a relevant indicator of strain capacity [33]. It is evident from Table 2.6 that the strain capacity is enhanced by the addition of fibres. For instance, the δ_{fmax} value for the control mix, *0P*, was 0.04 mm, while the δ_{fmax} values for *0BF* and *0RF* mixes were 0.06 and 0.22 mm, respectively. This enhancement can be explained by the bridging action of the fibres. The strain capacity of the RTSF mix, *0RF*, was higher than that of the blend fibres mix, *0BF*, possibly due to the larger number of RTSF fibres bridging the cracks.

The strain capacity also increases with higher rubber contents in the concrete. Compared to the control mix, *0P*, the δ_{fmax} of the RuC mixes was increased by 25%, 50% and 250% for *20P, 40P* and *60P*, respectively. Turatsinze et al. [33] explained such behaviour by the ability of rubber particles to reduce stress concentration at the crack tip, thus delaying the coalescence and propagation of micro-cracks. Mixes with steel fibres and rubber developed the highest strain capacity values, indicating a synergy between rubber and steel fibres in enhancing strain capacity.

2.4.3.4 Residual flexural strength and energy absorption behaviour

The load versus deflection curves shown in Figure 2.10 confirm that the post-peak branches of the SFRC prisms without rubber were significantly enhanced as a result of the inclusion of fibres. The fibres continue bridging the cracks and resisting their opening even after the peak load, dissipating energy through the pull-out mechanism.

Although rubber particles had an adverse effect on the flexural strength of the concrete prisms, they improved slightly the post-peak energy absorption. This enhancement can be explained by the ability of the rubber particles to undergo large deformation in tension and promote high energy absorption. As a result of the interlocking and friction at fibre–matrix and fibre-rubber interfaces, steel fibres substantially enhanced the post-peak energy absorption and dissipation of RuC mixes, which at large displacements show higher flexural capacity than the specimens without rubber.

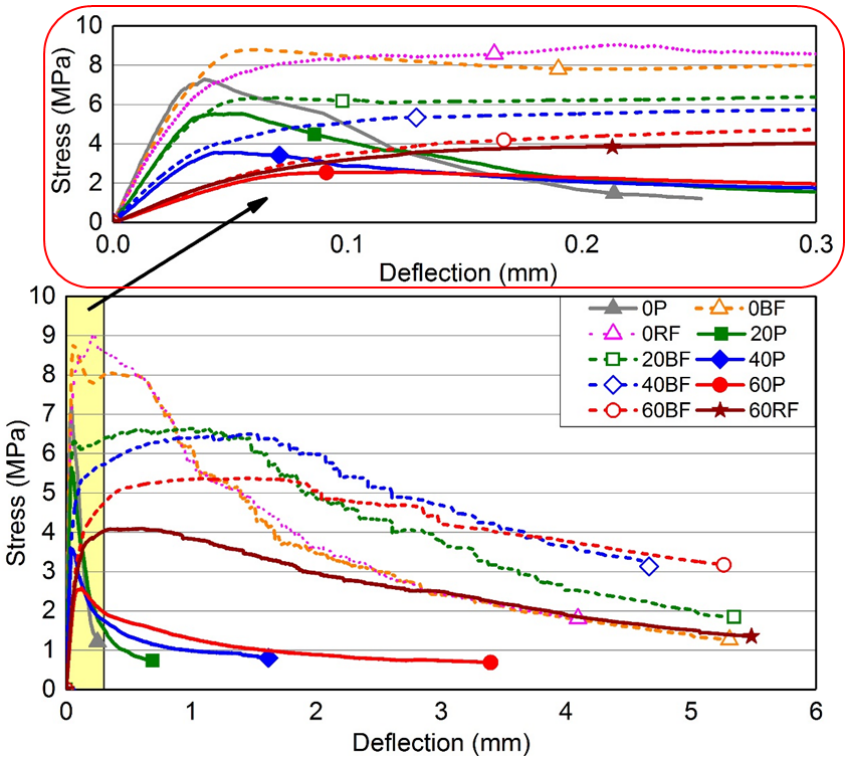

Figure 2.10: Average stress versus deflection curves for all concrete mixes studied

As expected, concrete prisms with a blend of fibres (MSF and RTSF) show superior post-peak energy absorption behaviour than those with RTSF alone. RTSF are overall better distributed and in general help control micro-cracks, while MSF are better at controlling cracks once they open and develop. Though the difference in performance is not obvious for normal concrete in Figure 2.10, this is well demonstrated at 60% rubber content when the *60BF* controls the cracks much better than *60RF*. In another study [43], the mixes with blend fibres are shown to outperform both the RTSF and MSF only mixes.

To further examine the post-peak energy absorption behaviour of the mixes, the residual flexural strength (f_{Ri}) and the characteristic residual flexural strength values ($f_{Ri,c}$) were obtained (see Table 2.7) at given intervals of CMOD (0.5, 1.5, 2.5, 3.5) according to RILEM recommendation [52]. The residual flexural strength can be considered a measure of toughness or even ductility of the SFRC mixes. Higher values of $f_{R,i}$ mean higher post-cracking load carrying capacity and higher ductility. The characteristic residual flexural strength $f_{Ri,c}$ accounts for the variability of the residual flexural strength results. SFRRuC mixes showed a lower rate of reduction in residual strength than FRC mixes. This may be attributed to the presence of rubber particles that prolong the crack path and increase the contact area of the failure surface with the rubber particles, which make some contribution to the tensile strength, but also enable the steel fibres to engage better across the crack.

Table 2.7 Residual and characteristic flexural strength values of concrete assessed

Mix No.	Mix ID	f_{Ri} (MPa)				$f_{Ri,c}$ (MPa)				fib (2010) classification	
		f_{R1}	f_{R2}	f_{R3}	f_{R4}	$f_{R1,c}$	$f_{R2,c}$	$f_{R3,c}$	$f_{R4,c}$	$f_{R3,c}/f_{R1,c}$	Class
1	*0P*	-	-	-	-	-	-	-	-	-	-
2	*0BF*	8.1	5.3	3.5	2.7	6.1	3.5	2.4	1.2	0.39	- (< 0.5)
3	*0RF*	8.4	5.2	3.7	2.8	8.3	4.7	2.9	1.8	0.35	- (< 0.5)
4	*20P*	-	-	-	-	-	-	-	-	-	-
5	*20BF*	6.5	6.6	5.4	4.3	4.4	4.9	3.3	2.3	0.75	4.4*b*
6	*40P*	-	-	-	-	-	-	-	-	-	-
7	*40BF*	5.9	6.4	6.4	5.4	4.9	5.8	5.6	4.6	1.14	4.9*d*
8	*60P*	-	-	-	-	-	-	-	-	-	-
9	*60BF*	5.1	5.4	5.3	4.7	4.4	5.2	5.1	3.8	1.16	4.4*d*
10	*60RF*	4.1	3.7	3.1	2.6	3.6	3.2	2.8	2.6	0.78	3.6*b*

* ***a*** if $0.5 < f_{R3,c}/f_{R1,c} < 0.7$; ***b*** if $0.7 \leq f_{R3,c}/f_{R1,c} \leq 0.9$; ***c*** if $0.9 \leq f_{R3,c}/f_{R1,c} \leq 1.1$;***d*** if $1.1 \leq f_{R3,c}/f_{R1,c} \leq 3$;e if $1.3 \leq f_{R3,c}/f_{R1,c}$

According to fib model code [58] for structural applications with normal and high-strength concrete, SFRC can be classified according to the post-cracking residual strength (considering the value of $f_{R1,c}$), and the ratio $f_{R3,c}/f_{R1,c}$. The higher the value of $f_{R1,c}$ and/or the ratio $f_{R3,c}/f_{R1,c}$, the higher the class. As observed in Table 2.7 mixes *40BF* and *60BF* show the best overall performance among all mixes, whereas SFRC mixes (without rubber) can not be classified as their $f_{R3,c}/f_{R1,c}$ ratio is less than 0.5. Nevertheless, all SFRC mixes (conventional and rubberised) fulfilled the requirements of EN 14889-1 [60] – 1.5 MPa at 0.5 mm CMOD and 1.0 MPa at 3.5 mm CMOD – and could be used for practical applications.

The aim of this study is to develop a more flexible Portland cement concrete pavement. However, as flexible pavement standards/specifications relate to asphalt concrete, it is not possible to use them for a direct comparison, though the flexural performance of SFRRuC is far superior to that of asphalt concrete. Hence, SFRRuC pavements, though flexible, should comply with standards/specifications for rigid pavements. The major issue here is that the rigid pavement standards relay on the compressive and flexural strengths. Though all SFRRuC mixes studied here meet the flexural strength characteristics, as described in pavement design standard BS EN 13877-1[54], not all of them can meet the compressive requirements. However, provided that durability requirements are met, this should not be a big issue but would require modification on the standard.

2.4.4 Free shrinkage behaviour

Typical curves of total shrinkage versus time are shown in Figure 2.11. The vertical dotted line shown at 8 days indicates the start of drying shrinkage. The values predicted according to Eurocode 2 [61] for conventional concrete (accounting for temperature and humidity) are also included for comparison.

Both conventional concrete and SFRC mixes show lower autogenous and drying shrinkage strains than those predicted by Eurocode 2 (EC2). The difference between predicted and actual values for these mixes can be attributed to the presence of high quantities of silica fume and fly ash, not accounted for in the Eurocode 2 equation. It is also clear that the addition of rubber increases the overall shrinkage strains at 57 days by 15.5% for *20P*, 59% for *40P* and 127% for *60P*. This increase in free shrinkage strain with increasing rubber content is due to the lower stiffness of rubber particles compared to conventional aggregates, which reduces the overall internal restrain. The higher porosity and diffusivity of rubberised concrete prims can also contribute to increasing the rate of moisture loss and accelerating drying shrinkage.

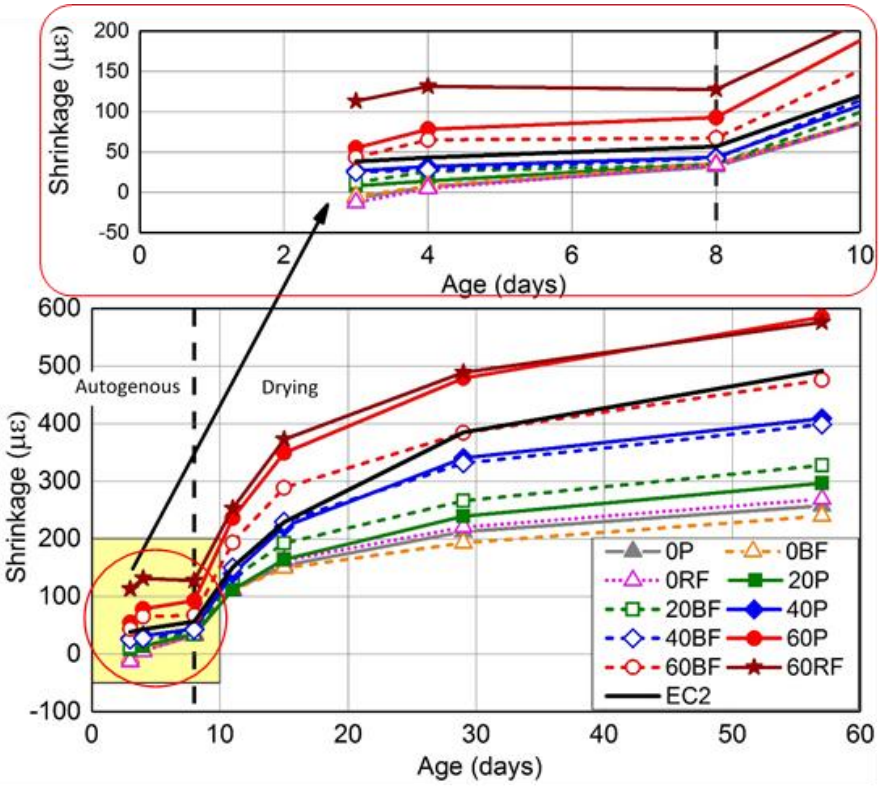

Figure 2.11: Total free shrinkage for all concrete mixes

2.5 Conclusions

This study assessed the fresh state and mechanical properties of steel-fibre reinforced rubberised concretes (SFRRuC), in which waste tyre rubber partially replaced aggregates, and blends of manufactured and recycled tyre steel fibres were used as reinforcement. Based on the experimental results, the following conclusions can be drawn:

- The replacement of conventional aggregates with rubber particles reduces workability and unit weight, and increases air content of the fresh concrete mixes. Steel fibres further lower workability and increase air content, whilst marginally increasing unit weight.
- The mechanical properties (compressive and flexural strength, as well as the modulus of elasticity) decrease with increasing rubber content. Steel fibres in appropriate amounts (up to 40 kg/m^3) enhance the mechanical properties of conventional concrete (up to 30% compressive strength) and provide modest increases in the modulus of elasticity.
- Free shrinkage strain increases with increasing rubber content as a result of the lower stiffness of rubber particles.
- In rubberised concrete, the addition of steel fibre reinforcement mitigates the loss in flexural strength (from 50% to 9.6% loss, compared to conventional concrete) and slightly improves compressive strength and modulus of elasticity (up to 12.5% and 28.4%, respectively), hence, they are an important component when RuC is to be used for structural purposes.
- Concrete strain capacity and post-peak energy absorption behaviour are enhanced by the addition of fibres and are further improved by the inclusion of rubber, completely transforming the flexural performance of RuC and enabling it to resist structural loads.
- A high performance (class d according to fib 2010 model code [58]) and highly flexible steel fibre reinforce rubberised concrete can be produced with 60% rubber content and blended fibres (20 kg/m^3 of MSF and 20 kg/m^3 of RTSF), suitable for pavement applications.

It is concluded that SFRRuC is a promising candidate material for use in structural concrete applications with increased toughness and flexibility requirements, such as road pavements and slabs on grade. Future work should be directed towards investigating the long-term performance of this innovative concrete in aggressive environments.

Acknowledgements

The research leading to these results has received funding from the European 393 Union Seventh Framework 394 Programme [FP7/2007- 2013] under grant agreement n° 603722. The authors would also like to thank all of the material suppliers and companies for their in-kind contribution of materials for this research study: Tarmac UK, Sika, Aggregate Industries UK Ltd and Twincon Ltd. The first author PhD studies are sponsored by King Saud University and Ministry of Education in the Kingdom of Saudi Arabia.

2.6 References

[1] ETRA, *The European Tyre Recycling Association*, 2016, Available at: http://www.etra-eu.org [Last accessed: 02/01/2018].

[2] Council of the European Union, *Council Directive 1999/31/EC of 26 April 1999 on the landfill of waste*, 1999.

[3] N.N. Eldin and A.B. Senouci, *Measurement and prediction of the strength of rubberized concrete,* Cement and Concrete Composites 16 (4) (1994) 287–298.

[4] A. Benazzouk, O. Douzane, K. Mezreb, B. Laidoudi, and M. Queneudec, *Thermal conductivity of cement composites containing rubber waste particles: Experimental study and modelling,* Construction and Building Materials 22 (4) (2008) 573–579.

[5] B.S. Mohammed, K.M.A. Hossain, J.T.E. Swee, G. Wong, and M. Abdullahi, *Properties of crumb rubber hollow concrete block,* Journal of Cleaner Production 23 (1) (2012) 57–67.

[6] Council of the European Union, *Council Directive 2008/98/EC on waste (Waste Framework Directive)*, 2008.

[7] M. Bravo and J. de Brito, *Concrete made with used tyre aggregate: durability-related performance,* Journal of Cleaner Production 25 (2012) 42–50.

[8] B.S. Thomas and R.C. Gupta, *A comprehensive review on the applications of waste tire rubber in cement concrete,* Renewable and Sustainable Energy Reviews 54 (2016) 1323-1333.

[9] K.S. Son, I. Hajirasouliha, and K. Pilakoutas, *Strength and deformability of waste tyre rubber-filled reinforced concrete columns,* Construction and Building Mateials 25 (1) (2011) 218-226.

[10] O. Youssf, M.A. ElGawady, J.E. Mills, and X. Ma, *An experimental investigation of crumb rubber concrete confined by fibre reinforced polymer tubes,* Construction and Building Materials 53 (2014) 522-532.

[11] S. Raffoul, R. Garcia, K. Pilakoutas, M. Guadagnini, and N.F. Medina, *Optimisation of rubberised concrete with high rubber content: An experimental investigation,* Construction and Building Materials 124 (2016) 391–404.

[12] D. Bompa, A. Elghazouli, B. Xu, P. Stafford, and A. Ruiz-Teran, *Experimental assessment and constitutive modelling of rubberised concrete materials,* Construction and Building Materials 137 (2017) 246–260.

[13] A. Grinys, H. Sivilevičius, D. Pupeikis, and E. Ivanauskas, *Fracture of concrete containing crumb rubber,* Journal of Civil Engineering and Management 19 (3) (2013) 447-455.

[14] F. Liu, W. Zheng, L. Li, W. Feng, and G. Ning, *Mechanical and fatigue performance of rubber concrete,* Construction and Building Materials 47 (2013) 711–719.

[15] P. Sukontasukkul and C. Chaikaew, *Properties of concrete pedestrian block mixed with crumb rubber,* Construction and Building Materials 20 (7) (2006) 450–457.

[16] T.C. Ling, H.M. Nor, and S.K. Lim, *Using recycled waste tyres in concrete paving blocks,* Proceedings of the ICE - Waste and Resource Management 163 (1) (2010) 37–45.

[17] C.A. Issa and G. Salem, *Utilization of recycled crumb rubber as fine aggregates in concrete mix design,* Construction and Building Materials 42 (2013) 48–52.

[18] E. Güneyisi, M. Gesoglu, N. Naji, and S. İpek, *Evaluation of the rheological behavior of fresh self-compacting rubberized concrete by using the Herschel–Bulkley and modified Bingham models,* Archives of Civil and Mechanical Engineering 16 (1) (2016) 9–19.

[19] D. Flores-Medina, N.F. Medina, and F. Hernández-Olivares, *Static mechanical properties of waste rests of recycled rubber and high quality recycled rubber from crumbed tyres used as aggregate in dry consistency concretes,* Materials and Structures 47 (7) (2014) 1185–1193.

[20] Z. Khatib and F. Bayomy, *Rubberized portland cement concrete,* Journal of Materials in Civil Engineering 11 (3) (1999) 206–213.

[21] A.R. Khaloo, M. Dehestani, and P. Rahmatabadi, *Mechanical properties of concrete containing a high volume of tire–rubber particles,* Waste Management (Oxford) 28 (12) (2008) 2472-2482.

[22] A.E. Richardson, K. Coventry, and G. Ward, *Freeze/thaw protection of concrete with optimum rubber crumb content,* Journal of Cleaner Production 23 (1) (2012) 96–103.

[23] M. Batayneh, I. Marie, and I. Asi, *Promoting the use of crumb rubber concrete in developing countries,* Waste Management (Oxford) 28 (11) (2008) 2171–2176.

[24] M.C. Bignozzi and F. Sandrolini, *Tyre rubber waste recycling in self-compacting concrete,* Cement and Concrete Research 36 (4) (2006) 735–739.

[25] E. Ganjian, M. Khorami, and A.A. Maghsoudi, *Scrap-tyre-rubber replacement for aggregate and filler in concrete,* Construction and Building Materials 23 (5) (2009) 1828-1836.

[26] USFD, *Thin wire reinforcement for concrete'.* B.P. Application (2001), Editor, UK.

[27] K. Pilakoutas, K. Neocleous, and H. Tlemat, *Reuse of tyre steel fibres as concrete reinforcement,* Proceedings of the ICE-Engineering Sustainability 157 (3) (2004) 131-138. ISSN 1478-4629.

[28] K. Neocleous, H. Angelakopoulos, K. Pilakoutas, and M. Guadagnini, *Fibre-reinforced roller-compacted concrete transport pavements,* Proceedings of the ICE-Transport 164 (TR2) (2011) 97–109.

[29] H. Tlemat, K. Pilakoutas, and K. Neocleous, *Stress-strain characteristic of SFRC using recycled fibres,* Materials and Structures 39 (3) (2006) 365–377.

[30] H. Angelakopoulos, K. Neocleous, and K. Pilakoutas, *Steel fibre reinforced roller compacted concrete pavements,* Challenges for Civil Construction (2008) 16–18.

[31] M.A. Aiello, F. Leuzzi, G. Centonze, and A. Maffezzoli, *Use of steel fibres recovered from waste tyres as reinforcement in concrete: Pull-out behaviour, compressive and flexural strength,* Waste Management 29 (6) (2009) 1960–1970.

[32] A.G. Graeff, K. Pilakoutas, K. Neocleous, and M.V.N. Peres, *Fatigue resistance and cracking mechanism of concrete pavements reinforced with recycled steel fibres recovered from post-consumer tyres,* Engineering Structures 45 (2012) 385–395.

[33] A. Turatsinze, J.L. Granju, and S. Bonnet, *Positive synergy between steel-fibres and rubber aggregates: Effect on the resistance of cement-based mortars to shrinkage cracking,* Cement and Concrete Research 36 (9) (2006) 1692–1697.

[34] T. Nguyen, A. Toumi, and A. Turatsinze, *Mechanical properties of steel fibre reinforced and rubberised cement-based mortars,* Materials and Design 31 (1) (2010) 641–647.

[35] N. Ganesan, J.B. Raj, and A. Shashikala, *Flexural fatigue behavior of self compacting rubberized concrete,* Construction and Building Materials 44 (2013) 7–14.

[36] J.-h. Xie, Y.-c. Guo, L.-s. Liu, and Z.-h. Xie, *Compressive and flexural behaviours of a new steel-fibre-reinforced recycled aggregate concrete with crumb rubber,* Construction and Building Materials 79 (2015) 263–272.

[37] N.F. Medina, D.F. Medina, F. Hernández-Olivares, and M. Navacerrada, *Mechanical and thermal properties of concrete incorporating rubber and fibres from tyre recycling,* Construction and Building Materials 144 (2017) 563–573.

[38] BSI, EN 197-1*, Cement — Part 1: Composition, specifications and conformity criteria for common cements,* BSI 389 Chiswick High Road, London W4 4AL, UK, 2011.

[39] ASTM, C136*, Standard test method for sieve analysis of fine and coarse aggregates* 10.1520/C0136-06, ASTM International, West Conshohocken, PA, 2006.

[40] BSI, EN 1097-6*, Tests for mechanical and physical properties of aggregates, Determination of particle density and water absorption,* BSI 389 Chiswick High Road, London W4 4AL, UK, 2013.

[41] BSI, EN 1097-3*, Tests for mechanical and physical properties of aggregates, Determination of loose bulk density and voids,* BSI 389 Chiswick High Road, London W4 4AL, UK, 1998.

[42] BSI, EN 933-3*, Tests for geometrical properties of aggregates, Determination of particle shape – Flakiness index,* BSI 389 Chiswick High Road, London W4 4AL, UK, 2012.

[43] H. Hu, P. Papastergiou, H. Angelakopoulos, M. Guadagnini, and K. Pilakoutas, *Mechanical properties of SFRC using blended manufactured and recycled tyre steel fibres,* Construction and Building Materials 163 (2018) 376–389.

[44] BSI, EN 12350-2*, Testing fresh concrete, Part 2: Slump-test,* BSI 389 Chiswick High Road, London W4 4AL, UK, 2009.

[45] BSI, *EN 12350-7, Testing fresh concrete, Part 7: Air content — Pressure,* BSI 389 Chiswick High Road, London W4 4AL, UK, 2009.

[46] BSI, EN 12350-6*, Testing fresh concrete Part 6: Density,* BSI 389 Chiswick High Road, London W4 4AL, UK, 2009.

[47] BSI, EN 12390-2*, Testing hardened concrete, Part 2: Making and curing specimens for strength tests,* BSI 389 Chiswick High Road, London W4 4AL, UK, 2009.

[48] BSI, EN 14651:+A1:2007*, Test method for metallic fibre concrete — Measuring the flexural tensile strength (limit of proportionality (LOP), residual) ICS 91.100.30,* BSI 389 Chiswick High Road, London W4 4AL, UK, 200.

[49] BSI, EN 12390-3*, Testing hardened concrete, Part3: Compressive strength of test specimens,* BSI 389 Chiswick High Road, London W4 4AL, UK, 2009.

[50] R. Garcia, K. Pilakoutas, I. Hajirasouliha, M. Guadagnini, N. Kyriakides, and M.A. Ciupala, *Seismic retrofitting of RC buildings using CFRP and post-tensioned metal straps: shake table tests,* Bulletin of Earthquake Engineering (2015) 1-27.

[51] JCI, SF-4*, Method of test for flexural strength and flexural toughness of steel fiber reinforced concrete,* Japan Concrete Institute, Tokio, Japan, 1984.

[52] RILEM, TC 162-TDF*, Test and design methods for steel fibre reinforced concrete, Bending test,* Final Reccomendation, Materials and Structures 35 (2002) 579–582.

[53] BSI, EN 12617-4*, Products and systems for the protection and repair of concrete structures — Test methods —Part 4: Determination of shrinkage and expansion,* BSI 389 Chiswick High Road, London W4 4AL, UK, 2002.

[54] BSI, EN 13877-1*, Concrete pavements Part 1: Materials,* BSI 389 Chiswick High Road London W4 4AL, UK, 2013.

[55] BSI, EN 206-1*, Concrete —Part 1: Specification, performance,production and conformity,* BSI 389 Chiswick High Road London W4 4AL, UK, 2000.

[56] R. Siddique and T.R. Naik, *Properties of concrete containing scrap-tire rubber–an overview,* Waste Management (Oxford) 24 (6) (2004) 563–569.

[57] O.A. Abaza and Z.S. Hussein, *Flexural behavior of steel fiber-reinforced rubberized concrete,* Journal of Materials in Civil Engineering 28 (1) (2015) 04015076.

[58] fib, *Model Code for Concrete Structures 2010,* Federal Institute of Technology Lausanne–EPFL, Section Génie Civil, Swizerland, 2010 p.146.

[59] M.A. Aiello and F. Leuzzi. *Waste tyre rubberized concrete: properties at fresh and hardened state.* Waste Management 30 (8–9) (2010) 1696–1704.

[60] BSI, EN 14889-1*, Fibres for concrete — Part 1: Steel fibres — Definitions, specifications and conformity,* BSI 389 Chiswick High Road, London W4 4AL, UK, 2006.

[61] BSI, EN 1992-1-1*, Eurocode 2: Design of concrete structures — Part 1-1: General rules and rules for buildings,* BSI 389 Chiswick High Road, London W4 4AL, UK, 2004.

Chapter 3

Durability of Steel Fibre Reinforced Rubberised Concrete (SFRRuC) Exposed to Chlorides

A. Alsaif, S.A. Bernal, M. Guadagnini, and K. Pilakoutas. Durability of steel fibre reinforced rubberised concrete Exposed to chloride. Construction and Building Materials 188 (2018) 130-142.

Author contribution statement

Dr Bernal, Dr Guadagnini and Prof. Pilakoutas supervised the PhD study of the first author. All authors discussed the results and commented on the manuscript.

This study assesses the durability and transport properties of low water/binder ratio (0.35) steel fibre reinforced rubberised concrete (SFRRuC) mixes, which are proposed to be used as flexible concrete pavements. Waste tyre rubber is incorporated in concrete as fine and coarse aggregate replacement and blends of manufactured steel fibres and recycled tyre steel fibres are used as internal reinforcement. The fresh, mechanical and transport properties of plain concrete are compared with those of SFRRuC mixes having different substitutions of rubber aggregates (0, 30 and 60% by volume). The chloride corrosion effects due to exposure to a simulated accelerated marine environment (intermittent wet-dry cycles in 3% NaCl solution) is also evaluated. The results show that, although water permeability (e.g. volume of permeable voids and sorptivity) and chloride ingress increase with rubber content, this increase is minor and water and chlorides permeability are generally within the range of highly durable concrete mixes. No visual signs of deterioration or cracking (except superficial rust) were observed on the surface of the concrete specimens subjected to 150 or 300 days of accelerated chloride corrosion exposure and a slight increase in the mechanical properties is observed. This study shows that the examined low water/binder SFRRuC mixes promote good durability characteristics, making these composite materials suitable for flexible concrete pavement applications.

This chapter consists of a "stand alone" journal paper and contains a relevant bibliography at the end of the chapter. Appendix B provides additional information and further test results.

3.1 Introduction

Several factors are considered when designing road pavements including traffic loading, sub-grade status, environmental conditions, as well as cost and availability of construction materials. Two different systems of pavements are conventionally used in roads construction: flexible asphalt or rigid concrete. A flexible pavement typically consists of a series of layers and its design is based on distributing the load through the component layers. On the other hand, a rigid pavement typically consists of one Portland cement concrete structural layer and its design is based on the flexural resistance of this layer. Flexible asphalt pavements have low stiffness and as such they can better accommodate deformations arising from temperature changes, loads and soil movements, however, lack the durability resistance of rigid concrete pavements which are longer lasting [1]. It is therefore desirable to develop a pavement system with comparable flexibility to asphalt pavement, and ability to withstand higher stresses as well as environmental attack during its service life. One attractive alternative proposed by the authors is concrete pavements that include high amounts of recycled rubber particles (chips and/or crumbs), as a partial replacement of natural aggregates, and recycled steel fibre reinforcement. These composite concretes, referred to as steel fibre reinforced rubberised concretes (SFRRuC), can be designed to have high flexibility similar to asphalt and flexural strengths similar to steel fibre reinforced concrete (SFRC) [1].

Over the past two decades, research interest in the potential use of waste tyre rubber (WTR) as partial replacement of natural aggregates in the production of concretes (rubberised concretes – RuC) has steadily grown [2-6]. RuC present reduced workability and increased air content, compared to conventional concretes, as a result of the rough surface texture of the rubber particles [4, 7-9]. Though RuC can show higher ductility and increased toughness compared to conventional concrete [8-10], this is at the expense of loss in strength and stiffness [11, 12]. Different strategies to improve the mechanical performance of RuC have been investigated in recent years, including the addition of supplementary cementitious materials to the binder mix to reduce the porosity and aid early age strength development. For example, Raffoul et al. [9] observed a 40% enhancement in the compressive strength of RuC when 20 wt.% of cement was replaced with equal amount of silica fume and fly ash. This enhancement was attributed to the better particle packing and cohesion of the concrete mix as a result of the reactivity of these materials and the consequent pozzolanic reaction.

The addition of fibres to RuC can enhance the mechanical performance of these composite concretes. Xie et al. [13] reported that the inclusion of manufactured steel fibres (MSF) in RuC,

mitigated the reduction in compressive strength while increasing residual flexural strength. Similar outcomes were reported in other studies by the authors [1, 2] where SFRRuC presented better mechanical properties than plain RuC. Although the fresh and mechanical properties of RuC and SFRRuC have been studied by several researchers, there is still a dearth of data in this field, especially when rubber aggregates are incorporated in the large volumes (exceeding 20% replacement by volume of total natural aggregates). It should be noted that, large volumes of rubber aggregates replacements in concrete are necessary to attain flexibility in concrete pavements.

Few studies examined the durability and transport properties of RuC, with notable discrepancies being reported on the effect of rubber particles on long-term performance. Water permeability and water absorption by immersion generally increase with rubber content [14-16]. This has been attributed to the additional water required in RuC mixes to maintain workability, and the high void volumes between rubber particles and cement paste due to the hydrophobicity of rubber. Conversely, several researchers have observed a reduction in water absorption of RuC (up to 12.5% rubber for fine aggregates) using the method of immersion and related this behaviour to the impervious nature of rubber particles. Benazzouk et al. [17] reports that the addition of rubber crumbs of up to 40% volume in cement pastes reduced sorptivity, hydraulic diffusivity and air permeability. Similar observations are reported by Segre and Joekes [18] who also attributed this behaviour to the hydrophobic nature of rubber. The transport properties of these composite concretes are strongly dependent on the distinctive features of the starting concrete matrix, whose performance can significantly vary as a function of mix design, age and curing conditions, among other factors, which explains the variability in results obtained from different investigations.

In a recent study, the authors [1] studied the mechanical properties of SFRRuC mixes in which fine and coarse aggregates were partially replaced with rubber (0%, 20%, 40% or 60% replacement by volume), and different types of steel fibres (MSF and/or recycled tyre steel fibres- RTSF) added in volumes of up to 40 kg/m^3. In addition to the increased toughness and flexibility attained, it was observed that all the examined SFRRuC mixes were able to achieve flexural strengths that meet the flexural strength limits prescribed in pavement design EN 13877-1 [19]. Concrete pavement slabs, however, are susceptible to several deteriorative processes that can be caused by the ingress of aggressive substances into concrete, such as corrosion due to attack by chlorides or carbonation. The rate of transport of aggressive agents is related to a large degree to the concrete's degree of saturation and air permeability [17].

Aggressive substances such as chlorides can also penetrate into concrete due to diffusion and capillary action.

The chloride permeability in RuC remains largely unknown and studies examining this [20, 21] reveal increased chloride permeability with rubber content, which can be significantly reduced with the addition of fly ash and/or silicate fume. This is consistent with the reduced water absorption and permeability achieved in concretes with these additions [15, 20]. To date, there are very few studies on the transport and durability properties of RuC with large volumes of rubber replacement [7, 22, 23], while the transport and durability properties of SFRRuC has not been studied yet. Furthermore, there is limited understanding on the mechanism governing chloride-induced corrosion of steel fibres in RuC and its potential effect on long-term performance. However, there is a good consensus that the main factors controlling durability of SFRC, when exposed to chlorides, include: (i) the age and the exposure conditions, (ii) the steel fibre type and size, (iii) the concrete matrix quality and (iv) the presence of cracks [24]. Consequently, it is important to understand the transport and durability properties of SFRRuC before using it in flexible concrete pavements.

In this study, the fresh state, mechanical strength, and transport properties of SFRC, and SFRRuC are investigated and compared. The fresh properties assessed include workability, air content and fresh density. The mechanical performance is examined in terms of compressive strength and flexural behaviour including flexural strength, elastic modulus and residual flexural strength. The transport properties examined are volume of permeable voids, gas permeability, sorptivity and chloride penetrability (chloride ion penetration depth and diffusion). The chloride corrosion effects due to exposure to a simulated accelerated marine environment (intermittent wet-dry cycles in 3% NaCl solution) are also evaluated.

3.2 Experimental Programme

3.2.1 Materials and mix designs

3.2.1.1 Materials

A Portland limestone cement CEM II-52.5 N, in compliance with EN 197-1 [25] and containing 80-94% Portland cement clinker, 10 –15% limestone and 0-5% minor additional constituents, was adopted as the primary binder in this study. Silica fume (SF) and fuel ash (FA) were also used (10 wt.% for each) to improve particle packing (or filling) in the mixture [9] as well as to reduce permeability and enhance concrete strength. Two types of high range water reducer HRWR

admixtures, plasticiser and superplasticiser, were also added to achieve the desired workability. A water/binder (Portland cements + silica fume + fly ash) ratio of 0.35 was used in all mixes.

The coarse aggregates were river gravel with particle sizes of 5/10 mm and 10/20 mm, specific gravity (SG) of 2.65 and water absorption (A) of 1.2%. The fine aggregates were river sand with particles sizes of 0/5 mm, SG of 2.64 and A of 0.5%.

The rubber aggregates were recovered by the mechanical shredding of vehicular tyres. Rubber particles were sourced in the following size ranges: 0/0.5 mm, 0.5/2 mm and 2/6 mm, 5/10 mm, and 10/20 mm. A relative density of 0.8 (measured using a representative volume of rubber) was used for the rubber to determine the appropriate replacement by volume. Figure 3.1 shows the particles size distribution for the used natural (N) and rubber (R) aggregates, obtained according to ASTM C136 [26].

A blend of two different types of steel fibres were used: 1) undulated MSF, and b) cleaned and screened recycled tyre steel fibres (RTSF). The physical and mechanical properties of both types of steel fibre are shown in Table 3.1.

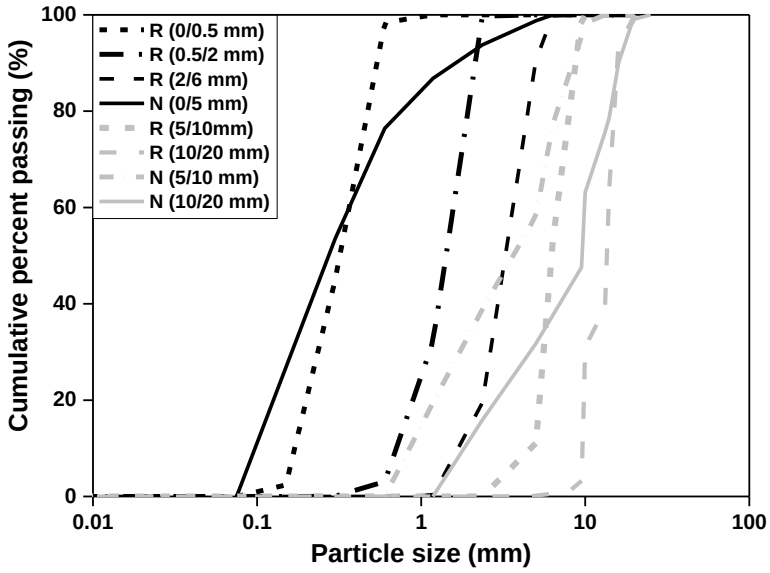

Figure 3.1: Particle size distributions for natural aggregates and rubber particles

Table 3.1 Physical and mechanical properties of steel fibres

Fibre type	Length (mm)	Diameter (mm)	Density (g/cm3)	Tensile strength (MPa)
MSF	*55*	0.8	7.8	1100
RTSF	*15-45 (> 60% by mass)*	<0.3	7.8	2000

3.2.1.2 Concrete mix designs

An optimized conventional concrete mix design [9] with target cylinder compressive strength of 60 MPa at 28 days of curing, typically used in bridge piers for XD3 exposure class, was adopted in this study. It was confirmed by the authors in a previous study [1] that this mix design suites the replacement up to 60% of WTR and does not cause much degradation in concrete fresh properties, yet maintaining a mechanical performance suitable for pavement construction.

The key parameters examined experimentally are: (i) the content of rubber (0%, 30% and 60%) replacing both fine and coarse aggregates by volume, (ii) the content of fibres (0 or a blend of 20 kg/m^3 MSF + 20 kg/m^3 RTSF), (iii) the curing conditions (mist room or 3% NaCl), (iv) the age of testing (28, 90, 150 or 300 days). The concrete mixes examined in this study are less than these of previous research [1] performed by the authors on the mechanical properties of SFRRuC. This is because, in the previous research, it was found that both plain and rubberised blended SFRC mixes (MSF and RTSF- 20 kg/m^3 each) showed superior mechanical performance than RuC mixes without fibres or with RTSF alone. Hence, RuC mixes without steel fibres or with only RTSF are eliminated in this study. Additionally, to reduce the large number of specimens needed to conduct parallel durability studies, the current research examined SFRRuC mix with 30% rubber replacement, which is in the middle range between 20% and 40% SFRRuC mixes examined in the previous research.

Table 3.2 shows the rubber replacement ratios and fibre contents of the four mixes examined in this study. The mix nomenclature is described below: Each mix name follows the format NM, where N stands for the percentage of aggregate replacement (0 – conventional concrete with no rubber replacement, 30 or 60%), whilst M shows information about the reinforcement; P stands for plain concrete without fibres and BF stands for blended fibre mixes consisting 20 kg/m^3 of MSF and 20 kg/m^3 of RTSF). For example, *60BF* mix contains 60% rubber replacement and contains both MSF (20 kg/m^3) and RTSF (20 kg/m^3). Table 3.3 presents the concrete mix designs per m^3 of concrete.

Table 3.2 Concrete mix ID and variables

Concrete mixes ID	% Rubber replacing aggregates by volume		MSF (kg/m^3)	RTSF (kg/m^3)
	Fine	Coarse		
0P	0	0	0	0
0BF	0	0	20	20
30BF	30	30	20	20
60BF	60	60	20	20

Table 3.3 Mixes proportions for 1 m^3 of fresh concrete

Components	Concrete mixes			
	0P	*0BF*	*30BF*	*60BF*
CEM II (kg/m^3)	340	340	340	340
SF (kg/m^3)	42.5	42.5	42.5	42.5
FA (kg/m^3)	42.5	42.5	42.5	42.5
Water (l/m3)	150	150	150	150
Plasticiser (l/m^3)	2.5	2.5	3.25	4.25
Superplasticiser (l/m^3)	5.1	5.1	5.1	5.1
Natural aggregates				
0/5 mm (kg/m^3)	820	820	574	328
5/10 mm (kg/m^3)	364	364	254	146
10/20 mm (kg/m^3)	637	637	446	255
Rubber				
0/0.5 mm (kg/m^3)	0	0	16.5	33
0.5/2 mm (kg/m^3)	0	0	24.8	49.6
2/6 mm (kg/m^3)	0	0	33	66
5/10 mm (kg/m^3)	0	0	33	66
10/20 mm (kg/m^3)	0	0	57.7	115.4
Fibres				
MSF (kg/m^3)	0	20	20	20
RTSF (kg/m^3)	0	20	20	20

3.2.1.3 Mixing, casting and curing procedure

Due to the limited capacity of the pan mixer used, each mix was cast in three batches. The concrete constituents were mixed according to the sequence shown in Figure 3.2.

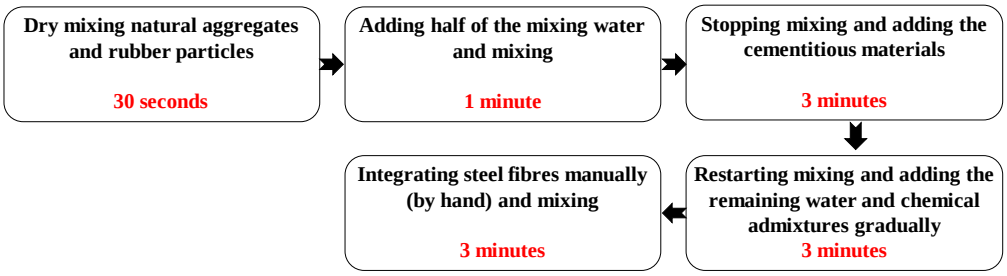

Figure 3.2: Sequence of mixing

Concrete was cast in two layers (according to EN 12390-2) [27] and vibrated on a shaking table (25s per layer). The fresh concrete was covered with plastic sheets and left under standard laboratory conditions (20 $^{\circ}C \pm 2$ and 50 $\pm$ 5% relative humidity (RH)) for 48 h. The specimens were then demoulded and stored in a mist room (21 $^{\circ}C \pm 2$ and 95 $\pm$ 5% RH) to cure for 28 days. Following a period of 21 days, 150 x 300 mm and 100 x 200 mm cylinders were removed from the mist room and sliced up, parallel to the trowelled surface, into five shorter cylinders (150 x

50 mm each) and two shorter cylinders (100 x 100 mm each), respectively. All concrete slices were placed back in the mist room until the end of mist curing (28 days).

3.2.2 Testing methods

3.2.2.1 Fresh state properties

Fresh concrete properties were assessed in terms of slump, air content and fresh density according to EN 12350-2 [28], EN 12350-7 [29], and EN 12350-6 [30], respectively.

3.2.2.2 Mechanical strength tests

Compression and flexural tests were performed on all of the specimens at the end of the drying period (4 days after removal from the mist room or NaCl solution). Three specimens were tested for each mix and environmental conditioning.

The Uniaxial compression tests were performed on concrete cubes (100 x 100 mm) according to EN 12390-3:2009 [31] at a loading rate of 0.4 MPa/s. Three-point bending tests were performed on prisms (100 x 100 x 500 mm) with 300 mm span, using an electromagnetic universal testing machine and a set-up similar to that suggested by RILEM [32]. A day before testing, a notch (5 mm thick and 15 mm deep) was sawn at the mid-span of the bottom side of each prism to force the crack to open at mid-span and a clip gauge was mounted across the notch (gauge length 12.5 mm) to measure the crack mouth opening displacement (CMOD) and control the test. All tests were CMOD-controlled at a constant rate of 0.05 mm/min for CMOD from 0 to 0.1 mm, 0.2 mm/min for CMOD ranging from 0.1 to 4 mm and 0.8 mm/min for CMOD from 4 mm to 8 mm. The net mid-span deflection was measured using two linear variable differential transformers (LVDTs) mounted at the middle of a yoke (one on each side), as suggested by JSCE [33].

3.2.2.3 Gas and water permeability

Cylinders of 150 x 50 mm were tested after 28 and 300 days of curing in a mist room. Prior to testing, specimens were pre-conditioned (oven dried) to remove water from the concrete pores. Rather than using the standardised preconditioning temperature of 105 ºC, which causes cracking, mainly due to the removal of interlayer and bound water present in the hydration products [34-36], a temperature of 80 ºC was initially used on the 28 day specimens in an attempt to minimise cracking. Constant mass was achieved after 7 days of drying, but SFRRuC specimens exhibited cracks of average width around 0.065 mm which can be attributed to the different coefficient of thermal expansion of the rubber aggregates. Although the values

obtained from the cracked specimens are not expected to reflect the real permeability of SFRRuC, these values are still reported in the following and commented upon.

To minimise cracking induced during preconditioning, a reduced temperature of 40 ºC was adopted for treating the 300 day specimens. As expected, it took much longer to reach constant mass (between 30 to 40 days). Considering the extended time required to dry the concretes, it was decided not to expose the specimens to wet-dry chlorides exposure, as a direct correlation between gas and water permeability measurement and chloride penetrability would not be fair, as the concretes would have completely different ages by the time each of test was conducted.

Oxygen permeability tests were performed on three 150 x 50 mm cylinders per mix following the procedure recommended by RILEM TC 116-PCD-C [37], also called "Cembureau method", using 1 Bar of oxygen gas above the atmospheric pressure. Sorptivity measurements were conducted in two cylinders of similar size following the recommendation of the EN 13057 [38]. After performing the sorptivity test, the same cylinders were used to measure the volume of permeable voids (VPV) based on the procedures of ASTM C1202 [39], also called the vacuum saturation method.

3.2.2.4 Chloride permeability and corrosion

After 28 days of mist curing, chloride permeability was evaluated in two different exposure conditions: (i) fully immersing cylinders (100 x 100 mm) in a 3% NaCl solution (placed in sealed plastic containers in the mist room until testing); and (ii) wet-dry cycles (accelerated chloride corrosion simulation), by immersion in a 3% NaCl for 4 days followed by a drying period in standard laboratory environmental conditions for 3 days. Prisms (100 x 100 x 500 mm), cubes (100 mm) and cylinders (100 x 100 mm) were kept apart by at least 10 mm using a specially designed frame. All specimens were preconditioned for ion chloride penetration tests using the unidirectional non-steady state chloride diffusion-immersion method described in EN 12390-11 [40].

After preconditioning for 90, 150 and 300 days in NaCl solution, two 100 x 100 mm cylinders per mix per condition were split into two halves at mid-point according to the colorimetric method [41, 42]. From each freshly split cylinder, the piece with the split section nearly perpendicular to the exposed surface was chosen for the penetration depth measurement, and was immediately sprayed with 0.1 N silver nitrate ($AgNO_3$) solution. Silver nitrate reacts with the chloride ion present in the hardened matrix to form white AgCl (white in colour); whereas at greater depth,

silver nitrate reacts with the hydroxyl ion to form Ag_2O (dark brown), as described in formulas (1) and (2) [43].

$$Ag^+ + Cl^- \rightarrow AgCl \downarrow (silver - white) \quad (1)$$
$$Ag^+ + OH \rightarrow AgOH \rightarrow Ag_2O \downarrow (brown) \quad (2)$$

Chloride penetration depth was indicated by the boundary colour change within 10-15 minutes after spraying. The chloride penetration depth was marked at the colour change boundary and the depth was recorded as the average distance, taken from five sections (Figure 3.3). The cylinder that registered the maximum average depth was selected for analysis and used to drill out binder powder from the surface and colour change boundary to determine acid-soluble chloride concentrations.

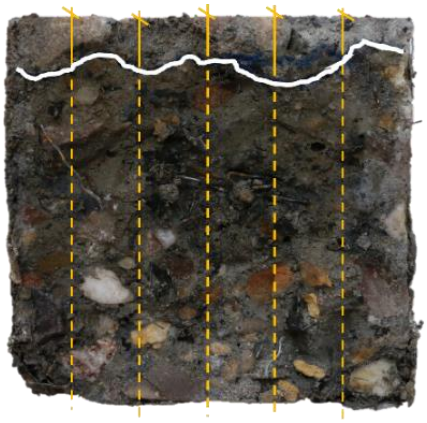

Figure 3.3: Representative SFFRuC freshly split, sprayed and marked for determination of chloride penetration depth

The acid-soluble (total) chloride concentration was measured at the 134.724 emission line using a Spectro-Ciros-Vision ICP-OES instrument which was calibrated with standards of known chloride concentrations made up in 20% nitric acid. The apparent chloride diffusion coefficients (D_{app}) were roughly estimated using the re-arrange error function solution of Fick's second law of diffusion shown in Eq. (3) [41, 42]:

$$D_{app} = \left(\frac{x}{2erf^{-1}\left(1-\frac{C_x}{C_s}\right)\sqrt{t}} \right)^2 \quad (3)$$

where x is the maximum average distance of colour change boundary from the concrete surface; C_x is the total chloride concentration at the colour change boundary at any time t; C_s is the total chloride concentration at the surface.

It should be noted that the D_{app} obtained using the traditional profile method specified in EN 12390-11 [40] is more accurate than that of colorimetric method. This is due to the fact that the

measurements and calculations of chloride concentration using colorimetric method can be influenced by many factors including concrete alkalinity, the amount and concentration of the sprayed $AgNO_3$ solution, pore solution volume of concrete, sampling method as well as method used for measuring the chloride content [42]. However, the colorimetric method is a quick, simple and relevant method for assessing the kinetics of chloride penetration in concrete specimens when non-steady state chloride diffusion test is carried out in laboratory condition. Many studies [41, 42, 44] have proven its feasibility to determine the average chloride penetration depth (the depth associated with the assumed ''critical'' chloride concentration with respect to corrosion risk ~ 0.4%. by unit mass of binder) and assess the D_{app}.

3.3 Results and Discussion

3.3.1 Fresh state properties

The slump, air content and fresh density of the concretes studied are presented in Table 3.4. The addition of fibres reduced the workability of the concrete, and this effect is more notable with the inclusion of both fibres and rubber in the SFRRuC mixes. For mixes *0BF*, *30BF* and *60BF*, the slump drops by 5%, 13% and 56%, respectively, when compared with the plain concrete, *0P*. The tendency of steel fibres to agglomerate contributed to the slump reduction. The decrease in slump as a result of adding rubber particles can be explained by the higher level of inter-particle friction between rubber particles and the other concrete constituents (owing to the rough surface texture and high coefficient of friction of rubber particles) [1, 4, 7-9]. Nevertheless, all mixes satisfy the slump requirements described in pavement design standard EN 13877-1 [19]. Moreover, similar to the finding in Ref. [9], no signs of segregation, bleeding or excessive “balling” were observed in any of the mixes.

Table 3.4 Fresh state properties of SFRRuC evaluated. Values in parenthesis correspond to one standard deviation of three measurements

Properties	Concrete mix			
	0P	*0BF*	*30BF*	*60BF*
Slump (mm)	223 (14)	212 (10)	193 (15)	98 (25)
Air content (%)	1.3 (0.5)	1.4 (0.1)	3.4 (1.1)	3.2 (0.2)
Fresh density (kg/m^3)	2405 (5)	2424 (9)	2124 (6)	1859 (4)

The addition of fibres alone did not induce notable changes in the air content of the concrete. The substitution of natural aggregate by rubber (mixes *30BF* and 60BF) in SFRC, however, significantly increased the air content of the fresh concrete by more than 100%. The rough and

hydrophobic nature of rubber particles tends to repel water and therefore increases the amount of entrapped air in the mix. The increased friction between fibres and rubber also cause fibres to agglomerate and trap more air [1, 45].

The fresh density of the SFRC mix, *0BF*, is slightly higher than that of the plain concrete mix, *0P*, owing to the high specific gravity of the added fibres (Table 3.1). The density of the fresh mix is significantly reduced when rubber particles are used to replace natural aggregates as a result of their lower density (section 3.2.1.1). For the SFRRuC, *30BF* and *60BF*, the density decreases by 13% and 30%, respectively, compared to the plain concrete.

3.3.2 Effect of chloride exposure in mechanical performance

3.3.2.1 Visual inspection

Figure 3.4 a) and b) show the appearance of specimens after 150 and 300 day exposure to accelerated chloride corrosion conditions, respectively. Prior to chloride exposure, there were no signs of rust on the concrete surface, which implies that the fibres were protected by a thin layer of cement paste. At the end of 150 days of wet-dry chloride exposure, however, the specimens showed minor signs of superficial rust (Figure 3.4a) in regions where the fibres were near the concrete surface. A large amount of rust is observed on the surface of the specimens exposed for 300 days (Figure 3.4b), mainly as a consequence of the corrosion of the steel frame used to hold the specimens. Nevertheless, at all periods of the accelerated chloride corrosion exposure, no sign of deterioration or cracks were observed on the concretes.

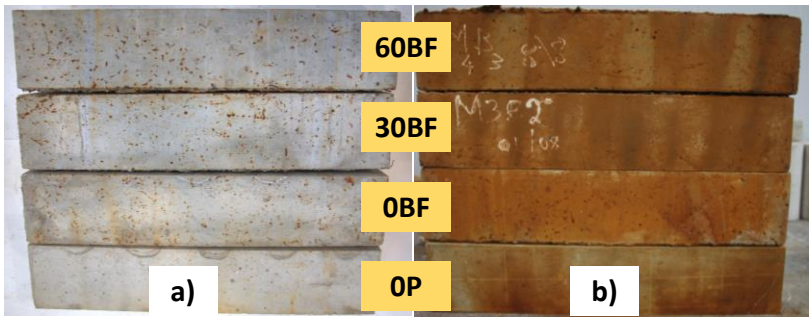

Figure 3.4: SFRRuC specimens after a) 150 days, and b) 300 days of wet-dry chloride exposure

Figure 3.5 shows the internal appearance of a SFRRuC splitted cube, *30BF*, after 300 days of wet-dry chloride exposure. Despite the external rusty appearance (Figure 3.4b), no evidence of rust is observed on the fibres embedded in these concretes. This indicates that steel reinforcement did not corrode to any significant extent under the wet-dry chloride exposure. This performance may be explained by the reduced chloride permeability of the concretes, as it will be discussed

in detail in the following sections, and the discrete nature of steel fibres embedded in the matrix, generating smaller potential differences along the steel surface and reduced cathode/anode ratios compared to conventional steel rebars [24].

Figure 3.5: Section through a SFRRuC specimen after 300 days of wet-dry chloride exposure

In addition, the dense and uniform fibre-matrix interfacial transition zone (ITZ), composed mainly of rich segregated lime, acts as a high alkalinity barrier and protects fibres in the bulk SFRC against chloride and oxygen ingress [24].

3.3.3 Compressive strength

The influence of wet-dry chloride exposure on the compressive strength of SFRRuC is presented in Figure 3.6. Error bars represent one standard deviation of three measurements. Comparable compressive strength values are seen for the plain concrete, *0P*, and the SFRC, *0BF*, before and after chloride exposure. As expected, the replacement of natural aggregates with rubber particles led to a substantial reduction in compressive strength. Prior to chloride exposure, reductions of up to 54% and 86% in compressive strength, respectively, with respect to *0BF*. The loss in compressive strength is mainly due to the lower stiffness and higher Poisson ratio of rubber in comparison to that of natural aggregates. The weak adhesion between cement paste and rubber particles may also contribute to the strength degradation, as discussed by the authors in Ref. [1] and Khaloo et al. in Ref. [12].

All mixes after 150 and 300 days of wet-dry chloride exposure present a slightly increased compressive strength, compared to the 28-day values measured prior to the chloride exposure. The increase in strength is attributed to the continuous hydration of the cementitious paste over the period of exposure, owing to the high amount of pozzolanic materials used for replacing Portland cement in all the concrete mixes.

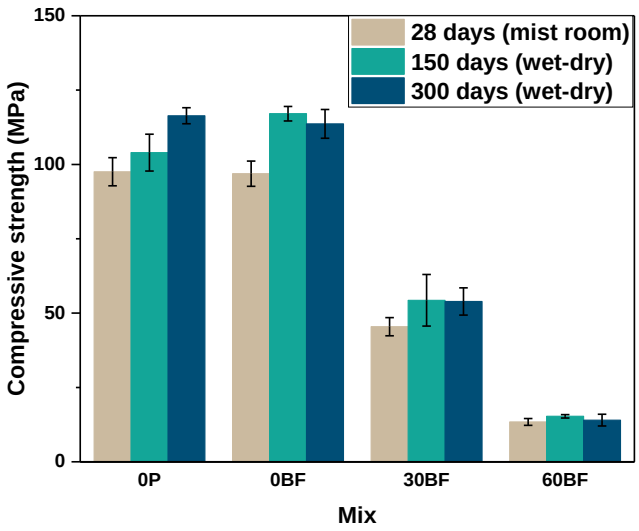

Figure 3.6: Compressive strength of concretes assessed before and after 150 and 300 days of wet-dry chloride exposure

3.3.4 Flexural behaviour

The mean values of flexural strength at 28 days and after 150 and 300 days of wet-dry chloride exposure are presented in Figure 3.7. Error bars represent one standard deviation of three measurements. The addition of fibres to plain concrete, mix *0BF*, enhances the 28-day flexural strength by 28%, compared to *0P*. The partial replacement of natural aggregates by rubber particles reduced the flexural strength of the tested concretes, but to a lesser extent than the compressive strength (Figure 3.6). The 28-day flexural strength reduction of SFRRuC mixes, *30BF* and *60BF*, in comparison to *0BF* is 31% and 56%, respectively. The contribution of steel fibres in enhancing the flexural strength was anticipated as the thin fibres, RTSF, tend to "sew" the micro-cracks that develop in the matrix during loading, while the thick fibres, MSF, tend to control the propagation of wider cracks and redistribute stresses [1, 46].

For all mixes, the flexural strength results are higher at the end of 150 days of wet-dry chloride exposure than those of 28-day mist cured specimens, as a consequence of the ongoing hydration of the cement in the concretes.

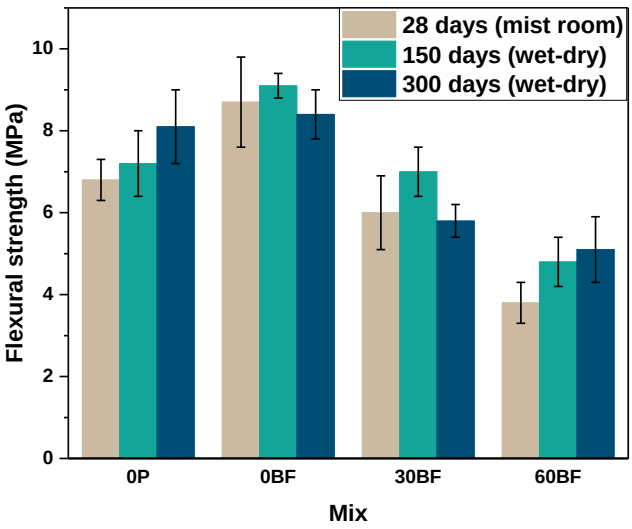

Figure 3.7: Flexural strength of concretes assessed before and after 150 and 300 days of wet-dry chloride exposure

No clear trend can be identified in the flexural strength values of the specimens at the end of 300 days of wet-dry cycles. While *0P* and *60BF* mixes present higher flexural strength values, compared to those of 150 days of wet-dry cycles, the flexural strength values of *0BF* and *30BF* mixes are even lower than their respective strength at 28-days. This variation may be the result of the high natural variability in these specimens. It is unlikely that the flexural strength of *0BF* and *30BF* specimens was reduced due corrosion attack, as evidence of rust in the fibres embedded in these specimens was not observed (see section 3.3.2.1).

Figure 3.8 shows the average elastic modulus obtained from three prisms per mix over the three periods of testing. Error bars represent one standard deviation of three measurements. Flexural elastic modulus was determined based on the theory elastic deflection and by using the secant modulus of the load-deflection curves (from 0 to 30% of the peak load).

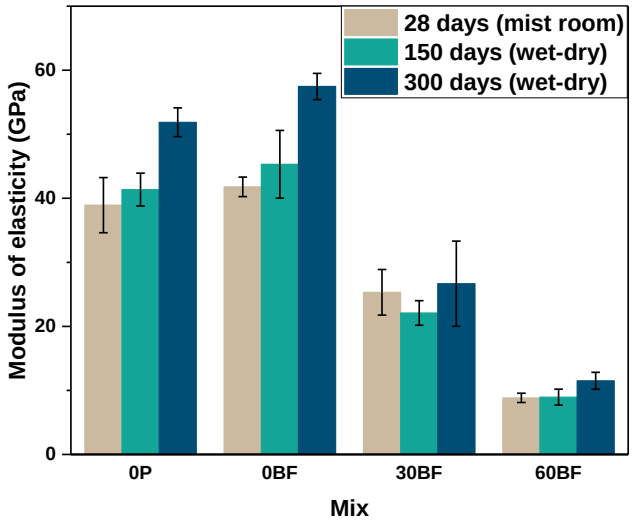

Figure 3.8: Elastic modulus of all tested concrete specimens before and after 150 and 300 days of wet-dry chloride exposure

The addition of 40 kg/m^3 of fibres did not affect the elastic modulus of concrete by much. However, a notable decrease in the elastic modulus is observed from the replacement of natural aggregates with rubber particles; reductions up to 38% for *30BF* and 79% for *60BF* compared to *0BF*. The reduction in the elastic modulus is mainly caused by the low stiffness of the rubber particles and to a lower degree by the high air content in these concretes, as discussed in section 3.3.1. The low elastic modulus of *60BF*, however, is still comparable to that of typical of flexible pavements, i.e. around 8 GPa [47].

A general increase in the average elastic modulus of all mixes after 150 and 300 days of wet-dry cycles was identified, compared to 28-day compressive strength. Although enhancement in elastic modulus was expected as the compressive strength increases with time, the large increase seen for normal concrete after 300 days can be partly attributed to variability between the three prisms which came from three different batches, and partly to the fact that the elastic modulus is determined indirectly from deflections.

Figure 3.9 presents the average flexural stress-CMOD curves registered in all prisms over the three periods of testing. The sudden stress loss after the peak load for the plain concrete mixes indicates their brittle behaviour in tension. On the other hand, all SFRC and SFRRuC mixes show enhanced post-cracking load bearing capacity and significant energy absorption. This is a result of the fibres bridging the cracks and controlling their propagation even after the peak load, dissipating energy through pull-out and mobilising and fracturing a larger volume of concrete. It is also evident that the post-peak energy absorption behaviour of the SFRC and SFRRuC specimens is not reduced after exposure to wet-dry cycles. This confirms that steel

reinforcement did not corrode to any significant extent under the wet-dry chloride exposure adopted in this study.

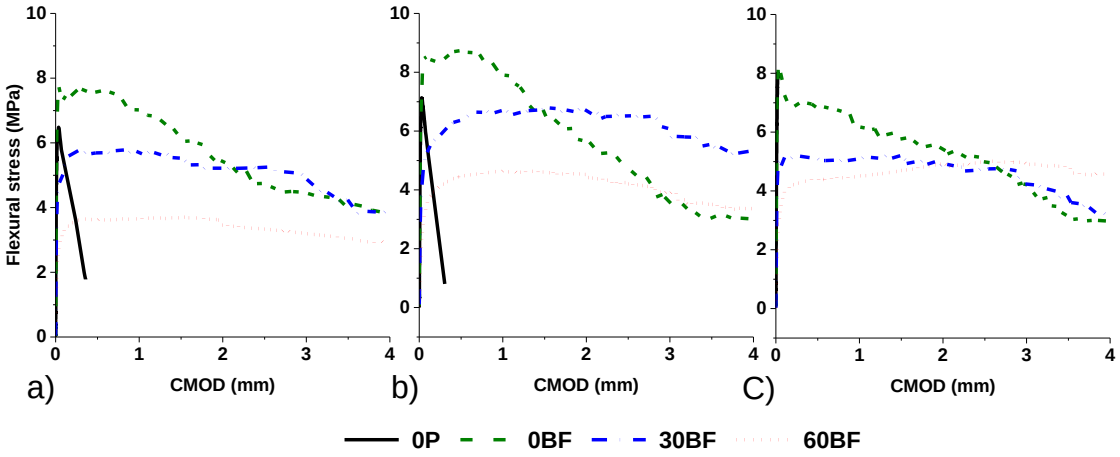

Figure 3.9: Flexural stress-CMOD curves of the tested concrete specimens a) before, and after wet-dry chlorides exposure for b) 150 and c) 300 days

3.3.5 Transport properties

3.3.5.1 Evaporable moisture and volume of permeable voids

The loss of mass due to water evaporation after preconditioning the specimens at 80 ºC (28 day cured) and 40 ºC (300 day cured) was determined as the ratio between the total amount of evaporated water and the dry mass of the specimen. The mean values (average of five measurements) of evaporable moisture concentrations results, W_e, are shown in Figure 3.10a, and the volume of permeable voids, VPV, are presented in Figure 3.10b. Error bars correspond to one standard deviation of five measurements for W_e and two measurements for VPV. A direct relationship between the W_e and VPV is observed for all the tested concretes, independently of the preconditioning temperature and curing age, where higher values of evaporated water are obtained in more porous concretes.

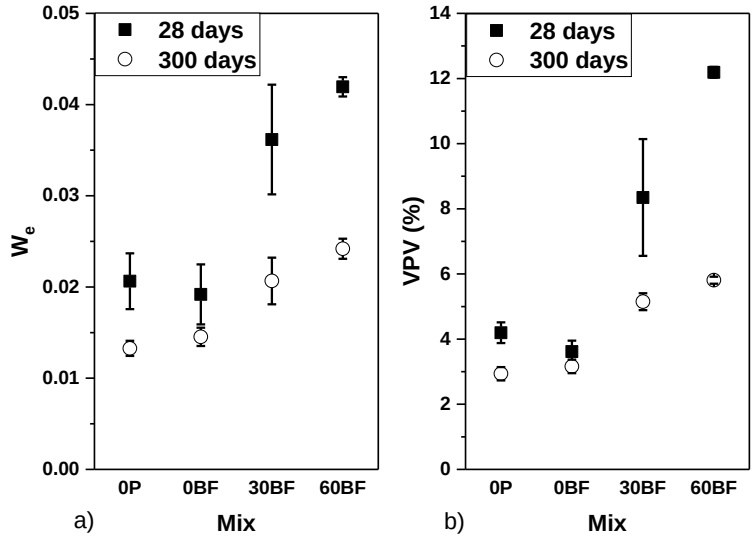

Figure 3.10: a) Evaporable moisture, and b) volume of permeable voids of all tested concretes

The addition of fibres generally results in reduced shrinkage cracking and in the establishment of more tortuous and disconnected pore network [48], thus reducing VPV. For 28 days cured samples, *0BF* mix exhibits, as expected, a decrease in VPV, though marginal and within the observed experimental error (average of 13%), whereas the SFRRuC mixes exhibit a large increase in VPV. This can be attributed to the rubber particles, the rough surface and hydrophobic nature of which can help trap air on their surface and make their interface more porous and highly absorptive to water [49, 50].

Minor changes in the VPV values are observed in concretes *0P* and *0BF* for the two curing conditions. This is unexpected as more mature concretes typically have lower permeability, but it may be the result of the already high quality of the concrete matrix which makes it dense to start with. In concrete composites with rubber aggregates, *30BF* and *60BF*, extended curing times reduce the VPV values by 24% and 93%, respectively. It should be pointed out that SFRRuC specimens exhibited severe cracking upon preconditioning at 80°C, which increased their permeability and caused the high VPV results recorded.

Baroghel-Bouny [51] proposed a classification of the durability of reinforced concrete structures based on "universal" durability indicators determined on a broad range of concretes cured in water. According to the proposed system, concrete mixes with VPV between 6-9% are categorised as highly durable. The VPV values of all the mixes examined in this study are lower than 6%, after 300 days of curing, even when rubber particles are used as partial aggregate replacement, which puts them in the highly durable category.

3.3.5.2 Oxygen permeability

The oxygen permeability is not only influenced by the overall porosity, but also by the proportion of continuity of larger pores where most of the flow will occur [52, 53]. Figure 3.11 shows the oxygen permeability results for 28 day cured specimens (preconditioned at 80 °C) and 300 day cured specimens (preconditioned at 40 °C), expressed as the intrinsic permeability '*K*'. Error bars correspond to one standard deviation of three measurements. Due to the extremely high permeability of the specimens resulting from the surface cracking upon preconditioning at 80°C, the gas permeability for the 28 day cured specimens with rubber particles could not be determined (the oxygen found its way out very quickly).

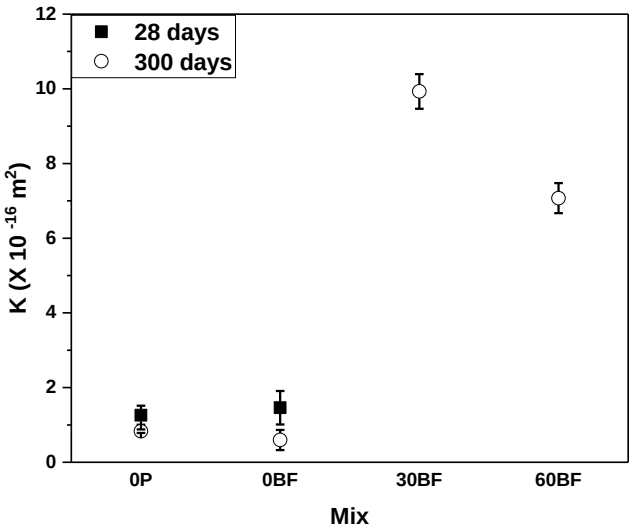

Figure 3.11: Oxygen permeability results for all tested mixes

Considering the standard deviations as well as the experimental errors for both 28 and 300 days results, the oxygen permeability values for SFRC specimens, *0BF*, are comparable with those of plain concrete, *0P*, indicating that the fibres did not modify much the permeability of the concretes tested. SFRRuC specimens, *30BF* and *60BF*, on the other hand, show significantly higher permeability values, up to 12 and 8.5 times respectively, with respect to the plain concrete mix, *0P*. These concretes presented comparable air contents (Table 3.4) and VPV values (Figure 3.10b), despite the differences in rubber content. The increased oxygen permeability recorded for the assessed specimens may be attributed to the compressibility of rubber particles when pressure is applied. As rubber deforms, the oxygen gas can more easily find its way through the specimen and around the rubber particles. If that is the case, then gas permeability may not be the best way to determine the permeability of RuC.

3.3.5.3 Water sorptivity

The main mechanism that governs sorptivity is capillary suction of water when a specimen is partially saturated [52, 54]. The difference in pressure causes the movement of water front through a porous material. Hence, sorptivity is derived by measuring the slope of the amount of water uptake per unit area as a function of the square root of time. The sorptivity results measured for 28 and 300 days cured specimens are shown in Figure 3.12. Error bars correspond to one standard deviation of two measurements

For the 28 day cured samples, the addition of fibres to plain concrete, mix *0BF*, causes marginal decrease in the sorptivity value, with an average of 12% with respect to the plain concrete mix, *0P*. For 300 day, however, *0BF* specimens record marginally higher sorptivity values, with an average of 9%, than that of *0P* specimens. These results are in good agreement with the VPV values (Figure 3.10b) confirming that the extended curing time had only a minor effect on the sorptivity and on the already high quality of the concrete matrix evaluated in this study.

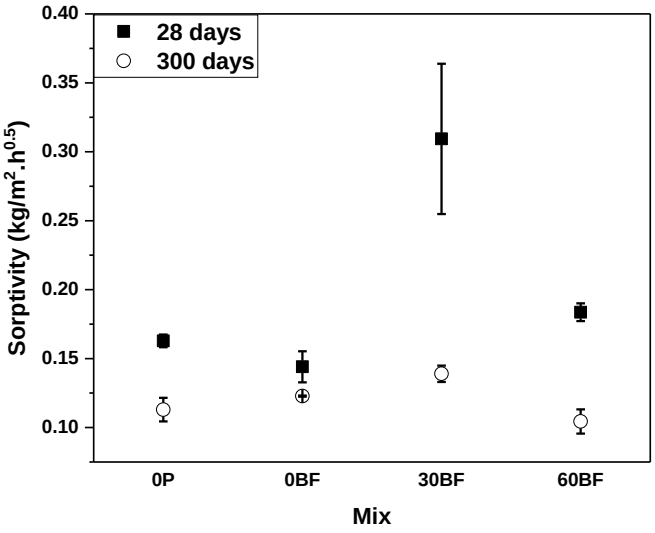

Figure 3.12: Sorptivity values of all tested mixes

The 28 days sorptivity results of the SFRRuC specimens show different trends. While the *30BF* specimens record the highest sorptiviy values, an average 90% higher than *0P* mix, *60BF* specimens shows slightly higher sorptivity value, average of 13% compared to *0P*. Unlike VPV and chloride penetration tests, where the specimens are fully immersed for a long period of time, specimens evaluated for sorptivity were partially immersed in water (2 mm depth from the trowelled surface) and the water uptake measurements were recorded during the first 24 hours of first immersion, as specified in EN 13057 [38]. Therefore, the quality of the concrete surface that is in contact with water plays a major role in imbibing the water through the fine

capillary pores. As it has been reported previously [45, 50], the rough texture of rubber particles cause both fine and coarse pores to increase with increasing rubber content. Hence, in addition to the surface cracking upon preconditioning at 80°C, the authors hypothesised that the high values of sorptivity for the *30BF* specimens may be attributed to the large amount of fine pores which dominated the initial sorptivity behaviour. On the other hand, the high amount of large course rubber particles in the *60BF* specimens located on the concrete surface in contact with water (see Figure 3.13) could have limited the water absorption rate (owing to the non-sorptive nature of rubber particles) and dominated the initial sorptivity behaviour. To confirm this, the specimens were left partially immersed for a longer period (15 days) and the water uptake was measured. Similar to VPV, it was observed that the sorptivity of the concrete is higher with increasing the rubber content. This suggests that when water imbibed through the contact surface in *60BF*, the amount of fine pores also dominated the water ingress into the sample, consistent with the differences in pore network between the surface and the core of the specimens.

30BF **60BF**

Figure 3.13: Cross section view of the SFRRuC specimens used for the sorptivity test

Extending the curing time for *30BF* and *60BF*, i.e. 300 days, cause significant reduction in the sorptivity values, with average of 67% and 20%, respectively, when compared with the values registered for concretes cured for 28 days. This is mainly related to the absence of surface cracking upon preconditioning at 40°C, which results in more realistic sorptivity values.

When calculating the concrete sorptivity using the depth penetration approach [52, 55, 56], all mixes examined here record sorptivity values less than 6 mm/h$^{0.5}$, which places them in the excellent durability class based on the durability index proposed by Alexander et al. [57] and adopted in Refs. [52, 55, 56].

3.3.5.4 Chloride ion penetration

Figure 3.14 shows the chloride penetration zone after spraying 0.1 N $AgNO_3$ at the end of 90 and 150 days of chloride exposure in fully-saturated and wet-dry conditions. As the continuous hydration of concrete specimens that contain high amount of silica fume gradually darken the colour of the matrix (see Figure 3.14), it was not possible to detect the penetration zone in any of the specimens exposed to chlorides for 300 days due to the similarity in colour between matrix and the rubber particles. This drawback of the colorimetric method for assessing chloride permeability in concretes containing blended cement and silica fume has also been previously reported [58].

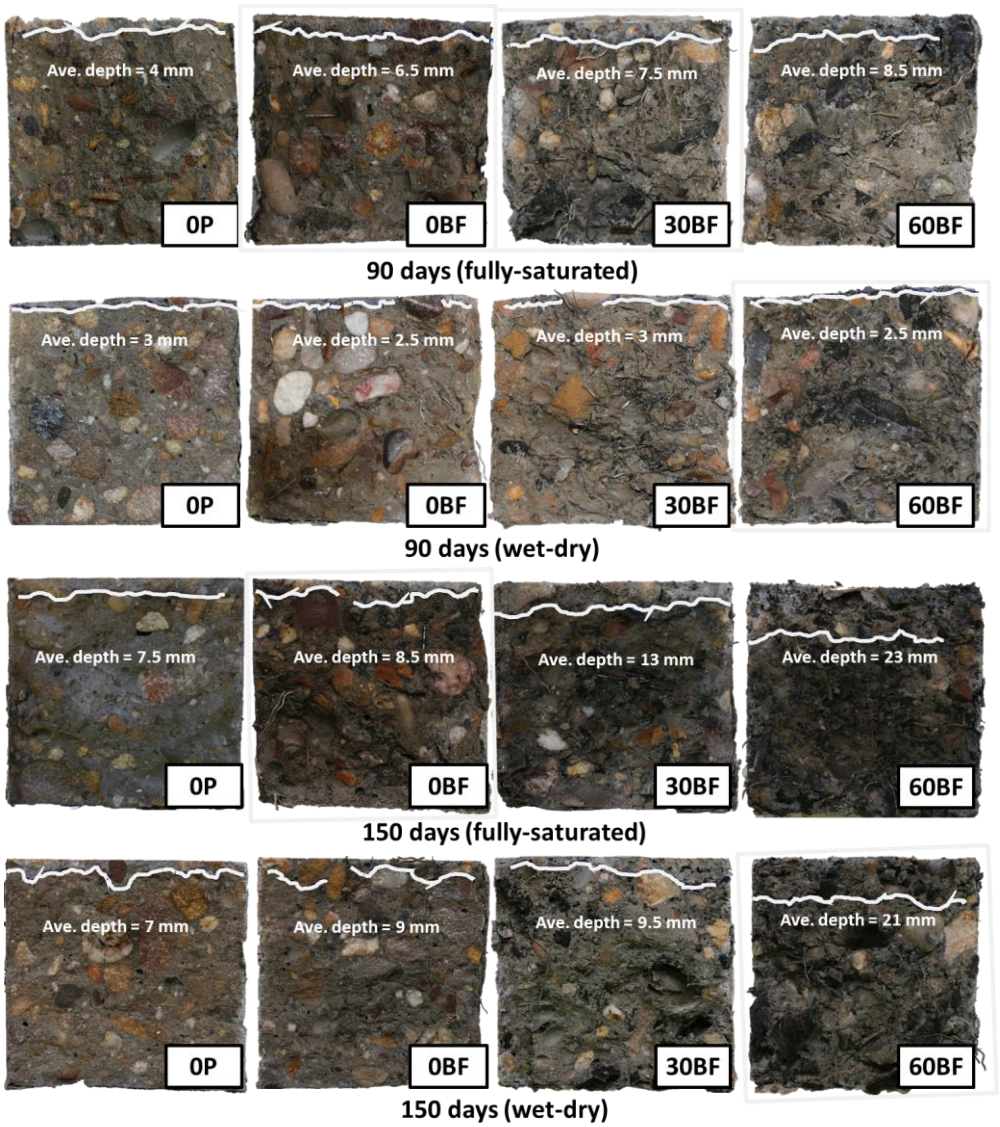

Figure 3.14: Chloride contaminated zone of all concrete mixes at the end of 90 and 150 days of chloride exposure in fully-saturated and wet-dry conditions

Figure 3.15 shows a comparison between the average chloride penetration depths for all concrete specimens. Error bars correspond to one standard deviation of the average depth measured in two different specimens. For concretes exposed to wet-dry cycles, the chloride penetration depth is in general lower than those of fully-saturated specimens. In fully-saturated specimens the chloride ingress is mainly governed by the diffusion mechanism. The process of chloride ingress into concrete exposed to wet-dry cycles is a combination of diffusion and absorption, as in partially saturated concretes the chloride solution is absorbed by capillary suction and concentrated by evaporation of water [59]. These results somehow contradict what has been reported for other blended cement concretes [59], where the wet-dry cycle exposure to chlorides typically leads to deeper chloride penetration compared to fully-saturated ones. The duration of the wet-dry cycles, and particularly the degree of dryness achieved, controls the extent of ingress of chlorides, as higher degrees of dryness facilitate deeper chloride penetration during subsequent wet cycles [60]. Due to the low permeability of these concretes, it seems the drying cycle was not sufficient to remove water beyond the concrete surface, hindering capillary sorption of chlorides rich solution into the concrete.

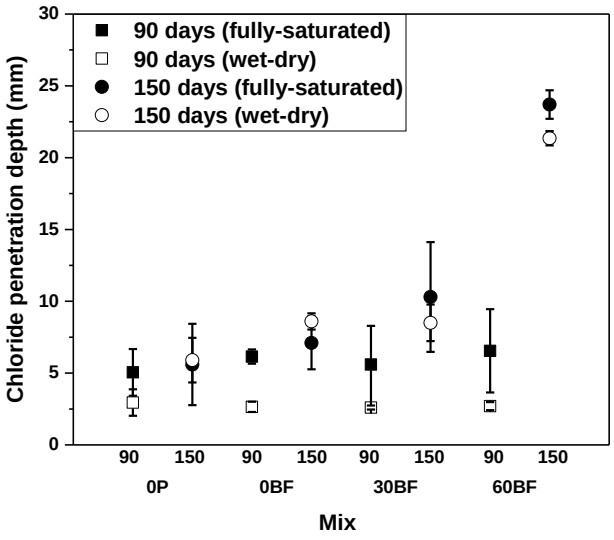

Figure 3.15: Chloride penetration depth for all concrete mixes assessed at the end of 90 and 150 days of chloride exposure in fully-saturated and wet-dry conditions

The data presented in Figure 3.15 also indicate that the chloride penetration depth at the end of 90 days of exposure was small and comparable, being in the range of 5–7 mm for the fully-saturated specimens, and 2–3 mm for the wet-dry specimens. This suggests that up to 90 days of chloride exposure, the penetration rate was not aggravated by the addition of rubber. At the end of 150 days of chloride exposure, however, the depth of chloride penetration in both

conditions generally increased with rubber content. This is consistent with the higher values of VPV obtained for SFRRuC specimens (sections 3.3.5.1).

For practical purposes, due to the small chloride penetration depths at 90 days and difficulty in identifying chloride penetration depths at 300 days of chloride exposure, only specimens at 150 days of exposure (in both conditions) were considered for the determination of total chloride concentration and apparent chloride diffusion coefficient. Table 3.5 presents the total chloride concentrations by weight of binder as well as the roughly estimated apparent chloride diffusion coefficient measured at the colour change boundary for all of the assessed concretes. The chloride concentrations for the plain concrete and SFRC mixes, *0P* and *0BF*, were less than 10 ppm (i.e. the detection limit of the instrument used), hence it was not possible to detect the exact total chloride concentrations and then calculate the apparent diffusion coefficients for these mixes.

Table 3.5 Chloride concentration and the roughly estimated apparent chloride diffusion coefficient in concretes after 150 days of chlorides exposure

Mix	Maximum average chloride penetration depth, x (mm)		Chloride concentration at surface, C_s (wt% of binder)		Chloride concentration at colour change boundary, C_x (wt% of binder)		Apparent diffusion coefficient (10^{-12} m^2/s)	
	fully-saturated	wet-dry	fully-saturated	wet-dry	fully-saturated	wet-dry	fully-saturated	wet-dry
0P	7.6	7	0.159	0.640	<10 ppm	<10 ppm	-	-
0BF	8.5	9	0.339	0.248	<10 ppm	<10 ppm	-	-
30BF	13	9.5	1.752	2.229	0.109	0.234	1.87	1.33
60BF	23	21	1.398	2.858	0.151	0.157	7.90	4.62

SFRRuC mixes, *30BF* and *60BF*, present lower chloride concentrations values (at both conditions) than 0.4% by weight of cement, which is the most commonly assumed critical total chloride concentration value inducing corrosion [58, 61]. This indicates that even with the increased VPV and sorptivity caused by the replacement of natural aggregates with rubber particles (sections 3.3.5.1 and 3.3.5.3), the assessed concretes present high resistance to chloride penetration for 150 days of chloride exposure.

SFRRuC mixes, *30BF* and *60BF*, show an increase in the apparent chloride diffusion coefficient at higher rubber contents, possibly due to their higher VPV and sorptivity. The apparent chloride diffusion coefficients of the fully-saturated and wet-dry specimens are comparable for the *30BF* mixes, indicating that under the testing conditions used in this study, the drying cycle had a

negligible effect on chloride penetration. Similar results have been identified in high quality Portland cement based concretes produced with silica fume, due to their refined porosity requiring longer drying times to obtain a particular moisture content [59]. Moreover, Kim et al. [44] evaluated the D_{app} at colour change boundary, following colorimetric method, for ordinary Portland concrete specimens made with 0.4 w/c ratio and immersed in marine environment for 6 months. It was found that the D_{app} was around 1.7 (10^{-12} m^2/s), in line with the values obtained here for *30BF*. On the other hand, *60BF* specimen in fully-saturated condition registers almost twice the diffusion coefficient than that in wet-dry condition. Nevertheless, with the apparent diffusion coefficients values observed here, SFRRuC mixes can be considered as medium to highly durable concrete mixes according to the durability indicators suggested in [51, 62].

For inspection purposes, the authors collected concrete samples at 50 mm depth from the exposed surface from those specimens exposed to chloride for 300 days, in both conditions, and the total chloride concentrations were measured. The total chloride concentrations for all of the examined samples were less than 10 ppm. This confirms the good resistance to chloride penetrability of all mixes.

3.4 Conclusion

This study examined the fresh, mechanical and transport properties as well as chloride corrosion effects in SFRRuC due to exposure to a simulated marine environment. Natural aggregates were partially replaced with waste tyre rubber particles and blends of MSF and RTSF were used as internal steel reinforcement. The following can be concluded:

- The addition of fibres marginally decreases workability and increases air content and unit weight. The substitution of rubber aggregates in SFRRuC mixes significantly reduces workability and unit weight (due to the lower density of rubber) and increases air content by more than 100%.

- No visual signs of deterioration or cracks (except superficial rust) were observed on the surface of concrete specimens subjected to 150 or 300 days of accelerated chloride exposure. Furthermore, no evidence of rust is observed internally on the fibres embedded in concretes indicating that steel reinforcement did not corrode to any significant extent under the wet-dry chloride exposure. This shows that blend fibres make a positive contribution to the durability of both conventional and RuC.

- The use of increasingly higher volumes of rubber aggregate in SFRRuC mixes reduces progressively the compressive strength and elastic modulus of concrete. Flexural strength is also affected, though to a lesser extent due to the presence of fibres. Hence, fibres are an essential component in the design of flexible concrete pavements.

- As a consequence of the ongoing hydration of the cementitious materials, a slight general increase in the mechanical properties of all mixes after 150 and 300 days of wet-dry chloride exposure was identified in comparison to the 28-day mechanical properties.

- While VPV and sorptivity generally increase with increased rubber content, the change with respect to plain concrete is minor. All mixes examined after 300 days of mist curing show VPV values lower than 6% and sorptivity values lower than 6 mm/h$^{0.5}$, which means that they can be classified as highly durable concrete mixes.

- The depth of chloride penetration in both conditions (fully-saturated and wet-dry) generally increases with rubber content. At the colour change boundary, *30BF* and *60BF* specimens record lower chloride concentrations than 0.4% by weight of cement (critical concentration inducing corrosion) and present apparent diffusion coefficients values within the range of highly durable concrete mixes.

It is concluded that the combination of rubber particles, up to 60%, and steel fibres can lead to an innovative concrete with increased ductility and flexibility as well as good transport characteristics. Future work should be focused on examining the capability of this promising concrete to withstand aggressive environments such as freeze-thaw resistance and fatigue performance.

Acknowledgements

The current experimental work was undertaken under the FP7 European funded collaborative project “Anagennisi: Innovative reuse of all tyre components in concrete” (Contract agreement number: 603722). The following companies offered materials and valuable in-kind contribution: Tarmac UK, Twincon Ltd, Aggregate Industries UK and Ltd Sika. Mr Alsaif would like to thank King Saud University and the Ministry of Education (Kingdom of Saudi Arabia) for sponsoring his PhD studies. Dr S.A. Bernal participation in this study has been sponsored by EPSRC through her ECF (EP/R001642/1).

3.5 References

[1] A. Alsaif, L. Koutas, S.A. Bernal, M. Guadagnini, and K. Pilakoutas, *Mechanical performance of steel fibre reinforced rubberised concrete for flexible concrete pavements,* Construction and Building Materials 172 (2018) 533–543.

[2] S. Raffoul, R. Garcia, D. Escolano-Margarit, M. Guadagnini, I. Hajirasouliha, and K. Pilakoutas, *Behaviour of unconfined and FRP-confined rubberised concrete in axial compression,* Construction and Building Materials 147 (2017) 388–397.

[3] F. Hernández-Olivares and G. Barluenga, *Fire performance of recycled rubber-filled high-strength concrete,* Cement and Concrete Research 34 (1) (2004) 109–117.

[4] N.N. Eldin and A.B. Senouci, *Measurement and prediction of the strength of rubberized concrete,* Cement and Concrete Composites 16 (4) (1994) 287–298.

[5] N.F. Medina, D.F. Medina, F. Hernández-Olivares, and M. Navacerrada, *Mechanical and thermal properties of concrete incorporating rubber and fibres from tyre recycling,* Construction and Building Materials 144 (2017) 563–573.

[6] D. Flores-Medina, N.F. Medina, and F. Hernández-Olivares, *Static mechanical properties of waste rests of recycled rubber and high quality recycled rubber from crumbed tyres used as aggregate in dry consistency concretes,* Materials and Structures 47 (7) (2014) 1185–1193.

[7] A. Benazzouk, O. Douzane, T. Langlet, K. Mezreb, J. Roucoult, and M. Quéneudec, *Physico-mechanical properties and water absorption of cement composite containing shredded rubber wastes,* Cement and Concrete Composites 29 (10) (2007) 732–740.

[8] F. Liu, W. Zheng, L. Li, W. Feng, and G. Ning, *Mechanical and fatigue performance of rubber concrete,* Construction and Building Materials 47 (2013) 711–719.

[9] S. Raffoul, R. Garcia, K. Pilakoutas, M. Guadagnini, and N.F. Medina, *Optimisation of rubberised concrete with high rubber content: An experimental investigation,* Construction and Building Materials 124 (2016) 391–404.

[10] A. Grinys, H. Sivilevičius, D. Pupeikis, and E. Ivanauskas, *Fracture of concrete containing crumb rubber,* Journal of Civil Engineering and Management 19 (3) (2013) 447–455.

[11] Z. Khatib and F. Bayomy, *Rubberized portland cement concrete,* Journal of Materials in Civil Engineering 11 (3) (1999) 206–213.

[12] A.R. Khaloo, M. Dehestani, and P. Rahmatabadi, *Mechanical properties of concrete containing a high volume of tire–rubber particles,* Waste Management (Oxford) 28 (12) (2008) 2472–2482.

[13] J.-H. Xie, Y.-C. Guo, L.-S. Liu, and Z.-H. Xie, *Compressive and flexural behaviours of a new steel-fibre-reinforced recycled aggregate concrete with crumb rubber,* Construction and Building Materials 79 (2015) 263–272.

[14] A. Turatsinze and M. Garros, *On the modulus of elasticity and strain capacity of self-compacting concrete incorporating rubber aggregates,* Resources, Conservation and Recycling 52 (10) (2008) 1209–1215.

[15] O. Onuaguluchi and D.K. Panesar, *Hardened properties of concrete mixtures containing pre-coated crumb rubber and silica fume,* Journal of Cleaner Production 82 (2014) 125–131.

[16] M. Bravo and J. de Brito, *Concrete made with used tyre aggregate: durability-related performance,* Journal of Cleaner Production 25 (2012) 42–50.

[17] A. Benazzouk, O. Douzane, and M. Quéneudec, *Transport of fluids in cement–rubber composite,* Cement and Concrete Composites 26 (1) (2004) 21–29.

[18] N. Segre and I. Joekes, *Use of tire rubber particles as addition to cement paste,* Cement and Concrete Research 30 (9) (2000) 1421–1425.

[19] BSI, EN 13877-1, *Concrete pavements Part 1: Materials,* BSI 389 Chiswick High Road, London W4 4AL, UK, 2013.

[20] M. Gesoğlu and E. Güneyisi, *Permeability properties of self-compacting rubberized concretes,* Construction and Building Materials 25 (8) (2011) 3319–3326.
[21] M. Gesoglu and E. Guneyisi, *Strength development and chloride penetration in rubberized concretes with and without silica fume,* Materials and Structures 40 (9) (2007) 953–964.
[22] A.J. Kardos and S.A. Durham, *Strength, durability, and environmental properties of concrete utilizing recycled tire particles for pavement applications,* Construction and Building Materials 98 (2015) 832–845.
[23] İ.B. Topçu and A. Demir, *Durability of rubberized mortar and concrete,* Journal of Materials In Civil Engineering 19 (2) (2007) 173–178.
[24] V. Marcos-Meson, A. Michel, A. Solgaard, G. Fischer, C. Edvardsen, and T.L. Skovhus, *Corrosion resistance of steel fibre reinforced concrete - A literature review,* Cement and Concrete Research 103 (2018) 1–20.
[25] BSI, EN 197-1, *Cement — Part 1: Composition, specifications and conformity criteria for common cements,* BSI 389 Chiswick High Road, London W4 4AL, UK, 2011.
[26] ASTM, C136, *Standard test method for sieve analysis of fine and coarse aggregates,* ASTM International, West Conshohocken, PA, doi:10.1520/C0136-06, 2006.
[27] BSI, EN 12390-2, *Testing hardened concrete, Part 2: Making and curing specimens for strength tests,* BSI 389 Chiswick High Road, London W4 4AL, UK, 2009.
[28] BSI, *EN 12350-2, Testing fresh concrete, Part 2: Slump-test,* BSI 389 Chiswick High Road, London W4 4AL, UK, 2009.
[29] BSI, EN 12350-7, *Testing fresh concrete, Part 7: Air content — Pressure,* BSI 389 Chiswick High Road, London W4 4AL, UK, 2009.
[30] BSI, EN 12350-6, *Testing fresh concrete Part 6: Density,* BSI 389 Chiswick High Road, London W4 4AL, UK, 2009.
[31] BSI, EN 12390-3, *Testing hardened concrete, Part3: Compressive strength of test specimens,* BSI 389 Chiswick High Road, London W4 4AL, UK, 2009.
[32] RILEM, *TC 162-TDF, Test and design methods for steel fibre reinforced concrete, Bending test, Final Reccomendation,* Materials and Structures 35 (2002) 579-582.
[33] JSCE, SF-4, *Method of test for flexural strength and flexural toughness of steel fiber reinforced concrete, Japan Concrete Institute, Tokio, Japan,* 1984.
[34] R.F. Feldman and V.S. Ramachandran, *Differentiation of interlayer and adsorbed water in hydrated Portland cement by thermal analysis,* Cement and Concrete Research 1 (6) (1971) 607–620.
[35] M. Farage, J. Sercombe, and C. Galle, *Rehydration and microstructure of cement paste after heating at temperatures up to 300 C,* Cement and Concrete Research 33 (7) (2003) 1047–1056.
[36] A. Graeff, *Long term performance of recycled steel fibre reinforced concrete for pavement applications*, in *Department of Civil and Structural Engineering*, 2011, The University of Sheffield, Sheffield.
[37] RILEM, TC 116-PCD, *Test for gas permeability of concrete. A, B and C: Permeability of concrete as a criterion of its durability,* Materials and Structures 32 (1999) 174–179.
[38] BSI, EN 13057:200, *Products and systems for the protection and repair of concrete structures - Test methods - Determination of resistance of capillary absorption,* BSI 389 Chiswick High Road, London W4 4AL, UK, 2002.
[39] C. ASTM, *1202,* Rapid Chloride Permeability 1997.
[40] BSI, EN 12390-11, *Testing hardened concrete - Part 11: Determination of the chloride resistance of concrete, unidirectional diffusion,* BSI 389 Chiswick High Road, London W4 4AL, UK, 2015.
[41] V. Baroghel-Bouny, P. Belin, M. Maultzsch, and D. Henry. *AgNO3 spray tests: advantages, weaknesses, and various applications to quantify chloride ingress into*

concrete. Part 1: Non-steady-state diffusion tests and exposure to natural conditions, Materials and Structures 40 (8) (2007) 759.

[42] F. He, C. Shi, Q. Yuan, C. Chen, and K. Zheng, *AgNO 3-based colorimetric methods for measurement of chloride penetration in concrete,* Construction and Building Materials 26 (1) (2012) 1–8.

[43] I. Ismail, S.A. Bernal, J.L. Provis, R. San Nicolas, D.G. Brice, A.R. Kilcullen, S. Hamdan, and J.S. van Deventer, *Influence of fly ash on the water and chloride permeability of alkali-activated slag mortars and concretes,* Construction and Building Materials 48 (2013) 1187–1201.

[44] M.-Y. Kim, E.-I. Yang, and S.-T. Yi, *Application of the colorimetric method to chloride diffusion evaluation in concrete structures,* Construction and Building Materials (2013) 239–245.

[45] R. Siddique and T.R. Naik, *Properties of concrete containing scrap-tire rubber–an overview,* Waste Management (Oxford) 24 (6) (2004) 563–569.

[46] H. Hu, P. Papastergiou, H. Angelakopoulos, M. Guadagnini, and K. Pilakoutas, *Mechanical properties of SFRC using blended manufactured and recycled tyre steel fibres,* Construction and Building Materials 163 (2018) 376–389.

[47] Council of the European Union, *Council Directive 1999/31/EC of 26 April 1999 on the landfill of waste*, 1999.

[48] A.P. Singh and D. Singhal, *Permeability of steel fibre reinforced concrete influence of fibre parameters,* Procedia Engineering 14 (2011) 2823–2829.

[49] O. Karahan, E. Özbay, K. Hossain, M. Lachemi, and C.D. Atiş, *Fresh, mechanical, transport, and durability properties of self-consolidating rubberized concrete,* ACI Materials Journal 109 (4) (2012).

[50] P. Sukontasukkul and K. Tiamlom, *Expansion under water and drying shrinkage of rubberized concrete mixed with crumb rubber with different size,* Construction and Building Materials 29 (2012) 520–526.

[51] V. Baroghel-Bouny, *Evaluation and prediction of reinforced concrete durability by means of durability indicators. Part I: new performance-based approach*, Concrete Life'06-International RILEM-JCI Seminar on Concrete Durability and Service Life Planning: Curing, Crack Control, Performance in Harsh Environments, RILEM Publications SARL, 2006.

[52] A. Du Preez and M. Alexander, *A site study of durability indexes for concrete in marine conditions,* Materials and Structures 37 (3) (2004) 146–154.

[53] J.R. Mackechnie, *Predictions of reinforced concrete durability in the marine environment, University of Cape Town, 1995.*

[54] F. Pelisser, N. Zavarise, T.A. Longo, and A.M. Bernardin, *Concrete made with recycled tire rubber: effect of alkaline activation and silica fume addition,* Journal of Cleaner Production 19 (6) (2011) 757–763.

[55] F. Olorunsogo and N. Padayachee, *Performance of recycled aggregate concrete monitored by durability indexes,* Cement and Concrete Research 32 (2) (2002) 179–185.

[56] M. Alexander and B. Magee, *Durability performance of concrete containing condensed silica fume,* Cement and Concrete Research 29 (6) (1999) 917–922.

[57] M. Alexander, J. Mackechnie, and Y. Ballim, *Guide to the use of durability indexes for achieving durability in concrete structures,* Research Monograph (1999) 2.

[58] V. Baroghel-Bouny, P. Belin, M. Maultzsch, and D. Henry, *$AgNO_3$ spray tests: advantages, weaknesses, and various applications to quantify chloride ingress into concrete. Part 1: Non-steady-state diffusion tests and exposure to natural conditions,* Materials and Structures 40 (8) (2007) 759–781.

[59] K. Hong and R.D. Hooton, *Effects of cyclic chloride exposure on penetration of concrete cover,* Cement and Concrete Research 29 (9) (1999) 1379–1386.

[60] A.M. Neville, *Properties of concrete,* 4th edition, John Wiley & Sons, Harlow,UK, 1996, p. 844.

[61] G. Glass and N. Buenfeld, *The presentation of the chloride threshold level for corrosion of steel in concrete,* Corrosion Science 39 (5) (1997) 1001–1013.997;39(5):1001-1013.

[62] S. Assié, G. Escadeillas, and V. Waller, *Estimates of self-compacting concrete 'potential'durability.* Construction and Building Materials 21 (10) (2007) 1909–1917.

Chapter 4

Freeze-Thaw Resistance of Steel Fibre Reinforced Rubberised Concrete (SFRRuC)

A. Alsaif, S.A. Bernal, M. Guadagnini, and K. Pilakoutas. Freeze-Thaw Resistance of Steel Fibre Reinforced Rubberised Concrete. Construction and Building Materials 195 (2019) 450-458.

Author contribution statement

Dr Bernal, Dr Guadagnini and Prof. Pilakoutas supervised the PhD study of the first author. All authors discussed the results and commented on the manuscript.

This study evaluates the freeze-thaw performance of steel fibre reinforced rubberised concretes (SFRRuC) engineered for flexible concrete pavements. The effect of large volumes of fine and coarse rubber particles (i.e. 30% and 60% volumetric replacement of natural aggregates) is determined for concretes reinforced with 40 kg/m^3 of a blend of manufactured steel fibres and recycled tyre steel fibres. The freeze-thaw performance is assessed through surface scaling, internal damage, residual compressive strength and flexural behaviour. The results show that SFRRuC are able to withstand 56 freeze-thaw cycles with acceptable scaling and without presenting internal damage or degradation in mechanical performance. This indicates that SFRRuC can perform well under extreme freeze-thaw conditions and can be used to construct long-lasting flexible pavements as a sustainable alternative to asphalt concretes.

This chapter consists of a "stand alone" journal paper and contains a relevant bibliography at the end of the chapter. Appendix C provides additional information and further test results.

4.1 Introduction

The use of concrete pavement slabs in regions experiencing severe freeze-thaw cycles is challenging, as concretes used for this application must withstand harsh environmental conditions during their service-life. One of the main factors compromising the durability of concrete pavements in such conditions is that drastic changes in temperature produce extra internal stresses causing concrete deterioration [1, 2]. Ice lenses can also form beneath the concrete surface as a result of uneven frost action on the subgrade and can potentially create unsupported regions in the pavement structure and cause additional flexural stresses [3]. Furthermore, de-icing salts, which are used to melt ice and snow, contain high volumes of sodium and/or magnesium chloride and can induce corrosion of the steel reinforcement and surface spalling [4, 5]. Hence, it is required to design concretes that can meet the mechanical strength requirements for paving, with the ability to withstand aggressive in-service conditions such as chlorides attack and freeze-thaw.

According to the European Tyre Recycling Association (ETRA) [6], each year in the 28 European member states and Norway around 300 million post-consumer tyres are discarded as waste. Much of these end up in landfills or are incinerated, despite the fact that they contain high performance constituent materials. According to ETRA [6], the composition of car tyres on the European Union market (by weight) are 48% rubber, 22% carbon black, 15% metal, 5% textile, and 10% others. Strict environmental protocols have been considered in most developed countries to control the disposal of waste tyres and the European Directive 1991/31/EC [7] has forbidden the land filling of whole post-consumer tyres since 2003 and shredded tyres since 2006 [8-10]. The European Directive 2008/98/EC [11] has provided a disposal hierarchy to encourage the management of post-consumer tyres that places reuse and recycling above incineration. A possible waste management solution is to find use for the post-consumer tyre materials in the construction industry. This improves sustainability by preventing environmental pollution as well as saving natural aggregate from depletion, and it is economically viable as some of the costly conventional materials (e.g. steel fibres) can be saved.

During the last three decades, rubber aggregates have been used in asphalt-rubber mixtures for pavement applications [12]. It has been noted that the use of rubber helps to reduce noise and increase resistance to temperature variation and freeze-thaw action, thus lowering maintenance costs and enhancing service life [13, 14]. The use of rubber aggregates as a partial substitution of natural aggregates in concrete has also been investigated by several researchers

[8, 15-17]. It has been demonstrated that, compared to conventional concrete, rubberised concrete (RuC) has larger deformability [15, 18], lower density [19-21], and higher sound absorption, skid and impact resistance as well as enhanced electrical and thermal insulation [10, 22-24]. Conversely, RuC suffers from increased air content as well as reduced workability, strength and stiffness [8, 25, 26]. As a result, RuC is rarely used in structural applications.

The durability properties of RuC are also not well understood. Few studies have assessed the freeze-thaw resistance of RuC and most focused on the resistance of RuC containing crumb rubber only [1, 2, 27-30]. Savas et al. [30] investigated the freeze-thaw resistance of RuC containing different amounts of crumb rubber. They observed that RuC mixes with replacement ratios of 10% and 15% by weight of cement (2–6 mm in size) exhibited durability factors (DFs) higher than the minimum 60% after 300 freeze-thaw cycles specified by ASTM C666/C666M-15 [31], whereas mixes with 20% and 30% could not meet the minimum DF recommended. Similarly, Kardos and Durham [32] assessed the rapid freeze-thaw resistance of plain concrete and RuC mixes with up to 50% sand replacement by volume. The authors found that RuC containing 10% crumb rubber exhibited the highest DF followed by the 20% RuC while the plain concrete and 30% RuC, showed comparable DFs. The 40% RuC and 50% RuC failed to withstand freeze-thaw action after 300 cycles as their DFs fell below 60%. Richardson et al. [28, 29], on the other hand, indicated that the addition of 0.6% by weight of crumb rubber with size smaller than 0.5 mm provided significant freeze-thaw protection in concrete.

Deterioration of concrete subjected to repeated freeze-thaw actions occur due to the formation of micro ice bodies within the concrete pores, which expand up to 9% compared to the volume of water [33, 34]. If the concrete paste becomes critically saturated and there is no space for this volume expansion, hydraulic pressures and tensile stresses can be generated in the pores, contributing to pore enlargement [35]. Consequently, the enlarged pores can be filled with water from the environment due to water uptake phenomena, causing larger tensile stress when frozen again and eventually leading to deterioration. Hence, the pore structure governs the rate and level of damage caused by freeze-thaw. More interconnected and larger pores are expected to lead to more water uptake and damage. The freeze-thaw resistance of concrete can be improved by providing air-entraining agents to create empty and closely spaced bubbles, which act as receiver of the excess water, thus relieving the pressure created in the concrete due to ice formation. In full saturation conditions, however, “the hydraulic pressure theory” is not applicable since non-frozen water cannot find a way to escape [36]. It is believed that crumb rubber particles can promote the formation of pores of similar quality to those created by air-

entraining agents [28, 37]. Khalo et al. [25] attributed the entrapment of air to the hydrophobic nature and rough surfaces of rubber particles, which entrap air during the mixing process. Hence, it is evident that the amount and size of rubber particles incorporated play a major role in the RuC freeze-thaw resistance, but there appears to be a limit to the replacement ratio that can lead to beneficial results. It has been reported for rubberised mortars and concretes that the amount of rubber replacement should be limited to a maximum of 10% [2] or 30% [32] by volume of fine aggregate in order to obtain acceptable durability.

In a recent study, the authors [38] demonstrated that the inclusion of fibres in RuC with high volumes of rubber (e.g. 30% or 60%) promote the development of SFRRuC with enhanced flexibility and ductility characteristics and flexural strengths that comply with the specifications defined in pavement design EN 13877-1 [39]. It has also been identified [40] that the substitution of natural aggregate by rubber particles increases the permeability of SFRRuC (i.e. volume of permeable voids and sorptivity) as rubber content increases. However, this increment is minor and the permeability properties of these concretes lie within the range of highly durable concretes. Furthermore, SFRRuC exhibit very high resistance to chloride permeability when assessed under accelerated wet-dry cycles [40]. The combination of such properties makes SFRRuC mixes ideal candidates for flexible concrete pavements. However, the effect of large volume of rubber on freeze-thaw resistance needs to be addressed. Due to the weak bond between cementitious materials and rubber particles [25, 26], micro-cracks forming in RuCs might propagate locally at a fast rate, making these materials more prone to damage. However, the authors hypothesised that this issue would be greatly mitigated by the inclusion of fibres in RuC as fibres tend to bridge micro-cracks and resist their opening. Hence, this study aims to examine the influence of freeze-thaw on the performance of SFRRuC under accelerated conditions. Performance is assessed through visual inspection of the specimens, mass loss, coefficient of thermal expansion (CTE), changes in relative dynamic modulus of elasticity (RDM), and residual mechanical properties including compressive strength, flexural strength, flexural modulus of elasticity and toughness.

4.2 Experimental Programme

4.2.1 Materials and concrete mix designs

4.2.1.1 Materials

Concrete mixtures were produced using a ternary blend of Portland lime cement type CEM II 52.5N, with silica fume (SF) and pulverised fuel ash (PFA) as cement replacements (10% by

weight for each). Two types of high range water-reducing admixtures were used: a) polycarboxylate polymer plasticiser and b) superplasticiser.

Natural river sand with particle size of 0/5 mm and specific gravity (SG) of 2.64 was used as fine aggregate (FA), while natural river gravel with particle sizes of 5/10 mm and 10/20 mm and a SG of 2.65 was employed as coarse aggregate (CA). Rubber aggregates used in this experimental study were recovered mechanically from post-consumer tyres. The fine rubber (FR) particles were supplied in three different sizes, 0/0.5 mm, 0.5/2 mm and 2/6 mm, and were used to replace 22.2%, 33.4%, 44.4% of FA volume, respectively. The course rubber (CR) particles were provided in two sizes, 5/10 mm and 10/20 mm, and were used to replace the CA in equal amounts. The specific gravity of 0.8, determined by the authors [38], was employed to calculate the volume of rubber particles. Figure 4.1 shows the particle size distribution of all aggregates used in this study, obtained according to ASTM-C136 [41].

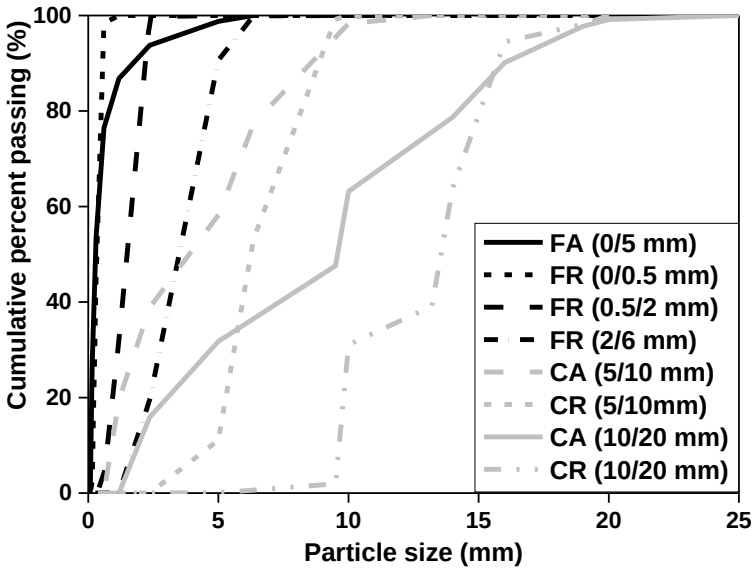

Figure 4.1: Particle size distributions

4.2.1.2 Concrete mix designs

Four different concrete mixes were prepared in this study including a plain concrete mix, a steel fibre reinforced concrete (SFRC) mix, and two SFRC rubberised concrete (SFRRuC) mixes, in which rubber aggregates were used as partial replacement for both FA and CA with 30% or 60% by volume. The amount of steel fibres added in the SFRC and SFRRuC mixes was 40 kg/m^3, as used in structural concrete, using equal amount of: a) crimped type manufactured steel fibres (MSF) with lengths of 55 mm and diameters of 0.8, and b) recycled tyre steel fibres (RTSF) with lengths between 15-45 mm (>60% by mass) and diameters <0.3 mm. Further details about the fibres characteristics are reported in [38, 42].

A mix ID was adopted for easy reference. It contains a number and a letter, where the number can be 0, 30 or 60, denoting the volumetric percentages of rubber aggregates used as partial replacement of natural aggregates, while the letter can be either P or BF (Plain or Blend of Fibres, respectively), referring to the absence or presence of the steel fibre reinforcement in the concrete mix. Table 4.1 shows the mixes IDs and variables.

Table 4.1 Mixes IDs and variables

Mix ID	*0P*	*0BF*	*30BF*	*60BF*
FR replacing FA by volume (%)	0	0	30	60
CR replacing CA by volume (%)	0	0	30	60
Amount of MSF (kg/m^3)	0	20	20	20
Amount of RTSF (kg/m^3)	0	20	20	20

All concretes assessed in this study were designed with 340 kg/m^3 of Portland cement, 42.5 kg/m^3 of SF, 42.5 kg/m^3 of PFA , 820 kg/m^3 of FA, 1001 kg/m^3 of CA, 150 l/m^3 of tap water (water /cement = 0.35), with 2.5 l/m^3 of plasticiser and 5.1 l/m^3 of superplasticiser. All mix design parameters were kept constant in this study except from the aggregates volume (see section 4.2.1.1). This study targeted slump of class S3 according to EN 206 [43] or higher (≥ 90 mm), therefore, the amount of plasticiser was also increased to 3.25 l/m^3 for *30BF* mix and to 4.25 l/m^3 for *60BF* mix to attain the targeted slump. The adopted concrete mix design was selected based on the outcomes of a previous study [21] evaluating RuC, in which it was identified that similar large volumes of aggregate replacements do not induce excessive degradation in fresh properties compared with reference concretes without rubber.

4.2.1.3 Mixing, casting and curing procedure

The production of the concrete mixes started with dry mixing natural and rubber aggregates for 30 s using a pan mixer. Half of the total amount of water was then introduced to the mixer, and the materials were mixed for another 1 min. Subsequently, mixing was halted for 3 min, to allow aggregates to gain saturation, and the cementitious materials were added. After that, mixing was continued for 3 min during which the remaining water and chemical admixtures were gradually added. Finally, the steel fibres were manually integrated, and mixing was continued for another 3 min.

Prior to casting, the concrete fresh properties including slump, air content and unit weight were assessed based on methods described in EN 12350-2 [44], EN 12350-7 [45], and EN 12350-6 [46],

respectively. Table 4.2 summarises the fresh properties of the concrete mixes. The results show that the inclusion of rubber particles in the fresh concrete mixes reduces the slump and unit weight, and increases the air content.

Table 4.2 Fresh properties of the tested concrete mixes

Mix ID	*0P*	*0BF*	*30BF*	*60BF*
Slump (mm)	235	200	155	110
Air content (%)	1.7	1.3	2.3	2.9
Unit weight (kg/m^3)	2401	2425	2175	1865

Concrete was cast in the moulds using two layers of casting (according to EN 12390-2) [47] and was vibrated on a shaking table (25s per layer). The specimens were then cured in the moulds for 48 h with wet hessian and sealed with plastic. Subsequently, all specimens were stored in a mist room at a temperature of 21 ℃ $\pm$ 2 and relative humidity of 95 $\pm$ 5% for 10 months. This curing age was selected considering that in countries experiencing severe winters, concrete casting on-site typically takes place in spring (or summer) and therefore it is most likely that the first freeze-thaw will be experienced within 10 months of age.

Four cubes and three prisms per mix were removed from the mist room, marked as 'F-T' and subjected to freeze-thaw conditions, while a similar number of specimens was kept as 'control' in the mist room. The compressive strength and flexural behaviour of all 'F-T' and 'control' specimens were evaluated at the end of the freeze-thaw conditioning period. Two prisms per mix were used to assess the coefficient of thermal expansion (CTE) as described in section 4.2.2.3.

4.2.2 Test set-up and instrumentation

4.2.2.1 Freeze-thaw testing

The freeze-thaw resistance of concrete cubes and prisms was assessed based on: (i) visual analysis in terms of damage caused by freeze-thaw action, (ii) mass loss due to cubes scaling following the recommendation of PD CEN/TS 12390-9 [48], (iii) beam tests according to PD CEN/TR15177 [49] to assess the internal damage of concrete prisms through the evaluation of their RDMs using the measurements obtained from ultrasonic pulse transit time (UPTT), and (iv) residual compressive strength and flexural behaviour.

The concrete specimens were placed in stainless steel containers and were fully immersed in a 3% NaCl solution. The containers were then placed into a chamber that was programmed to apply continuous cycles of freeze and thaw with temperature ranging from -15 ℃ to 20 ℃ and controlled through a thermocouple embedded in the centre of a concrete cube. Figure 4.2 shows the experimental temperature profile compared with the desired temperature profile specified in PD CEN/TS 12390-9 [48].

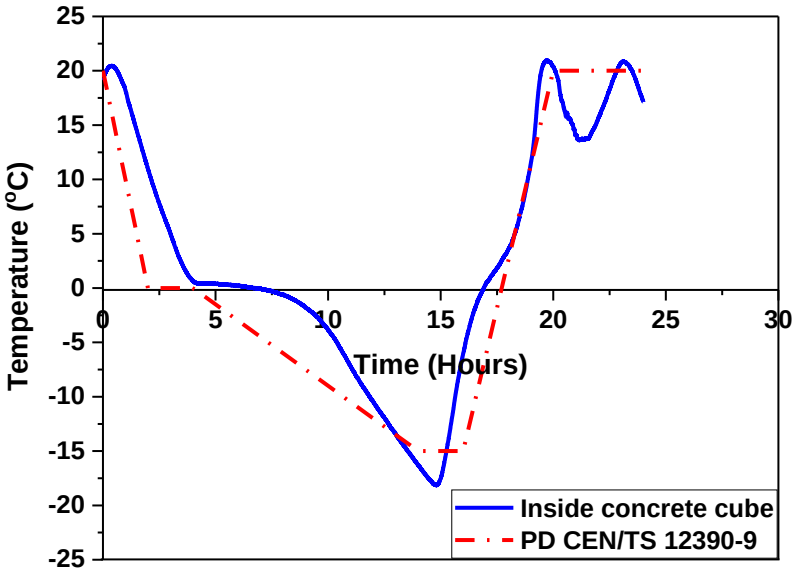

Figure 4.2: Temperature profile measured in the centre of a concrete cube using a thermocouple, compared with that of PD CEN/TS 12390-9 [48]

The mass loss and UPTT were determined after 7, 14, 28, 42 and 56 freeze-thaw cycles. At each of these defined cycles, during the thawing phase, the concrete cubes and prisms were removed and first visually examined in terms of surface damage. The cubes were then thoroughly brushed to remove any loose parts and then weighed. All detached materials were collected, oven dried for 24 hours at 105 ℃ and weighed to the nearest 0.1g. The percentage of cumulative mass loss after n cycles, was calculated according to Equation (1):

$$\text{Cummulative mass loss } (\%), \mathrm{n} = \frac{\sum_{i=1}^{n} \mathrm{M}_{d,n}}{M_0} \cdot 100 \qquad (1)$$

where, $M_{d,n}$ is the mass of the oven dried scaled material collected after cycle *n*, and M_0 is the initial mass of specimens after curing and before testing.

Similarly, the concrete prisms were thoroughly brushed, surface dried, and were then fitted with two transducers on the two opposite sides of the prisms to measure the UPTT. The transducers were pressed against the concrete surfaces, using the same pressure each time, until a constant

minimum value was achieved. The RDM of elasticity after *n* cycles, was calculated using Equation (2) below;

$$\mathrm{RDM,n}\ (\%) = \left(\frac{UPTT_0}{UPTT_n}\right)^2 \cdot 100 \qquad (2)$$

where $UPTT_0$ is the initial UPTT of the specimen, in μs, while UPTTn is the specimen UPTT after *n* freeze-thaw cycles, in μs. Cubes and prisms were then returned to the containers with fresh 3% NaCl solution and test was resumed.

4.2.2.2 Compressive cube tests and flexural tests on prisms

Concrete cubes were tested under uniaxial compressive loading according to EN 12390-3 [50] at a loading rate of 0.4 MPa/s. Concrete prisms were tested under 4-point bending test configuration following the recommendations of the JSCE [51], using an electromechanical testing machine. The net mid-span deflection was recorded by two linear variable differential transformers (LVDTs), placed on an aluminium yoke. The load was applied in displacement control at a constant rate of deflection at the mid-span of the prism of 0.2 mm/min until a deflection of 6 mm.

4.2.2.3 Coefficient of thermal expansion

The CTE was determined according to the TI-B 101 procedure [52] using two duplicate prisms per mix. The CTE of the rubber particles used in this study was also determined to be approximately 80 x 10^{-6} m/mK, which is 10 times higher than that of the limestone natural aggregates used in this study, and obtained from FDA [53]. Such significant difference in CTE may induce internal stresses during the freeze-thaw cycles.

4.3 Results and Discussion

4.3.1 Visual inspection

Figure 4.3 shows the appearance of the tested specimens before and after completing 56 cycles of freeze-thaw action. Surface scaling and concrete pop-outs are the two signs of deterioration that are observed in all tested specimens. Surface scaling (i.e. delamination) is expected to develop when internal stresses exceed the tensile or shear strength of the surface layer, whilst the build-up of pressure around the coarse aggregate particles can cause the concrete between the particles and the nearest concrete face to pop-outs [54].

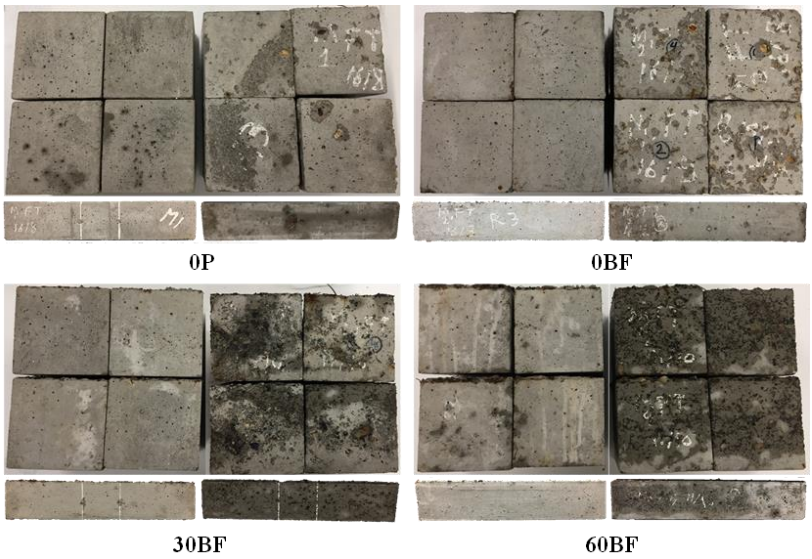

Figure 4.3: Specimens appearance before (left) and after (right) completing 56 cycles of freeze-thaw action

ASTM C672/C672M – 12 [55] specifies a visual rating category depending on the severity of surface scaling, as shown in Table 4.3. Based on the appearance of the concretes after exposure (Figure 4.3), concretes without rubber aggregates (i.e. *0P* and *0BF*) are rated 3, while SFRRuC specimens (i.e. *30BF* and *60BF*) are rated 4. The amount of concrete scaling and mortar coming off at the end of the freeze-thaw cycles is higher in rubberised concrete. This is a likely consequence of the higher volume of permeable voids (VPV) identified in SFRRuC (see Figure 4.4 [40]), and the resulting increase in water uptake of the samples during testing compared to specimens without rubber aggregates. It has been reported [56] that the connectivity of pores is higher at the surface of the concrete specimens and typically increases at higher freeze-thaw cycles. Therefore, concretes with higher permeability are expected to suffer more severe damage. Despite the fact that the SFRRuC specimens show moderate to severe scaling, they withstood 56 freeze-thaw cycles without severe damage.

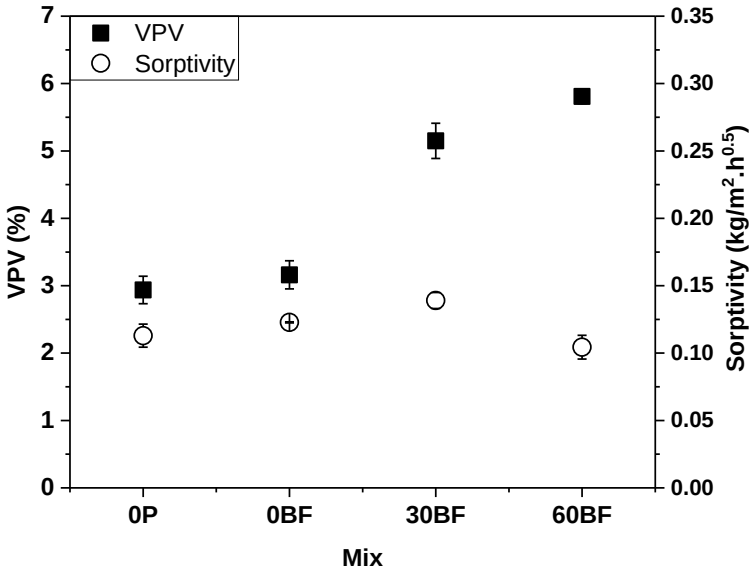

Figure 4.4: VPV (left) and sorptivity (right) of all tested concretes [40]

Table 4.3 Surface scaling rating adapted from ASTM C672/C672M – 12 [55]

Rating	Condition of surface
0	No scaling
1	Very slight scaling (3 mm [1/8 in.] depth max., no coarse aggregate visible
2	Slight to moderate scaling
3	Moderate scaling (some coarse aggregate visible)
4	Moderate to severe scaling
5	Sever scaling (coarse aggregate visible over entire surface)

4.3.2 Mass of scaled concretes

Figure 4.5 shows the mean cumulative mass loss versus the number of freeze-thaw cycles. Error bars represent one standard deviation of four measurements. It is evident that *0P* specimens exhibit minimal mass loss throughout the test, while *0BF* and *60BF* specimens show similar mass loss behaviour, which is higher than *0P*. The SFRRuC specimens with 30% rubber replacement, *30BF*, display the highest rate of mass loss, especially after 14 freeze-thaw cycles. A previous study by the authors [40] on the transport properties of the same four concrete mixes shows that *30BF* specimens present the highest sorptivity values (see Figure 4.4). The higher sorptivity for the *30BF* specimens was attributed to the large amount of fine pores which facilitated water uptake and caused these specimens to be more prone to damage due to freeze-thaw cycles. On the other hand, owing to the high amount of large coarse rubber particles and the non-sorptive nature of rubber, a reduction in sorptivity was observed in the *60BF* specimens.

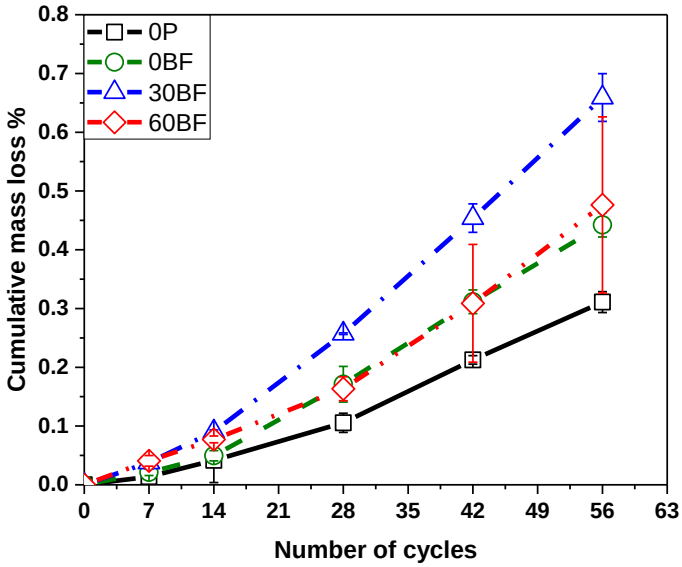

Figure 4.5: Cumulative mass loss as a function of freeze-thaw cycles

For all concrete mixes, the ratios between the masses of scaled materials after completing 56 freeze-thaw cycles (M_{56}) to that after 28 cycles (M_{28}) are lower than two, and the M_{56} are less than 1.0 kg/m^2 (see Table 4.4). Hence, they all fall under the acceptable resistance category, as specified by the Swedish standard SS 13 72 44 ED [57]. Consequently, this study contradicts previous work [2, 32] and shows that when using fibres, the amount of rubber aggregates can be significantly increased (up to 60%) without compromising durability.

The high resistance to freeze-thaw exhibited by the tested concretes can not be attributed to differences in thermal properties as minimal changes in the coefficient of thermal expansion (CTE) were obtained (see Table 4.5). This indicates that rubber aggregates may counteract the freeze-thaw effect even in highly porous concretes due to their low stiffness, which offers less resistance to expansion. It should also be noted that the addition of rubber increases air entrainment (see VPV in Figure 4.4 as found in [40]), which can also create a pressure release system for freeze-thaw phenomena [58]. Furthermore, rubber particles, with their excellent damping characteristic [20, 59], may contribute somehow in balancing the internal stresses and act like absorbers for the temperature and freeze-thaw induced stresses and deformations [4]. The fibre blends also participate by bridging and controlling cracks.

Table 4.4 Mass loss results for all concrete mixes

Mix	M_{56}/M_{28}	Mass of scaled materials after 56 cycles, M_{56} (kg/m^2)
0P	1.5	0.5
0BF	1.1	0.6
30BF	1.2	0.9
60BF	1.9	0.7

Table 4.5 Coefficient of thermal expansions obtained for all concrete mixes

Mix	Coefficient of thermal expansion × 10^{-6} m/mk
0P	10.3-12.2
0BF	10.3-11
30BF	9.0-11.6
60BF	9.7-12.9

4.3.3 Effect of freeze-thaw on mechanical performance

4.3.3.1 Compressive strength

Table 4.6 summarises the average compressive strength and standard deviation (in brackets) derived from testing four specimens for each of the examined concretes. As expected, the addition of blended fibres enhances the compressive strength of control specimen *0BF* by 7% with respect to *0P*. The partial replacement of natural aggregates with rubber particles, however, considerably reduces the compressive strength reporting an average reduction of 58% for *30BF* and 88% for *60BF* compared to *0BF*. The two mechanisms responsible for such degradation in compressive strength are: (i) the lower stiffness and higher Poisson ratio of rubber compared to natural aggregates, and (ii) bond defects between rubber particles and matrix [25, 26]. Further discussions regarding the compressive strength reduction mechanism in SFRRuC are reported in [38], where similar results were obtained.

Table 4.6 Average compressive strength results of all concrete mixes

Mix	Compressive strength (MPa)		
	Control	F-T	Change on control (%)
0P	111 (3.8)	108 (3.8)	-3
0BF	118 (0.9)	110 (7.7)	-7
30BF	50 (4.0)	40 (5.3)	-20
60BF	14 (3.0)	12 (2.0)	-14

After 56 cycles of freeze-thaw (F-T), all concrete specimens exhibit minor compressive strength loss compared to the control specimens of the same mixes. The slight reduction in the compressive strength indicates that the freeze-thaw action has affected mostly the surface of the concrete, without compromising its internal integrity.

A good correlation is identified between the compressive strength and cumulative mass loss for all concrete specimens at the end of the 56 cycles (see Figure 4.6). The *30BF* specimens show the highest amount of cumulative mass loss, 0.66%, and compressive strength loss, 20%, which were most likely caused by the higher sorptivity of this mix (see Figure 4.4).

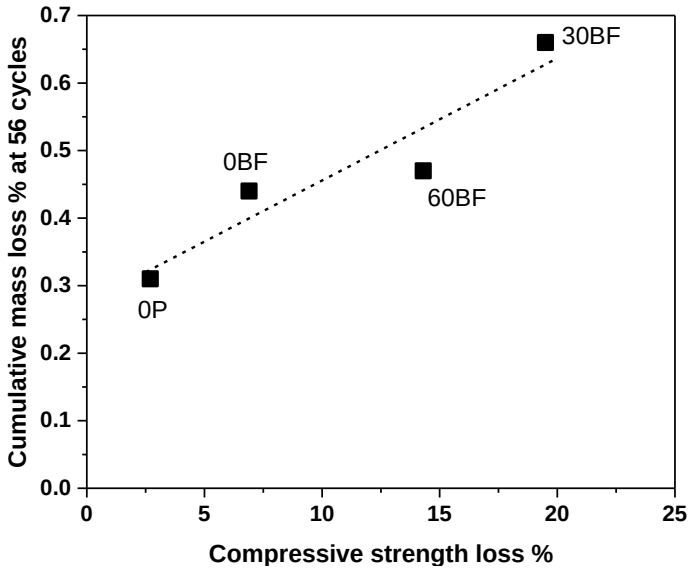

Figure 4.6: Correlation between the percentage of cumulative mass loss and compressive strength loss at the end of 56 freeze-thaw cycles

4.3.3.2 Flexural strength

Table 4.7 summarises the average values of flexural strength, modulus of elasticity and toughness of the control and F-T specimens as obtained from testing three specimens per mix. Values in brackets represent standard deviation.

Table 4.7 Average flexural strength, modulus of elasticity and toughness factor

Mix		*0P*	*0BF*	*30BF*	*60BF*
Flexural strength (MPa)	Control	8.1 (1.1)	9.4 (1.0)	6.1 (1.0)	3.7 (0.6)
	F-T	8.5 (1.3)	9.1 (0.5)	4.9 (0.8)	3.9 (0.6)
	Change on control (%)	5	-3	-20	5
Flexural modulus of elasticity (GPa)	Control	48 (2.2)	46 (0.1)	26 (0.5)	9.3 (1.0)
	F-T	47 (4.3)	44 (1.5)	25 (0.7)	8.8 (1.1)
	Change on control (%)	-3	-3	-3	-5
Flexural toughness factor (MPa)	Control	-	5.9 (0.3)	5.2 (0.9)	3.2 (0.5)
	F-T	-	5.2 (0.9)	3.8 (0.7)	3.4 (0.3)
	Change on control (%)	-	-12	-27	6

Table 4.7 shows that the addition of blended fibres enhances the flexural strength of *0BF* control specimens by 16%, compared to *0P*. On the other hand, the replacement of 30% and 60% of natural aggregates with rubber particles, as expected, reduces the flexural strength by 35% and 60% respectively, compared to *0BF*. It should be noted that the presence of steel fibres in SFRRuC mixes effectively mitigates the rate of reduction in flexural strength, compared to that in compressive strength, due to the ability of the fibres to control micro-cracking, as discussed in Alsaif et al. [38].

After completing 56 cycles of freeze-thaw action, the concretes *0P*, *0BF* and *60BF* show comparable flexural strength values to those of control specimens of the same mixes with small differences within one standard deviation. The flexural strength of the *30BF* specimens after 56 cycles of freeze thaw action, however, is 20% below that of the control specimens of the same mix, which is consistent with the reduction in compressive strength reported in Table 4.6. As mentioned earlier, the high sorptivity in the *30BF* mix [40] may have caused this reduction in strength. Nevertheless, all SFRRuC specimens studied here (both F-T and control) satisfy the flexural strength requirements specified in pavement design EN 13877-1[39].

4.3.3.3 Flexural modulus of elasticity

The elastic beam theory was adopted in this study to determine the secant modulus of elasticity of the load-deflection curves considering the region from 0 to 40% of the peak load. As shown in Table 4.7, the addition of steel fibres in conventional concrete specimens, *0BF*, marginally reduces the modulus of elasticity compared to *0P* specimens. This reduction was not anticipated as the addition of fibres was expected to slightly increase the modulus of elasticity of the composite due to their high stiffness, but may be explained by the increased volume of permeable voids, as discussed in [40]. The substantial decrease in the modulus of elasticity, however, for the SFRRuC specimens (48% for *30BF* and 80% for *60BF*) was expected due to the lower stiffness of the rubber aggregates, compared to the replaced natural aggregates [38]. After freeze-thaw action, minor reductions (3-5%) in the modulus of elasticity were recorded. The RDM was also investigated and it is discussed in the following section.

4.3.3.4 Relative dynamic modulus of elasticity

Figure 4.7 shows the mean RDM values as a function of the number of freeze-thaw cycles applied. Error bars represent one standard deviation of three measurements. It is worth mentioning that, during the periodical measurements, occasionally UPTT values went down due to difficulties of making contact with the sides of the concrete prism as these were severely roughened due to scaling. In general, the RDM values decrease with increasing number of freeze-thaw cycles. This is expected due to the typical increase in water uptake (capillary pores imbibe water) and, hence the UPTT values. It is also evident from Figure 4.7 that the rate of reduction in RDM values increases with the rubber content. This may indicate some loss in the bond between the rubber and cementitious materials [1], possibly due to the weak adhesion in the interfacial transition zone (ITZ). As all specimens survived 56 freeze-thaw cycles and their RDM values are above the threshold value of 80% defined by RILEM 2004 [60], all concrete mixes can be considered to be durable.

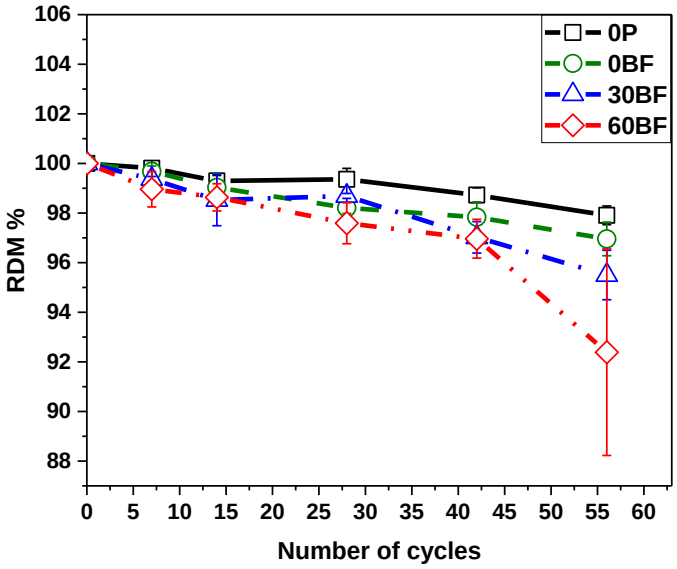

Figure 4.7: Change in relative dynamic modulus during freeze/thaw cycles

4.3.3.5 Load-deflection curve and flexural toughness factor

Figure 4.8 shows the average (of 3 prisms) stress-deflection curves. While the plain concrete specimens, *0P*, failed suddenly after reaching the peak stress, highlighting the brittleness of plain concrete in tension, *0BF*, *30BF* and *60BF* specimens continued sustaining further flexural stresses even after first crack. This is mainly due to the contribution of fibres in dissipating energy through their pull-out mechanism as well as in bridging cracks and resisting their opening [38]. Rubber particles also participated partially in enhancing the post-peak behaviour by absorbing some of the energy during loading and undergoing large deformation as identified by the authors in a previous study [38].

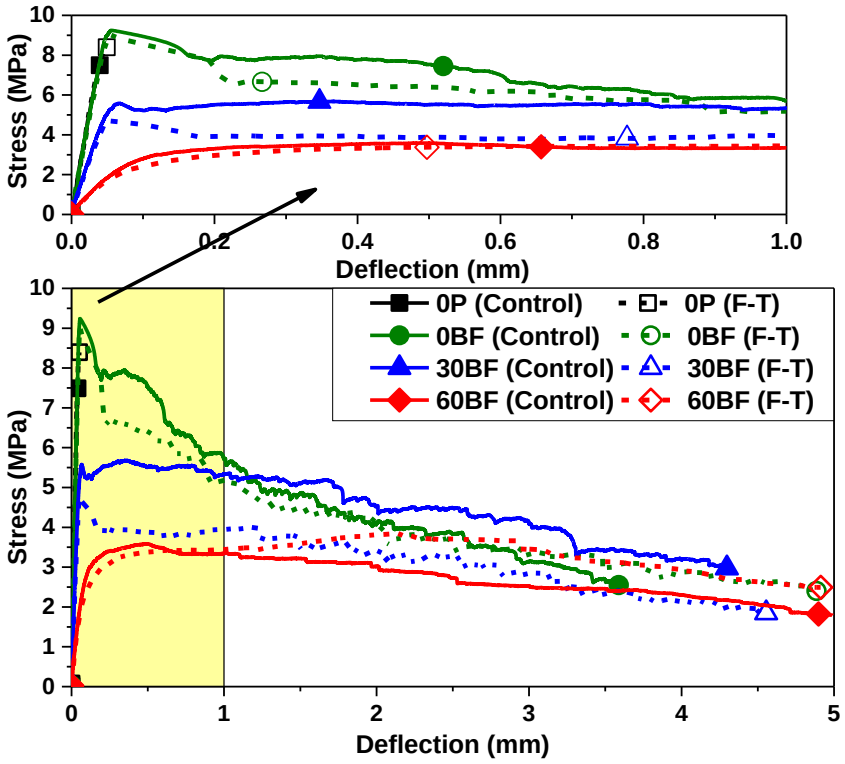

Figure 4.8: Average stress versus deflection curves for all concrete mixes

To further examine the effect of freeze-thaw action on the flexural behaviour of SFRC and SFRRuC, the flexural toughness factors were obtained (see Table 4.7) according to JSCE [51]. The toughness factor of the plain concrete mix, *0P*, is not included as its post-peak energy absorption behaviour is negligible. The area under the load-deflection curve is computed up to a deflection of δ_f = 2 mm and the flexural toughness factor is calculated according to Equation (3).

$$\text{Flexural toughness factor (MPa)} = \frac{Area\ under\ the\ curve \cdot L}{2 \cdot b \cdot h^2} \quad (3)$$

where L is the span length, in mm, b is the width of the specimen, in mm, h is the height of the specimen, in mm.

The toughness factor is found to decrease with increasing rubber content mainly due to the large reduction in flexural strength. After freeze-thaw action, the toughness factor decreases by 12% for *0BF* and 27% for *30BF* while it increases by 6% for *60BF*. Overall, F-T action did not have a major impact on flexural performance, except for *30BF* specimens due to their higher sorptivity (see Figure 4.4). This is mainly attributed to the presence of fibres which are more effective in enhancing flexural behaviour through mechanisms (crack bridging) that are not significantly affected by freeze-thaw.

4.3.4 General discussion on practical use

Previous research by the authors [38] showed that optimised flexible SFRRuC mixes were able to attain high ductility and flexibility, and achieve workability properties and flexural strengths that meet the specifications defined in pavement design [39]. It has also been identified in a subsequent research study [40] that the durability and permeability properties of these flexible SFRRuC mixes lie within the range of highly durable concrete based on commonly accepted "durability indicators" [57, 60-62]. In this article, the authors demonstrate the ability of these SFRRuC mixes to withstand 56 freeze-thaw cycles with acceptable scaling and without presenting internal damage or degradation in mechanical performance. Furthermore, the inclusion of a large amounts of waste tyre rubber leads to the development of flexible SFRRuC pavements with stiffness values similar to those of flexible asphalt pavements, i.e. around 8 GPa. Hence, these flexible SFRRuC are expected to accommodate subgrade induced movements and settlements arising from poor compaction during construction or temperature variations, including freeze-thaw. The body of this work shows that SFRRuC, which can be manufactured using conventional mixing techniques, is a promising solution for building sustainable road pavements.

4.4 Conclusion

This study assessed the freeze-thaw performance of steel fibre reinforced rubberised concretes (SFRRuC) produced with large contents of waste tyre rubber and reinforced with a blend of manufactured and recycled tyre steel fibres. Based on the experimental results, this study shows that all SFRRuC mixes successfully withstood 56 freeze-thaw cycles without being significantly damaged. The cubes show acceptable scaling resistance according to the Swedish Criteria SS 13 72 44 ED, while the prisms maintain RDMs values above the threshold value for internal damage (80%) specified in RILEM TC 176-IDC. Hence, as hypothesised by the authors, the inclusion of steel fibres in RuC greatly mitigates the negative effects of large volumes of rubber on freeze-thaw resistance.

The presence of steel fibres in SFRRuC mixes significantly reduces the rate of reduction in flexural strength due to the addition of large volumes of rubber, compared to that in compressive strength. All SFRRuC mixes show flexural strengths that satisfy the requirement for pavement design according to EN 13877-1.

Comparable mechanical performance is observed from specimens subjected to freeze-thaw and control specimens kept in the mist room, thus making SFRRuC a potentially sustainable flexible

concrete pavement solution capable of adequate freeze-thaw performance. For pavement applications, future studies should investigate the fatigue performance of this novel concrete.

Acknowledgements

The current experimental work was undertaken under the FP7 European funded collaborative project "Anagennisi: Innovative reuse of all tyre components in concrete" (Contract agreement number: 603722). The following companies offered materials and valuable in-kind contribution: Tarmac UK, Twincon Ltd, Aggregate Industries UK and Ltd Sika. Mr Alsaif would like to thank King Saud University and the Ministry of Education (Kingdom of Saudi Arabia) for sponsoring his PhD studies. Dr S.A. Bernal participation in this study has been sponsored by EPSRC through her ECF (EP/R001642/1).

4.5 References

[1] K.A. Paine, R. Dhir, R. Moroney, and K. Kopasakis, *Use of crumb rubber to achieve freeze/thaw resisting concrete*, in Challenges of Concrete Construction: Volume 6, Concrete for Extreme Conditions: Proceedings of the International Conference held at the University of Dundee, Scotland, UK, 2002, Thomas Telford Publishing.

[2] İ.B. Topçu and A. Demir, *Durability of rubberized mortar and concrete*, Journal of Materials in Civil Engineering 19 (2) (2007) 173-178.

[3] A. Vaitkus, J. Gražulytė, E. Skrodenis, and I. Kravcovas, *Design of frost resistant pavement structure based on road weather stations (RWSs) Data*, Sustainability 8 (12) (2016) 1328.

[4] O.A. Abaza and Z.S. Hussein, *flexural behavior of steel fiber-reinforced rRubberized concrete*, Journal of Materials in Civil Engineering 28 (1) (2015) 04015076.

[5] V. Baroghel-Bouny, P. Belin, M. Maultzsch, and D. Henry, *$AgNO_3$ spray tests: advantages, weaknesses, and various applications to quantify chloride ingress into concrete. Part 1: Non-steady-state diffusion tests and exposure to natural conditions*, Materials and Structures 40 (8) (2007) 759-781.

[6] ETRA, *The European Tyre Recycling Association*, 2016, Available at: http://www.etra-eu.org [Last accessed: 02/01/2018].

[7] Council of the European Union, *Council Directive 1999/31/EC of 26 April 1999 on the landfill of waste*, 1999.

[8] N.N. Eldin and A.B. Senouci, *Measurement and prediction of the strength of rubberized concrete*, Cement and Concrete Composites 16 (4) (1994) 287-298.

[9] A. Benazzouk, O. Douzane, K. Mezreb, B. Laidoudi, and M. Queneudec, *Thermal conductivity of cement composites containing rubber waste particles: Experimental study and modelling*, Construction and Building Materials 22 (4) (2008) 573-579.

[10] B.S. Mohammed, K.M.A. Hossain, J.T.E. Swee, G. Wong, and M. Abdullahi, *Properties of crumb rubber hollow concrete block*, Journal of Cleaner Production 23 (1) (2012) 57-67.

[11] Council of the European Union, *Council Directive 2008/98/EC on waste (Waste Framework Directive)*, 2008.

[12] J.A. Epps, *Uses of recycled rubber tires in highways*. Volume 198, 1994: Transportation Research Board.

[13] S.N. Amirkhanian and J.L. Burati Jr, *Utilization of waste tires in asphaltic materials,* Clemson University, SC (United States). Deptartment of Civil Engineering. Technical Report;PB-96-203062/XAB,CNN: Contract SPR-554; TRN: 62752193, 1996.

[14] B. Adhikari, D. De, and S. Maiti, *Reclamation and recycling of waste rubber*, Progress in Polymer Science 25 (7) (2000) 909-948.

[15] S. Raffoul, R. Garcia, D. Escolano-Margarit, M. Guadagnini, I. Hajirasouliha, and K. Pilakoutas, *Behaviour of unconfined and FRP-confined rubberised concrete in axial compression*, Construction and Building Materials 147 (2017) 388-397.

[16] F. Hernández-Olivares and G. Barluenga, *Fire performance of recycled rubber-filled high-strength concrete*, Cement and Concrete Research 34 (1) (2004) 109-117.

[17] F. Hernández-Olivares, G. Barluenga, M. Bollati, and B. Witoszek, *Static and dynamic behaviour of recycled tyre rubber-filled concrete*, Cement and Concrete Research 32 (10) (2002) 1587-1596.

[18] A. Alsaif, R. Garcia, M. Guadagnini, and K. Pilakoutas, *Behaviour of FRP-Confined Rubberised Concrete with Internal Recycled Tyre Steel Fibres*, in *High Tech Concrete: Where Technology and Engineering Meet: Proceedings of the 2017 fib Symposium, held in Maastricht, The Netherlands, June 12–14, 2017*, D.A. Hordijk and M. Luković, Editors. 2018, Springer International Publishing: Cham. p. 233-241.

[19] A. Grinys, H. Sivilevičius, D. Pupeikis, and E. Ivanauskas, *Fracture of concrete containing crumb rubber*, Journal of Civil Engineering and Management 19 (3) (2013) 447-455.

[20] F. Liu, W. Zheng, L. Li, W. Feng, and G. Ning, *Mechanical and fatigue performance of rubber concrete*, Construction and Building Materials 47 (2013) 711-719.

[21] S. Raffoul, R. Garcia, K. Pilakoutas, M. Guadagnini, and N.F. Medina, *Optimisation of rubberised concrete with high rubber content: An experimental investigation*, Construction and Building Materials 124 (2016) 391-404.

[22] P. Sukontasukkul and C. Chaikaew, *Properties of concrete pedestrian block mixed with crumb rubber*, Construction and Building Materials 20 (7) (2006) 450-457.

[23] T.C. Ling, H.M. Nor, and S.K. Lim, *Using recycled waste tyres in concrete paving blocks*, Proceedings of the ICE - Waste and Resource Management 163 (1) (2010) 37-45.

[24] C.A. Issa and G. Salem, *Utilization of recycled crumb rubber as fine aggregates in concrete mix design*, Construction and Building Materials 42 (2013) 48-52.

[25] A.R. Khaloo, M. Dehestani, and P. Rahmatabadi, *Mechanical properties of concrete containing a high volume of tire–rubber particles*, Waste Management 28 (12) (2008) 2472-2482.

[26] Z. Khatib and F. Bayomy, *Rubberized portland cement concrete*, Journal of Materials In Civil Engineering 11 (3) (1999) 206-213.

[27] X. Zhu, C. Miao, J. Liu, and J. Hong, *Influence of crumb rubber on frost resistance of concrete and effect mechanism*, Procedia Engineering 27 (2012) 206-213.

[28] A. Richardson, K. Coventry, V. Edmondson, and E. Dias, *Crumb rubber used in concrete to provide freeze–thaw protection (optimal particle size)*, Journal of Cleaner Production 112 (2016) 599-606.

[29] A.E. Richardson, K. Coventry, and G. Ward, *Freeze/thaw protection of concrete with optimum rubber crumb content*, Journal Of Cleaner Production 23 (1) (2012) 96-103.

[30] B. Savas, S. Ahmad, and D. Fedroff, *Freeze-thaw durability of concrete with ground waste tire rubber*, Transportation Research Record: Journal of the Transportation Research Board (1574) (1997) 80-88.

[31] ASTM, *C666/C666M − 15: Standard Test Method for Resistance of Concrete to Rapid Freezing and Thawing*, 2015.

[32] A.J. Kardos and S.A. Durham, *Strength, durability, and environmental properties of concrete utilizing recycled tire particles for pavement applications*, Construction and Building Materials 98 (2015) 832-845.

[33] T.C. Powers and T. Willis, *The air requirement of frost resistant concrete*, in *Highway Research Board Proceedings*, 1950.

[34] T.C. Powers, *A working hypothesis for further studies of frost resistance of concrete*, in *Journal Proceedings*, 1945.

[35] D.H. Bager, *Qualitative description of the micro ice body freeze-thaw damage mechanism in concrete*, in *Workshop proceeding no. 9: Nordic miniseminar: Freeze-Thaw Testing of Concrete – Input to revision of cen test methods*, 2010.

[36] B. Johannesson, *Dimensional and ice content changes of hardened concrete at different freezing and thawing temperatures*, Cement and Concrete Composites 32 (1) (2010) 73-83.

[37] A. Benazzouk, O. Douzane, T. Langlet, K. Mezreb, J. Roucoult, and M. Quéneudec, *Physico-mechanical properties and water absorption of cement composite containing shredded rubber wastes*, Cement and Concrete Composites 29 (10) (2007) 732-740.

[38] A. Alsaif, L. Koutas, S.A. Bernal, M. Guadagnini, and K. Pilakoutas, *Mechanical performance of steel fibre reinforced rubberised concrete for flexible concrete pavements*, Construction and Building Materials 172 (2018) 533-543.

[39] BSI, EN 13877-1, *Concrete pavements Part 1: Materials,* BSI 389 Chiswick High Road, London W4 4AL, UK, 2013.

[40] A. Alsaif, S.A. Bernal, M. Guadagnini, and K. Pilakoutas, *Durability of steel fibre reinforced rubberised concrete exposed to chlorides*, Construction and Building Materials 188 (2018) 130-142.

[41] ASTM, *C136, Standard test method for sieve analysis of fine and coarse aggregates, ASTM International, West Conshohocken, PA. doi:10.1520/C0136-06.*,2006.

[42] H. Hu, P. Papastergiou, H. Angelakopoulos, M. Guadagnini, and K. Pilakoutas, *Mechanical properties of SFRC using blended manufactured and recycled tyre steel fibres*, Construction and Building Materials 163 (2018) 376-389.

[43] BSI, BS 8500-1:2015+A1:2016*, Concrete – Complementary British Standard to BS EN 206. Part 1: Method of specifying and guidance for the specifier*, 2016.

[44] BSI, EN 12350-2*, Testing fresh concrete, Part 2: Slump-test,* BSI 389 Chiswick High Road, London W4 4AL, UK, 2009.

[45] BSI, EN 12350-7*, Testing fresh concrete, Part 7: Air content — Pressure,* BSI 389 Chiswick High Road, London W4 4AL, UK, 2009.

[46] BSI, EN 12350-6*, Testing fresh concrete Part 6: Density,* BSI 389 Chiswick High Road, London W4 4AL, UK, 2009.

[47] BSI, EN 12390-2*, Testing hardened concrete, Part 2: Making and curing specimens for strength tests,* BSI 389 Chiswick High Road, London W4 4AL, UK, 2009.

[48] BSI, PD CEN/TS 12390-9, *Testing hardened concrete - Part 9: Freeze-thaw resistance with de-icing salts - Scaling*, BSI 389 Chiswick High Road, London W4 4AL, UK, 2016.

[49] BSI, PD CEN/TR15177*, Testing the freeze-thaw resistance of concrete - Internal structural damage,* BSI 389 Chiswick High Road, London W4 4AL, UK, 2006.

[50] BSI, EN 12390-3*, Testing hardened concrete, Part3: Compressive strength of test specimens,* BSI 389 Chiswick High Road, London W4 4AL, UK, 2009.

[51] JSCE, SF-4*, Method of test for flexural strength and flexural toughness of steel fiber reinforced concrete,* Japan Concrete Institute, Tokio, Japan, 1984.

[52] TI-B, 101*, Test Method: Expansion Coefficient of Concrete,* Danish Technological Institute Building Technology, 1994.

[53] FDA, Federal Highway Administration Research and Technology*, Coordinating, Developing, and Delivering Highway Transportation Innovations*, 2016.

[54] T. Harrison, J.D. Dewar, and B. Brown, *Freeze-thaw Resisting Concrete: Its Achievement in the UK*, 2001: CIRIA.

[55] ASTM, C672 / C672M-12, *Standard Test Method for Scaling Resistance of Concrete Surfaces Exposed to Deicing Chemicals,* ASTM International, West Conshohocken, PA, www.astm.org, 2012.

[56] J. Yuan, Y. Liu, H. Li, and C. Yang, *Experimental investigation of the variation of concrete pores under the action of freeze-thaw cycles*, Procedia Engineering 161 (2016) 583-588.

[57] Swedish standards, SS 13 72 44 ED. 4*, Concrete Testing - Hardened Concrete - Scaling At Freezing,* Standardiserings-Kommissionen I Sverige, 2005.

[58] G. Skripkiūnas, A. Grinys, and E. Janavičius. *Porosity and durability of rubberized concrete*. in *The Second International Conference on Sustainable Construction Materials and Technologies*, 2010.

[59] K. Najim and M. Hall, *Mechanical and dynamic properties of self-compacting crumb rubber modified concrete*, Construction and Building Materials 27 (1) (2012) 521-530.

[60] RILEM, TC 176-IDC, *Internal damage of concrete due to frost action,* Final Recommendation, Prepared by L. Tang and P.-E. Petersson SP Swedish National Testing and Research Institute, Boras, Sweden. Materials and Structures / Mat6riaux et Constructions, Volume 37, December 2004, pp 754-759 in Slab test: Freeze/thaw resistance of concreteInternal deterioration 2004.

[61] V. Baroghel-Bouny, *Evaluation and prediction of reinforced concrete durability by means of durability indicators. Part I: new performance-based approach*, in *ConcreteLife'06-International RILEM-JCI Seminar on Concrete Durability and Service Life Planning: Curing, Crack Control, Performance in Harsh Environments*, 2006: RILEM Publications SARL.

[62] M. Alexander, J. Mackechnie, and Y. Ballim, *Guide to the use of durability indexes for achieving durability in concrete structures*, Research Monograph 2 (1999).

This page is intentionally left blank

Chapter 5

Fatigue Performance of Flexible Steel Fibre Reinforced Rubberised Concrete (SFRRuC) Pavements

A. Alsaif, R. Garcia, F.P. Figueiredo, K. Neocleous, A. Christofe, M. Guadagnini, and K. Pilakoutas, Fatigue performance of flexible steel fibre reinforced rubberised concrete pavement, Engineering Structures 193 (2019) 170-183.

Author contribution statement

Dr Garcia, Dr Guadagnini and Prof. Pilakoutas supervised the PhD study of the first author. Dr Neocleous and Mr Christofe contributed to the experimental analysis while Dr Figueiredo contributed to the numerical analysis. All authors discussed the results and commented on the manuscript.

Recycled rubber particles and steel fibres from end-of-life tyres have the potential to enhance the flexibility and ductility of concrete pavements and produce more sustainable pavement solutions. However, the fatigue behaviour of such pavements is not fully understood. This article investigates the mechanical and fatigue performance of steel fibre reinforced concrete (SFRC) and steel fibre reinforced rubberised concrete (SFRRuC). Specimens tested were cast using rubber particles as replacement of natural aggregates (0%, 30% and 60% by volume), and using a blend of manufactured and recycled tyre steel fibres (40 kg/m^3). Prisms were subjected to four-point flexural cyclic load (f=15 Hz) at stress ratios of 0.5, 0.7, 0.8 and 0.9. The results show that, compared to plain concrete, the addition of steel fibres alone improves the fatigue stress resistance of concrete by 11% (at 25% probability of failure). The replacement of natural aggregates with rubber particles improves the flexibility of SFRRuC (from 51 GPa elastic modules for plain concrete to 13 GPa for SFRRuC), but reduces its fatigue stress resistance by 42% (at 25% probability of failure). However, a probabilistic analysis of the fatigue life data and overall design considerations show that the flexible SFRRuC can be used for pavements. To account for the effect of fatigue load, the Concrete Society approach included in TR34 is modified to account for SFRRuC pavements. Finite element analyses show that flexible SFRRuC pavements can accommodate large subgrade movements and settlements and result in much smaller cracks (up to 24 times) compared to SFRC pavements.

This chapter consists of a "stand alone" journal paper and contains a relevant bibliography at the end of the chapter. Appendix D provides additional information and further test results.

5.1 Introduction

Rigid concrete pavements are widely used in the construction of long-lasting roads as they enable a better distribution of load over the subgrade and require overall smaller structural depth, compared to flexible asphalt pavements. However, road pavement slabs are subjected to continuous cyclic traffic and thermal loads that can deteriorate the material mechanical properties, propagate cracks and eventually cause fatigue fracture [1-3], leading to premature pavement failure. A potential solution to enhance the flexibility, toughness and fatigue resistance of concrete pavements is to replace part of the natural aggregates with waste tyre rubber (WTR) particles [4, 5]. Rubber aggregates are known to reduce stiffness and enhance impact and skid resistance of concrete [6-12], but can cause significant decrease in mechanical properties, especially at high rubber contents (up to 90% reduction in compressive strength for 100% natural aggregates replacement) [13-17]. Consequently, until now rubberised concrete (RuC) is mainly utilised in low-strength non-structural applications, e.g. concrete pedestrian blocks [11]. Few researchers studied the performance of RuC in structural applications and to date there are limited studies on the fatigue performance of RuC [7, 18-23]. Liu et al. [7] studied the effect of replacing small percentages of fine natural aggregates with crumb rubber particles (0 to 15% by volume) and found that the fatigue performance of the RuC mixes was better than that of ordinary concrete. The enhancement was attributed to the ability of rubber to resist crack propagation by filling internal spaces and absorbing energy through deformation.

To enhance the strength of RuC for structural applications (especially flexural strength), steel fibres can be used to produce steel fibre reinforced rubberised concrete (SFRRuC) [5, 20, 24-26]. In SFRRuC, rubber particles absorb energy and enhance the fracture characteristics of the material [14, 27], whereas the fibres control crack opening and propagation even after the peak load, thus dissipating energy through gradual fibre debonding [8]. Ganesan et al. [20] examined the flexural fatigue behaviour of self-compacting RuC (SCRuC) with and without manufactured steel fibres. They observed that the replacement of fine aggregates with crumb rubber particles (up to 20% by volume) improved the flexural fatigue strength by approximately 15%. The addition of crimped-type manufactured steel fibres (MSF) into SCRuC mixes further enhanced the fatigue strength by 10%. More recently, Gupta et al. [22] reported that the incorporation of rubber ash and rubber fibres in concrete as a replacement of fine natural aggregates (up to 35%

by volume) enhanced the flexural impact and fatigue resistance by up to 217% and 52%, respectively.

Whilst these studies examined the fatigue of mixes with small amounts of rubber (less than 20% by total aggregate volume), recent research [8] has proven that the use of large amounts of rubber (especially large rubber particles) is necessary to attain low stiffness pavements with the potential to accommodate subgrade movements. The authors [8] have recently proposed optimised flexible SFRRuC mixes with large amounts of rubber (60% by volume replacement of natural aggregates) and blends of MSF and recycled tyre steel fibres (RTSF) that meet the flexural strengths of EN 13877-1 [28]. The authors [29, 30] also demonstrated that the durability, long-term and permeability performance indicators of the optimised mixes, rank them as 'highly durable concrete'[31-34]. These properties make SFRRuC a promising candidate for sustainable road pavement slabs, particularly considering that reusing end-of-life tyre materials (WTR and RTSF) in concrete would contribute to the reduction of the environmental impact caused by discarded tyres (1.5 billion units/year [35]). However, to date, the flexural fatigue performance of SFRRuC with large amounts of rubber and steel fibres has not been investigated.

As the variability in flexural fatigue performance of steel fibre reinforced concrete (SFRC) and SFRRuC is expected to be high due to the combination of rubber and/or fibres [20, 22], a statistical approach may need to be adopted to quantify the reliability of experimental results and their suitability for use in pavement design. Probabilistic distribution models including the two-parameter Weibull distribution model, graphical interpolation model and the mathematical model are commonly used to statistically analyse fatigue life data and derive probabilistic relationships that can be used in design [1, 36, 37].

This study assesses the mechanical and fatigue performance of SFRRuC. Initially, the study examines the mechanical performance of SFRC and SFRRuC mixes with different replacement volumes of rubber aggregates (0, 30 and 60%) and a blend of MSF and RTSF. The results are compared in terms of uniaxial compressive strength, static flexural strength, elastic modulus, and flexural fatigue strength (number of fatigue cycles). Subsequently, three different probabilistic approaches are used to estimate the design fatigue stress ratio. The design implications of using SFRRuC in new pavements is shown by a practical example. Finite element analyses are performed using Abaqus® to demonstrate the capability of flexible SFRRuC pavements to accommodate subgrade movements and settlements. This study contributes towards developing economically and structurally sound alternative materials for sustainable flexible pavements, as well as towards using recycled materials derived from end-of-life tyres.

5.2 Experimental programme

5.2.1 Materials and casting procedure

Four optimised concrete mixes developed previously by the authors [8, 11, 29] were produced to cast the tested specimens. Three cubes (100 mm) and twelve prisms (100×100×500 mm) were cast and prepared for each mix. A binder made of 80% of a Portland limestone cement CEM II-52.5 N, 10% of silica fume (SF) and 10% of pulverised fuel ash (PFA) was used for all concrete mixes. The fine aggregate was medium-grade washed river sand with size 0/5 mm and specific gravity (SG) of 2.65, whereas the coarse aggregate was round river washed gravel with particle sizes of 5/10 mm and 10/20 mm and SG of 2.64. Chemical admixtures including plasticiser and superplasticiser were utilised to enhance workability and cohesion. A blend of 20 kg/m^3 of MSF (0.8, 55) and 20 kg/m^3 of RTSF (0.22, 23), as shown in Figure 5.1a, were used as reinforcement. Details on the characterisations of the steel fibres are reported in [8, 38].

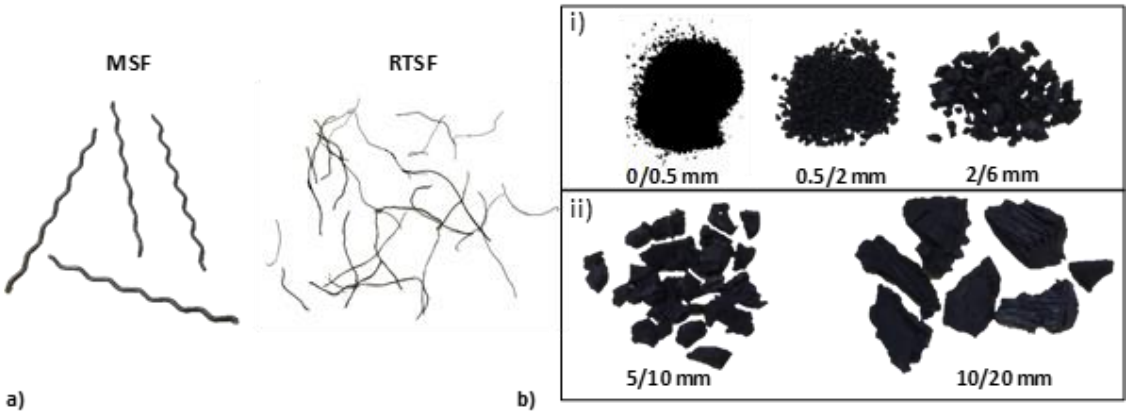

Figure 5.1: a) MSF and RTSF, b) rubber particles, used in this study

The natural aggregates were replaced with two different volumetric percentages of rubber particles (30% or 60%) of roughly similar size distribution to minimise packing issues. Figure 5.1b shows the rubber particles according to size. The fine rubber particles of sizes 0/0.5 mm, 0.5/2 mm and 2/6 mm were used in a 2:3:4 ratio, respectively, whilst the coarse rubber particles of sizes of 5/10 mm and 10/20 mm were used in a 1:1 ratio. The mass of rubber replacing the mineral aggregates was calculated using a relative density of 0.8 [8]. Figure 5.2 shows the particle size distribution of rubber and natural aggregates (NA) obtained according to ASTM-C136 [39].

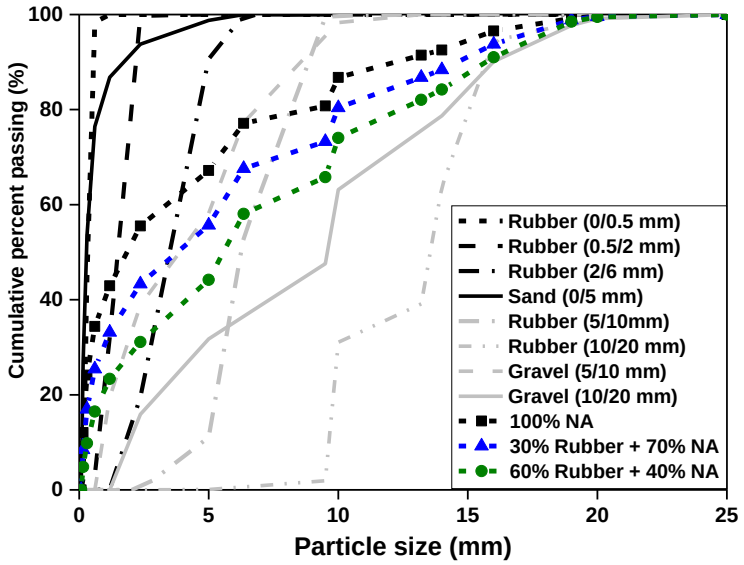

Figure 5.2: Particle size distributions rubber particles and natural aggregates

Table 5.1 summarises the mix proportions and corresponding IDs of the four concrete mixes examined in this study. The number in the ID represents the quantity of rubber particles replacing both fine and coarse aggregates (0%, 30% or 60% by volume), while P=Plain concrete and BF=blend fibres.

Table 5.1 Mix proportions for 1 m^3 of concrete, adapted from [8]

Components	Concrete mixes ID			
	0P	*0BF*	*30BF*	*60BF*
CEM II (kg/m^3)	340	340	340	340
Silica Fume (SF) (kg/m^3)	42.5	42.5	42.5	42.5
Pulverised Fuel Ash (PFA) (kg/m^3)	42.5	42.5	42.5	42.5
Fine aggregates 0/5 mm (kg/m^3)	820	820	574	328
Coarse aggregates 5/10 mm (kg/m^3)	364	364	254	146
Coarse aggregates 10/20 mm (kg/m^3)	637	637	446	255
Water (l/m^3)	150	150	150	150
Plasticiser (l/m^3)	2.5	2.5	3.25	4.25
Superplasticiser (l/m^3)	5.1	5.1	5.1	5.1
Fine rubber particles (kg/m^3)	0	0	165	330
Course rubber particles (kg/m^3)	0	0	24.8	49.6
MSF (kg/m^3)	0	20	20	20
RTSF (kg/m^3)	0	20	20	20
Total	2404	2444	2087	1733

To produce the SFRRuC mixes, natural and rubber aggregates were first added into a pan mixer and mixed for approximately 30 s in dry conditions. Half of the mixing water was then added, and the materials were mixed for 1 min. The mixer was halted for three minutes to add the binder materials. Subsequently, mixing restarted and the remaining water and admixtures were gradually added for another 3 min. Finally, the steel fibres were added manually, and mixing continued for 3 min. All specimens were cast in moulds using two layers of concrete (according to EN 12390-2 [40]), and each layer was compacted on a vibrating table for 25 s. Following casting, the specimens were covered with plastic sheets to retain moisture, and kept under standard laboratory conditions for 2 days. As a large number of specimens were needed for each mix, due to parallel durability studies [29, 30], three batches were cast for each mix. The number of specimens per mix was also limited by the capacity of the concrete mixer in the laboratory. All specimens were cured in a mist room for 28 days, after which they were stored under standard laboratory conditions until testing. All specimens were tested after 150 days following casting to ensure that they had developed their full strength.

5.2.2 Test setup and instrumentation

The uniaxial compressive tests on cubes were carried out using a cube crusher at a loading rate of 0.4 MPa/s, according to EN 12390-3 [41]. The prisms were subjected to static and fatigue four-point bending using a servo-hydraulic actuator with a capacity of 250 kN (±0.05% error). Two linear variable differential transducers (LVDTs) mounted onto each side of a yoke, as suggested by the JSCE guidelines [42] (see Figure 5.3), monitored the vertical mid-span displacement of the prisms. The static tests were performed at a displacement rate of 0.2 mm/min. Initially, three prisms per mix were tested statically to select the load limits for the fatigue tests and to monitor the development of cracks. The maximum amplitude of the fatigue load was calculated by multiplying a stress ratio (S=0.5, 0.7 or 0.9) by the average flexural strength obtained from the three specimens subjected to static load. As discussed in more detail in section 5.3.3, in some cases the stress ratio was multiplied by the characteristic flexural strength (instead of the average) to prevent premature failure of the prisms during the fatigue tests. The minimum amplitude of each loading cycle was set to 10% of the maximum fatigue load to avoid disengagement of the specimens during testing. The fatigue loading cycles were applied at a frequency of 15 Hz (sinusoidal wave), which is within the typical range (12-20 Hz) used for prism tests in order to avoid amplification or resonance problems [1, 19, 36, 43, 44]. The load cycles were applied in four point bending, ensuring a sufficient constant moment region to allow the development of cracked sections at a known stress level. The fatigue tests were terminated

either after two million cycles, or at failure of the prisms. Readings were saved at specific logarithmic steps as following (every cycle from 0 to 10 then every10th cycle up to 100 cycles, then every 100th cycle up to 1,000 cycles, then every 1,000th cycle up to 10,000 cycles, then every 10,000th cycle up to failure). The main output of the fatigue tests was the number of cycles at failure as well as the vertical displacements recorded by the LVDTs.

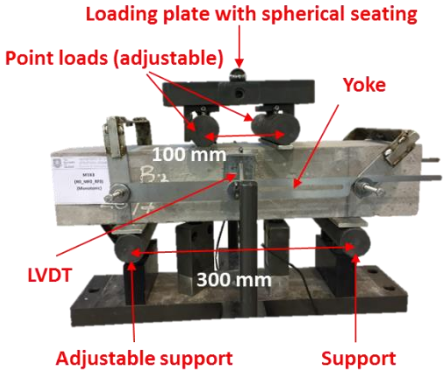

Figure 5.3: Flexural test set-up

5.3 Results and discussion

5.3.1 Failure mode

Typical failure modes of the tested cubes are shown in Figure 5.4. Whilst the plain concrete specimens (*0P*) failed in a brittle manner, the SFRC and SFRRuC specimens failed in a much more 'ductile' manner. As the inclusion of large amounts of rubber and steel fibres led to the development of more distributed (and thinner) cracking, compared to specimens without rubber (*0BF*), this confirms that ductility was improved by adding fibres and further enhanced by the rubber, as explained previously by the authors in [8].

Figure 5.4: Typical failure modes of concrete cubes

5.3.2 Static compressive and flexural strengths

Table 5.2 summarises the average cube compressive strength ($f_{cm,cube}$), static flexural elastic modulus (E_s), and static flexural strength ($f_{ctm,fl}$) including characteristic values ($f_{ctk,fl}$) for each

concrete mix. The coefficient of variation is also presented in brackets. The results in Table 5.2 indicate that the addition of a blend of steel fibres in conventional concrete (mix *0BF*) increases the compressive strength by 18% over the plain concrete mix (*0P*). A similar enhancement was observed in a previous study by the authors [8], who attributed the enhancement to the ability of steel fibres (especially RTSF) to control and delay micro-crack coalescence and the unstable propagation of cracking. However, mixes *0BF* and *0P* show the same elastic modulus and flexural strength despite the difference in compressive strength, which may be attributed to some air being trapped during the casting of 0BF prisms as observed by the authors in another study [8]. Indeed, the results in [8] showed that the increase in air content creates weaknesses inside the concrete matrix and decreases concrete density, which in turn affects both the strength and stiffness. Compared to mix *0P*, replacing large amounts of fine and coarse aggregates with rubber reduces the compressive strength by 49% and 85% for *30BF* and *60BF* mixes, respectively. Similarly, the elastic modulus and flexural strength of mix *30BF* drop by 57% and 34%, respectively, whereas these properties decrease by 75% and 42% for mix *60BF*. Nevertheless, in the design of road pavements, which work essentially in bending, having sufficient flexural strength is more important than having high compressive strength, provided durability is not compromised.

Table 5.2 Static compressive and flexural test results

Mix	$f_{cm,cube}$ (MPa)	E_s (MPa)	$f_{ctm,fl}$ (MPa)	$f_{ctk,fl}$ (MPa)	$\frac{f_{ctm,fl}}{\sqrt{f_{cm,cube}}}$
0P	102 (4.7)	51 (5.1)	7.0 (13.3)	5.2	0.693
0BF	120 (2.9)	51 (4.8)	7.0 (9.3)	5.8	0.639
30BF	52 (7.5)	22 (13.8)	4.6 (5.3)	4.1	0.638
60BF	15 (10.7)	13 (21.9)	4.1 (18.5)	2.6	1.058

The reduction in strength and stiffness in SFRRuC is mainly due to the lower stiffness and higher Poisson's ratio of rubber (nearly 0.5) when compared to natural aggregates, but also due to the poor adhesion between rubber and cement paste [8, 11, 15]. It should be noted that the compressive strength of the mixes degrades faster than the flexural strength, which confirms, as also discussed in [8], that the combination of fibres and rubber enhances the tensile capacity of SFRRuC. This is evident by noting that the ratio of the average static flexural strength to the square root of the average compressive strength ($\frac{f_{ctm,fl}}{\sqrt{f_{cm,cube}}}$) for *60BF* is much higher than for the other mixes.

It should be mentioned that the relatively large variability in $f_{ctm,fl}$ in Table 5.2 can be attributed to the fact that each specimen belonged to a different batch. To determine a safe initial loading protocol for the fatigue stress loads, the characteristic flexural strength ($f_{ctk,fl}$) of each mix was determined according to RILEM TC 162-TDF [45].

5.3.3 Flexural fatigue strength

Table 5.3 summarises the flexural fatigue results of the tested prisms. The results report the stress ratio (*S*) in decreasing order, as well as the fatigue life (*N*). For the initial tests (3 prisms per mix), the maximum and minimum amplitudes of the fatigue load were determined using the characteristic strength values ($f_{ctk,fl}$) and *S*=0.9 (see footnote * in Table 5.3). After examining the values *N* at this stress ratio, it was found that some of the plain concrete (*0P*) and SFRC specimens (*0BF*) sustained at least 2 million cycles. Conversely, the *N* values of the SFRRuC specimens (*30BF* and *60BF*) were much lower. Hence, it was decided to use average strength values ($f_{ctm,fl}$) and *S* of 0.8 and 0.9 for the tests on prisms *0P* and *0BF*, respectively. On the other hand, the flexural fatigue loads for the tests on prisms *30BF* and *60BF* were determined using characteristic values and *S* of 0.7 and 0.5.

Table 5.3 Fatigue flexural test results

Mix	Stress ratio, S, based on $f_{ctm,fl}$ ($f_{ctk,fl}$)	Specimen No.	Fatigue life, *N*	Mix	Stress ratio, S, based on $f_{ctm,fl}$ ($f_{ctk,fl}$)	Specimen No.	Fatigue life, *N*
0P	0.9 (1.26)	*0P*-1	195	*30BF*	0.78 (0.9*)	*30BF*-1	12,000+
		0P-2	438			*30BF*-2	217,700+
		0P-3	482			*30BF*-3	729,700+
	0.8 (1.12)	*0P*-1	1,200+		0.57 (0.7)	*30BF*-1	2,218
		0P-2	6,968			*30BF*-2	1,690,882
		0P-3	17,800+			*30BF*-3	2,000,000
	0.64 (0.9*)	*0P*-1	733,303		0.43 (0.5)	*30BF*-1	2,000,000
		0P-2	2,000,000			*30BF*-2	2,000,000
		0P-3	2,000,000			*30BF*-3	2,000,000
0BF	0.9 (1.13)	*0BF*-1	431	*60BF*	0.66 (0.9*)	*60BF*-1	3,754
		0BF-2	9,172			*60BF*-2	6,084
		0BF-3	102,718			*60BF*-3	59,690
	0.8 (1.0)	*0BF*-1	16,525		0.51(0.7)	*60BF*-1	58,937
		0BF-2	209,338			*60BF*-2	64,157
		0BF-3	356,807			*60BF*-3	315,080
	0.71 (0.9*)	*0BF*-1	852,009		0.37(0.5)	*60BF*-1	1,600,000
		0BF-2	2,000,000			*60BF*-2	2,000,000
		0BF-3	2,000,000			*60BF*-3	2,000,000

+ Number of cycles recorded in 100 cycle accuracy.
* Initial tests at 0.9$f_{ctk,fl}$

Figure 5.5 compares the logarithmic number of cycles (log *N*) endured by each specimen and the relative *S* calculated using $f_{ctm,fl}$ (quantitative comparisons are included in section 5.4). It is evident that the fatigue life data have a large scatter even for the same mixes and stress ratios, in particular for specimens with steel fibres and/or rubber particles. Though the uneven distribution of rubber and fibre orientation may significantly contribute to this high variability [1, 20], the fact that specimens from different batches were used also plays a significant role.

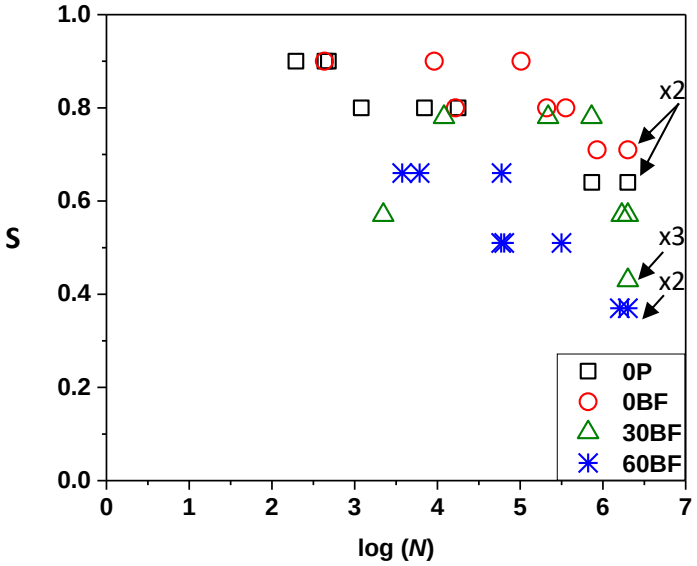

Figure 5.5: Test results in terms of logarithmic number of cycles (log N) and S (based on $f_{ctm,fl}$)

Figure 5.5 indicates that steel fibre blends improve the performance of specimens *0BF* by increasing its fatigue life. Previous research has proven that RTSF are effective in restraining the propagation of micro-cracks into meso-cracks, whilst MSF are more effective in holding macro-cracks together [1, 38].

The replacement of natural aggregates with rubber in SFRRuC significantly degrades the fatigue performance of specimens *30BF* and *60BF*. This can be attributed to the stiffness and strength degradation in the SFRRuC resulting from the different elastic properties of rubber, as well as to the weak bond between cement paste and rubber. SFRRuC is also highly porous [29], which also contributes to stiffness degradation during cyclic loading.

Figure 5.6 compares the load-deflection response under static and fatigue load for the examined mixes. The static curve is the average of three prisms, whereas the fatigue curve (one specimen) is representative of typical behaviour observed during the tests. Despite the fact that the applied S (calculated using $f_{ctm,fl}$) is different for all mixes, it is evident that the initial stiffness (slope) of the fatigue loops is similar to that of the static curve. However, the stiffness degrades gradually

with the number of fatigue cycles. Note also that the stiffness degrades faster with increasing rubber contents. It is also interesting to note that the *0P* and *0BF* failure occurred when the fatigue cycles touched the monotonic envelope. This may also be the case for *30BF* and *60BF* as one cycle was recorded for every logarithmic step. Though this does not necessarily help to predict fatigue life, but it can give an indication of the likely fatigue behaviour and, most importantly, the maximum displacement at failure.

The damage process in SFRRuC under fatigue loading is expected to progress in three stages: 1) during the first load cycles, flaws and micro-cracks form at the rubber/matrix interface and at the weak region within the concrete; 2) as loading progresses, micro-cracks develop at the rubber/matrix interface and at the fibre/matrix interface, with the former propagating at a faster rate. Although the fibres resist the opening of numerous micro-cracks, these tend to propagate and combine quickly to form macro-cracks; 3) at the final stages of loading (or at failure), a main crack develops after a sufficient number of macro-cracks have formed.

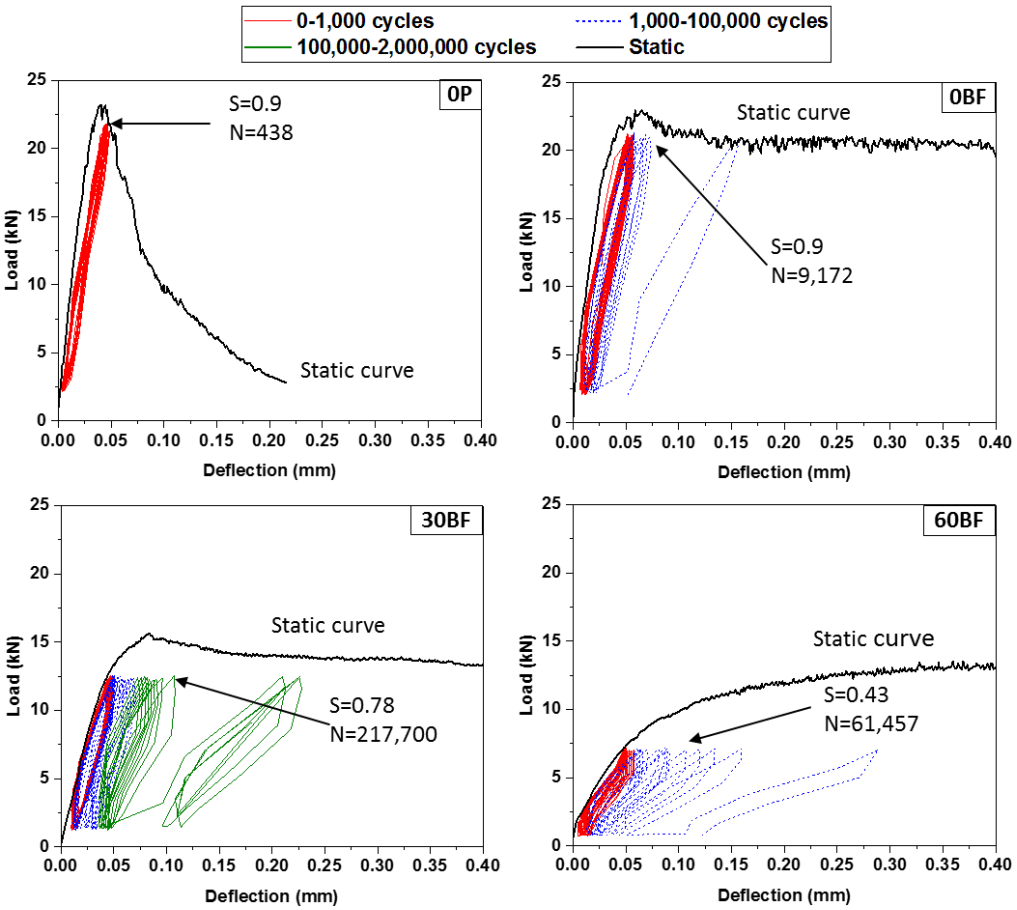

Figure 5.6: Load-deflection response under static and fatigue load for examined mixes

The fatigue loops of the SFRRuC (*30BF* and *60BF*) specimens are evidently "fatter" than those of *0P* and *0BF*, thus indicating that the addition of rubber enhances energy dissipation. However, a direct comparison of the energy dissipated by the specimens is not possible due to the different S applied during the tests. Note also that, due to their higher flexibility, SFRRuC specimens exhibit notably higher deflection at failure than that of normal concrete (*0P* and *0BF*). Despite the lower fatigue resistance of SFRRuC mixes with large volumes of rubber, their higher ductility and flexibility can still be used to accommodate subgrade movements of pavement slabs at lower stress levels. To assess the overall fatigue performance of SFRRuC pavement, a probabilistic approach can be adopted, as shown in the following sections.

5.4 Determination of fatigue-life distribution using probabilistic analysis

In this section, three models: 1) two-parameter Weibull distribution model, 2) graphical interpolation model and 3) the mathematical model are used to derive probabilities of failure (P_f) and *S–N* relationships for each mix, which can be used in pavement design. For comparison purposes, the P_f-*S–N* relationships are compared at probabilities of failure of 25% and 50% (or survival probabilities of 75% and 50%, respectively). These values are widely adopted in the fatigue design of pavements [1, 44-46]. In pavement design, it is usually considered that 2×10^6 cycles correspond to an infinite fatigue life [7, 20, 49] and this assumption is utilised in the following calculations.

5.4.1 Two-parameters Weibull distribution

The Weibull distribution has been widely used for the statistical analysis of fatigue life data in concrete [7, 36, 49, 50] because it is easy to apply, it is statistically sound and provides accurate results even with a small number of samples, and it has a hazard function that reflects the actual material behaviour in fatigue. The two-parameters of the Weibull distribution (α and u) can be calculated through either i) the graphical method, ii) the method of moments, or iii) the method of maximum-likelihood estimate. In this study, the fatigue life data for each mix and at a given stress ratio S (based on $f_{ctm,fl}$) are analysed, and α and u are estimated using methods i to iii above. The mean values of α and u (average of i to iii) are used to estimate the fatigue lives corresponding to P_f = 0.25 and 0.50, from which the P_f-*S–N* relationships are derived.

5.4.1.1 Graphical method

The Weibull distribution survival function is defined by [7, 50]:

$$P_s\,(N) = \exp\left[-\left(\frac{N}{u}\right)^{\alpha}\right] \quad (1)$$

where *N* is the fatigue life, *α* is the shape parameter (or Weibull slope) at the stress ratio *S*, and *u* is the scaling parameter (or characteristic life) at *S*.

By taking the logarithm twice on both sides of Eq. (1):

$$ln\left[ln\left(\frac{1}{P_s}\right)\right] = \alpha \ln(N) - \alpha \ln(u) \quad (2)$$

If it is assumed that $Y = ln\left[ln\left(\frac{1}{p_s}\right)\right]$, $X = ln(N)$ and $\beta = \alpha ln(u)$, then Eq. (2) can be rewritten as a linear equation:

$$Y = \alpha \mathrm{X} - \beta \quad (3)$$

where all the variables are as defined before. Hence, when the fatigue life data at a given stress follow a linear trend (correlation coefficient $r \geq 0.9$), such data are deemed to comply with the Weibull distribution and *α* and *u* can be obtained directly from regression analyses [7, 20]. Table 5.4 summarises the fatigue life data (in ascending order), P_s, *X* and *Y* of the tested specimens. In this table, the survival probability Ps is calculated using [49, 50]:

$$P_s = 1 - \frac{i}{K+1} \quad (4)$$

where *i* is the failure order number, and *K* is the number of specimens tested at a given stress ratio (*K*=3 prisms).

Table 5.4 Analysis of fatigue life data

Mix	S	Fatigue life, N	P_s	X	Y	Graphical method			Method of moments		Maximum likelih-hood moment		Average		Estimated fatigue life, N_e at P_f of	
						r	α	u	α	u	α	u	α_w	u_w	0.25	0.50
0P	0.9	195	0.75	5.27	-1.25	0.94	1.48	461	2.58	419	3.63	415	2.54	427	262	370
		438	0.50	6.08	-0.37											
		482	0.25	6.18	0.33											
	0.8	1,200	0.75	7.09	-1.25	0.99	0.57	11,208	1.03	8,758	1.13	9,029	0.90	9,569	2,400	6,371
		6,968	0.50	8.85	-0.37											
		17,800	0.25	9.79	0.33											
	0.64	733,303	0.75	13.51	-1.25	0.90	1.22	2,032,791	2.29	1,780,997	3.18	1,771,850	2.21	1,843,261	1,048,809	1,561,514
		2,000,000	0.50	14.51	-0.37											
		2,000,000	0.25	14.51	0.33											
0BF	0.9	431	0.75	6.07	-1.25	1.00	0.29	32,926	0.64	26,868	0.53	22,143	0.48	27,039	2,014	12,594
		9,172	0.50	9.12	-0.37											
		102,718	0.25	11.54	0.33											
	0.8	16,525	0.75	9.71	-1.25	0.96	0.46	272,603	1.15	204,081	1.06	198,163	0.88	222,700	54,233	146,979
		209,338	0.50	12.25	-0.37											
		356,807	0.25	12.78	0.33											
	0.71	852,009	0.75	13.66	-1.25	0.90	1.44	2,028,617	2.62	1,820,457	3.74	1,804,209	2.57	1,865,583	1,149,396	1,617,843
		2,000,000	0.50	14.51	-0.37											
		2,000,000	0.25	14.51	0.33											
30BF	0.78	12,000	0.75	9.39	-1.25	0.99	0.37	396,881	0.86	295,090	0.76	278,790	0.66	320,351	47,821	183,078
		217,700	0.50	12.29	-0.37											
		729,700	0.25	13.50	0.33											
	0.57	2,218	0.75	7.70	-1.25	0.91	0.18	1,999,505	1.16	1,295,849	0.47	818,064	0.60	1,357,428	169,741	736,371
		1,690,882	0.50	14.34	-0.37											
		2,000,000	0.25	14.51	0.33											
	0.43	2,000,000	0.75	14.51	-1.25	0.00[+]	0.00[+]	0.00[+]	0.00[+]	0.00[+]	0.00[+]	0.00[+]	0.00+	0.00+	2,000,000	2,000,000
		2,000,000	0.50	14.51	-0.37											
		2,000,000	0.25	14.51	0.33											
60BF	0.66	3,754	0.75	8.23	-1.25	0.91	0.49	26,817	0.71	18,660	0.84	20,913	0.67	21,909	3,434	12,701
		6,084	0.50	8.71	-0.37											
		59,690	0.25	11.00	0.33											
	0.51	58,937	0.75	10.98	-1.25	0.85[*]	0.71	193,571	1.00	145,901	1.29	159,403	0.99	164,629	46,870	113,763
		64,157	0.50	11.07	-0.37											
		315,080	0.25	12.66	0.33											
	0.37	1,600,000	0.75	14.29	-1.25	0.90	5.49	2,007,453	9.55	1,965,979	14.25	1,946,702	9.67	1,953,644	1,717,428	1,880,968
		2,000,000	0.50	14.51	-0.37											
		2,000,000	0.25	14.51	0.33											

[+] All of three specimens recorded 2M fatigue cycles, therefore, all point in the curve are aligned. [*] Correlation coefficient less than 0.9.

Figure 5.7 plots the values X and Y for mix *0BF*. The results show that the fatigue life data for the same stress ratio follow a linear trend. This confirms that α represents the slope of the curve, while u can be calculated using the curve intercept point β. Similar trends were observed for the rest of the data, and the results of α and u obtained from the graphical method are listed in Table 5.4. It is shown that in most cases $r \geq 0.9$, thus indicating that a linear relationship exists between X and Y. Since all the three prisms *30BF* at S=0.43 reached 2×10^6 fatigue cycles, the three points in the graph are aligned vertically, thus leading to a zero slope (i.e. α=0). Although r=0.85 for *60BF* at S=0.51, the probabilistic analysis is still carried out and the results are subsequently adjusted using the average values of the Weibull distribution parameters, as explained later.

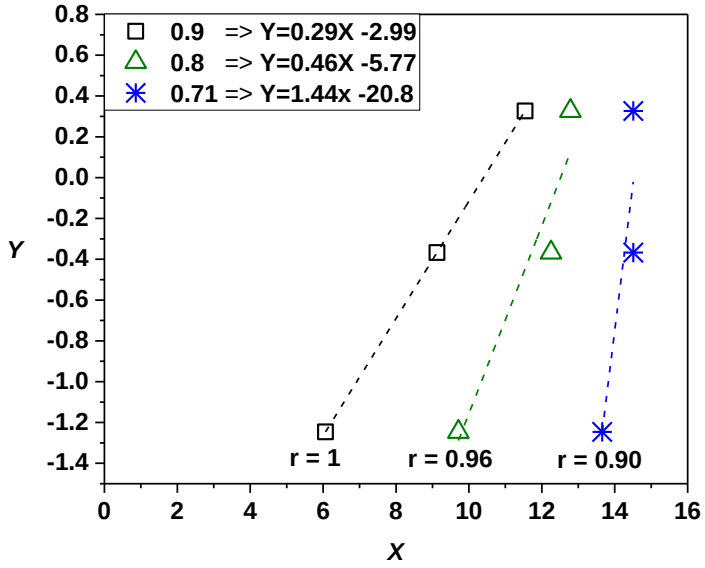

Figure 5.7: Graphical analysis of fatigue-life data for 0BF

5.4.1.2 Method of moments

This method calculates α and u at each stress ratio using the mean fatigue life (μ) of three prisms, and the corresponding coefficient of variation (CV) according to the following equations [36, 49-51]:

$$\alpha = (CV)^{-1.08} \tag{5}$$

and

$$u = \frac{\mu}{\Gamma\left(\frac{1}{\alpha}+1\right)} \tag{6}$$

where $\Gamma(\ )$ is the gamma function.

Table 5.4 summarises the values α and u for all concrete mixes at various stress ratios using the method of moments.

5.4.1.3 Method of maximum-likelihood estimate

The probability density function of the Weibull distribution can be written as [36, 50, 51]:

$$f_N(N) = \frac{\alpha}{\theta} N^{\alpha-1} \exp\left[\frac{N^{\alpha}}{\theta}\right] \quad (7)$$

where

$$\theta = u^{\alpha} \quad (8)$$

The maximum-likelihood function can be expressed as follows [36, 50, 51]:

$$\frac{\sum_{i=1}^{K} N_i^{\alpha^*} \ln(N_i)}{\sum_{i=1}^{K} N_i^{\alpha*}} - \frac{1}{\alpha^*} = \frac{1}{K} \sum_{i=1}^{K} \ln(N_i) \quad (9)$$

$$\theta^* = \frac{1}{K} \sum_{i=1}^{K} N_i^{\alpha^*} \quad (10)$$

where α^* and θ^* are the maximum-likelihood estimators for α and θ, respectively, and the rest of the variables are as defined before. Accordingly, the value α^* is first obtained iteratively using Eq. (9), and then replaced in Eq. (10) to calculate θ^*. The parameter u is finally calculated using α^* and θ^* (instead of α and θ) in Eq (8). Table 5.4 summarises the values α and u for all concrete mixes at various stress ratios using the method of maximum-likelihood estimate.

The results in Table 5.4 show that the three methods lead to significantly different values of α and u, with the graphical method yielding α and u values considerably different from those obtained by the other two methods. This is due to the small number of prisms (three) tested at each stress ratio, as well as to the large scatter in the fatigue life data. To address this issue and adopt a more conservative approach, the average values of α and u of the three methods are considered. The average values are shown as α_w and u_w in Table 5.4.

5.4.1.4 *Ps-S-N* relationships

The values α_w and u_w of the Weibull distribution parameters (Table 5.4) are used here to estimate the fatigue lives corresponding to P_f = 0.25 and 0.50 (P_s=0.75 and 0.50). The fatigue life N_e at certain S and P_f can be estimated using a rearranged version of Eq. (2) [36]:

$$N_e = ln^{-1}\left[\frac{ln\left[ln\left(\frac{1}{1-P_f}\right)\right] + \alpha_w \ln(u_w)}{\alpha_w}\right] \quad (11)$$

Table 5.4 compares the values N_e calculated using Eq. (11) at P_f = 0.25 and 0.50. The results show that, as expected, for the same stress ratio the value N_e increases with the probability of failure. Additionally, for the same probability of failure, N_e increases as the stress ratio decreases.

Using the estimated fatigue lives N_e in Table 5.4, the P_f-*S-N* relationships can be derived using the double logarithmic fatigue equation, which has been used in previous studies [7, 19]:

$$\log(S) = a + b\log(N_e) \quad (12)$$

Figure 5.8 shows the calculated P_f-*S-N* relationships for all concrete mixes using N_e values at P_f=0.25 and 0.50. The constants *a* and *b* in Eq. (12) are obtained from regression analyses of the data shown in Figure 5.8. It is shown that *r* is always close to 1 for all concrete mixes at both probability of failures, which confirms the linear trend of the test data. Note that the equations in Figure 5.8 can be used to calculate the stress ratio for a known fatigue life at P_f=0.25 and 0.50, as shown in section 5.4.4.

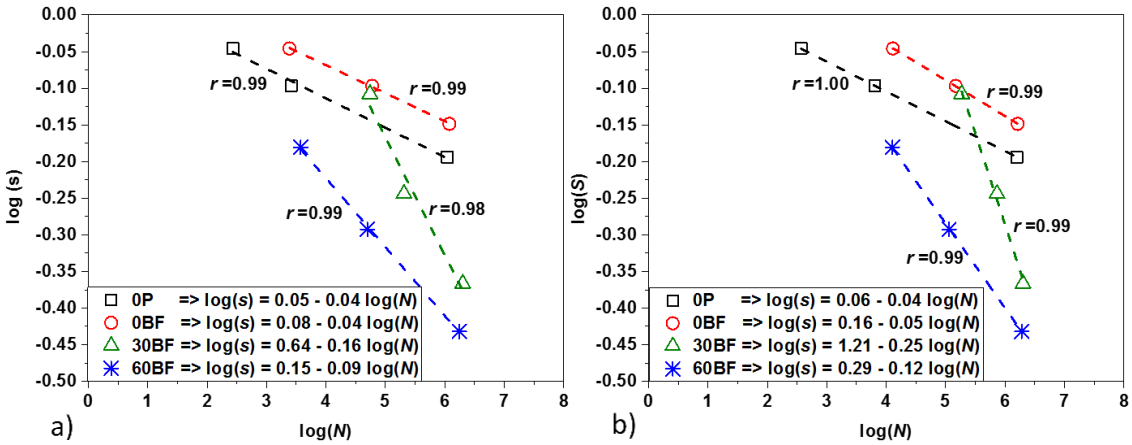

Figure 5.8: Fatigue curves of all concrete mixes corresponding to a) P_f = 0.25 and b) P_f = 0.50

5.4.2 Graphical interpolations

The graphical interpolation model is suitable for practical design because it presents concisely the P_f -*S-N* relationships, and it is fast and computationally simple. To generate the P_f -*S-N* relationships, the specimens are initially sorted in ascending order of fatigue life [44, 52, 53]. The probability of failure is defined as $\frac{j}{n+1}$, where *j* is the rank of the specimen and *n* is the number of specimens tested for each mix at a particular stress ratio. Table 5.5 shows the specimens of mix *0BF* ranked according to their fatigue life, as well as the calculated P_f values.

Table 5.5 Ranked specimens in terms of N according to stress ratio for mix 0BF

j	Fatigue life, *N*, at stress ratio of (based on $f_{ctm,fl}$)			$P_f = \frac{j}{(n+1)}$
	0.9	0.8	0.71	
1	431	16,525	852,009	0.25
2	9,172	209,338	2,000,000	0.50
3	102,718	356,807	2,000,000	0.75

The P_f-*S*-*N* relationships for mix *0BF* are shown in Figure 5.9a-c. In this method, a P_f-*N* curve is initially plotted for each stress ratio using P_f and log(*N*), as shown in Figure 5.9a for the data in Table 5.5. Based on linear regressions, the *S*-*N* curves are then derived using the stress ratios *S* (based on $f_{ctm,fl}$) and log(*N*) for each P_f, as shown in Figure 5.9b. The *S*-P_f curves in Figure 5.9c are finally obtained by graphical interpolation for different fatigue lives. For instance, for a fatigue life *N*=500,000 cycles (log (*N*)=5.7), the estimated stress ratio is S_e=0.76 (see Figure 5.9b) for P_f =0.50. Alternatively, the linear equations obtained by regression analyses in the *S*-*N* curves (see Figure 5.9b) can be used to estimate the stress ratio. Different *N* can be selected in the last step for comparison. In this study, *N*=500,000, 1,000,000 and 2,000,000 cycles are adopted. The P_f-*S* and *S*-*N* curves for mixes *0P*, *30BF* and *60BF* calculated following the above procedure are shown in Figure 5.10. Further comparisons of the results shown in Figure 5.9 and Figure 5.10 are included in section 5.4.4.

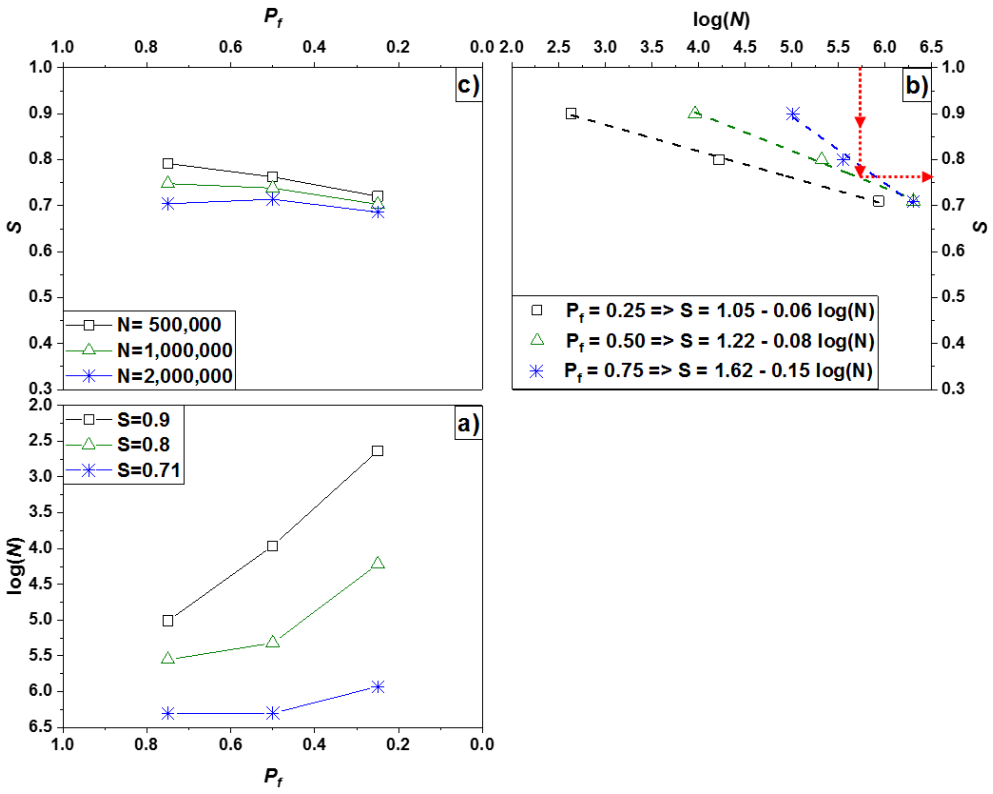

Figure 5.9: Graphical interpolation example for mix 0BF a) Pf -N, b) N-S and c) Pf -S curves

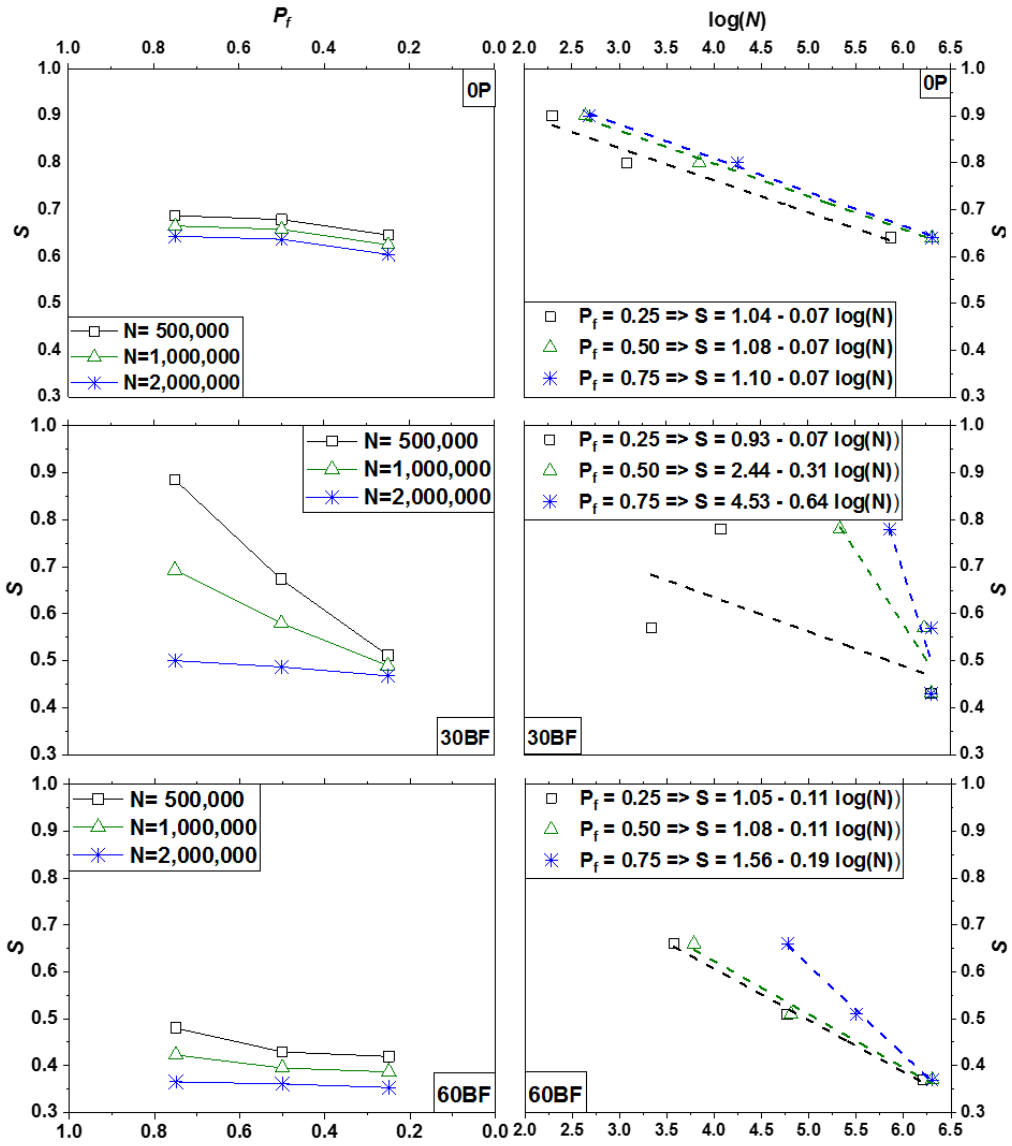

Figure 5.10: Graphical interpolation results for mixes 0P, 30BF and 60BF: S-Pf and S-N curves

5.4.3 Mathematical models

Previous research has proposed a mathematical function to derive P_f -S-N relationships for SFRC [1, 44, 52]. The mathematical function can be expressed as:

$$P_f = 1 - 10^{-a\,S^b\,(log\,N)^c} \quad (13)$$

where *a*, *b* and *c* are experimental coefficients derived from statistical analyses of the fatigue life data, as described in references [44, 52, 53]. The coefficient *a*, *b* and *c* obtained for the mixes examined in this study are summarised in Table 5.6. Such coefficients can be replaced in Eq. (13) to estimate the stress ratio S_e for any values of N and P_f.

Table 5.6 Experimental coefficients a, b and c calculated from the mathematical model

Mix	Experimental coefficients		
	a	*b*	*C*
0P	8.77E-04	21.50	8.39
0BF	1.43E-03	10.07	4.76
30BF	2.91E-04	1.71	4.62
60BF	2.27E-06	8.35	10.87

5.4.4 Comparison between models

Table 5.7 compares the estimated fatigue stress ratio S_e for a fatigue life of 2×10^6 cycles and P_f=25% and 50% obtained from the probabilistic models described in sections 5.4.1, 5.4.2 and 5.4.3. With the exception of *30BF*, the estimated fatigue stress ratios obtained from the three models agree well for all mixes at the same P_f. The low stress ratios given by the mathematical model for *30BF* can be attributed to the fact that the three specimens for S=0.43 reached 2×10^6 fatigue cycles (see Table 5.3), which leads to a very low coefficient *b* (see Table 5.6). The average stress ratio of the three models can be used for practical pavement design, as demonstrated by an example in the following section.

Table 5.7 Summary of the fatigue stress ratio obtained from three methods

Mix	P_f	Estimated S_e based on			Average stress ratio, $S_{e,ave}$
		Weibull distribution	Graphical interpolation	Mathematical	
0P	25%	0.62	0.60	0.61	0.61
	50%	0.63	0.64	0.64	0.64
0BF	25%	0.70	0.69	0.65	0.68
	50%	0.70	0.71	0.71	0.71
30BF	25%	0.42	0.47	0.24	0.45[+]
	50%	0.44	0.49	0.40	0.47[+]
60BF	25%	0.36	0.35	0.34	0.35
	50%	0.37	0.36	0.37	0.37

[+] Value calculated based on the Weibull distribution and graphical methods only.

5.5 Design implications

To assess the effect of the addition of steel fibres and/or rubber on the thickness *h* of rigid pavement slabs, a road section with a standard axle load *W* is assumed. According to Westergaard's empirical-theoretical model [54], the rigid pavement can be modelled as a thin elastic plate on a soil subgrade. The stress at the edge (critical location) is:

$$\sigma_{max} = \frac{0.572\,W}{h^2}\left[4\log\left(\frac{I}{\sqrt{1.6\,Z^2+h^2}-0.675\,h}\right)+0.359\right] \quad (14)$$

where σ_{max} is the maximum tensile stress of the slab modified to account for fatigue by multiplying the flexural strength ($f_{ctm,fl}$ listed in Table 5.2) by the average fatigue stress ratio $S_{e.ave}$ at P_f=25% (i.e. values from last column in Table 5.7); Z is an equivalent contact radius of the tyre; and *I* is the radius of the relative stiffness of the slab, defined by:

$$I = \sqrt[4]{\frac{E_s\ h^3}{12\,(1-\nu^2)\,M_k}} \quad (15)$$

where ν is the Poisson's ratio of the slab material; M_k is the modulus of elastic subgrade reaction; and E_s is shown in Table 5.2. In this study, M_k is the modulus of resilience of the soil and measures the ability of the ground to resist immediate elastic deformation under load.

The slab thickness *h* for all concrete mixes was calculated using the modified Westergaard's method and the following (typical) values: *W*=80 kN, M_k=80 MPa/m, and *Z*=190 mm (assuming a tyre pressure of 7 bar), and ν=0.2. The subgrade is taken to be a very well consolidated made of gravels and sandy gravels [55]. Although mixes *0P* and *0BF* have similar average static flexural strength and elastic modulus, the addition of fibres reduces the slab thickness by 7% (h=173 mm for *0P* vs h=161 mm for *0BF*). This is mainly due to the enhanced fatigue performance resulting from the addition of fibres, as discussed in section 5.3.3. On the other hand, the replacement of natural aggregates with rubber particles increases the slab thickness to 256 mm and 305 mm for mixes *30BF* and *60BF*, respectively. This is due to the reduced mechanical and fatigue properties of SFRRuC mixes (sections 5.3.2 and 5.3.3), which leads to a low radius of relative stiffness *I* (Eq. (15)).

Based on these results, it is evident that the modified Westergaard's method does not show the expected benefits of using steel fibres and/or rubber over plain concrete. This is because the method was originally developed for plain concrete, which behaves in a linear elastic manner up to tensile failure. As such, the effect of deformability (i.e. ductility and flexibility) which will help to accommodate subgrade movements are not accounted for in the equations. To assess the deformability of SFRRuC, the authors performed three-point bending tests on notched prisms

according to RILEM [45] and the stress versus crack mouth opening displacement (CMOD) curves are shown in Figure 5.11. The enhancement in flexibility is demonstrated by progressively larger CMODs at maximum stress with increasing rubber content, resulting from the ability of rubber to reduce stress concentration at the crack tip and to delay micro-crack propagation [24]. Likewise, the post-peak behaviour is also improved by the inclusion of fibres, and it is further enhanced by the rubber. For example, at a stress level of 3MPa, mixes *30BF* and *60BF* have larger CMODs than that of *0BF*, thus confirming the enhancement in ductility as discussed in section 5.3.1. Hence, in order to identify the benefits of using steel fibres and/or rubber in concrete, it is necessary to use design equations that take into account the flexibility and ductility that SFRRuC can offer.

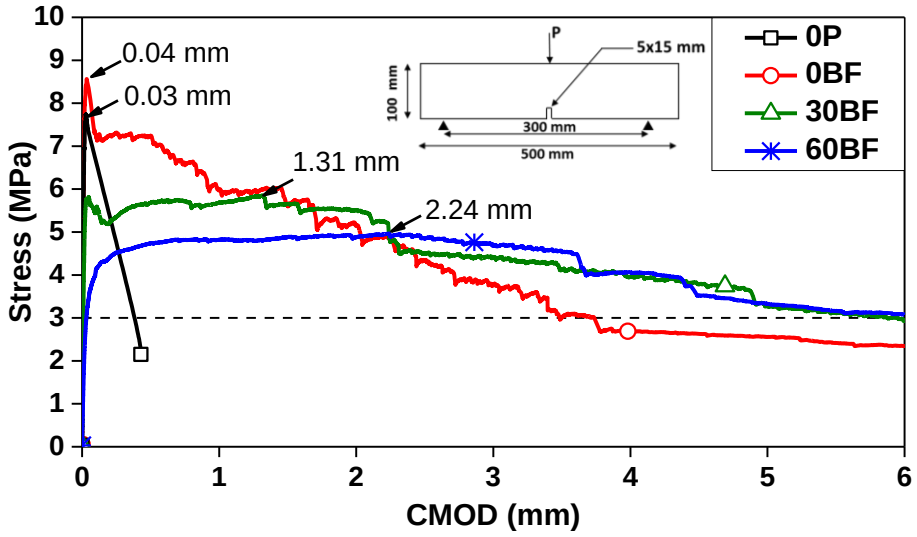

Figure 5.11: Average stress-CMOD curves for prisms

The Technical Report 34 (TR34) by the Concrete Society [56] can be used to show the advantages of using SFRRuC pavements. TR34 designs SFRC slabs at the ultimate limit state (ULS) using the yield line theory. Accordingly, the flexural moment at the bottom of the slab and along the sagging yield lines (M_p) are considered to be fully plastic (i.e. residual post-cracking behaviour exist), as shown in Eq. (16). At the same time, cracks must be avoided at the top surface of the slab and the moment capacity along the hogging yield lines (M_n), as shown in Eq. (17), should be always greater than the ultimate design moment of the concrete.

$$M_P = \frac{h^2}{1.5}\left(0.29\,\sigma_4 + 0.16\,\sigma_1\right) \tag{16}$$

$$M_n = \frac{f_{ctm,fl}}{1.5}\left(\frac{h^2}{6}\right) \tag{17}$$

where $\sigma_1 = 0.45 \cdot f_1$, and $\sigma_4 = 0.37 \cdot f_4$. In this study, values of f_1 is represented by the residual flexural strength at 0.5 mm CMOD and f_4 is represented by the residual flexural strength at 3.5

mm CMOD (as obtained from three-point bending tests on notched prisms [45]). The slab thickness h can be calculated using Eq. (18) [56] for a free edge load.

$$W = \frac{[\pi\,(M_P + M_n) + 4\,M_n]}{\left[1 - \left(\frac{2\,Z}{3\,l}\right)\right]} \tag{18}$$

The design approach adopted by TR34 neglects the effect of fatigue load. To address this drawback and account for fatigue, it is thus proposed to modify this approach and multiply $f_{ctm,fl}$ in Eq. (17) by $S_{e.ave}$ (section 5.4.4).

Figure 5.12 compares the slab thickness calculated using the modified TR34 approach and modified Westergaard's method. It is shown that the adoption of the proposed modified TR34 approach reduces the slab thickness calculated by the modified Westergaard's method by 20% for 0P, 32% for 0BF, 44% for 30BF and 50% 60BF mixes. These results confirm the benefits of using steel fibres and/or rubber in concrete. It is also shown that, although the fatigue strength of SFRRuC is relatively low, the thickness of slabs produced with this novel material is similar to that of slabs built with plain concrete. However, unlike plain concrete pavements, SFRRuC pavements represent a potential solution to accommodate subgrade movements during service life. Consequently, it is recommended to use the proposed modified TR34 approach for the design of SFRRuC flexible pavements.

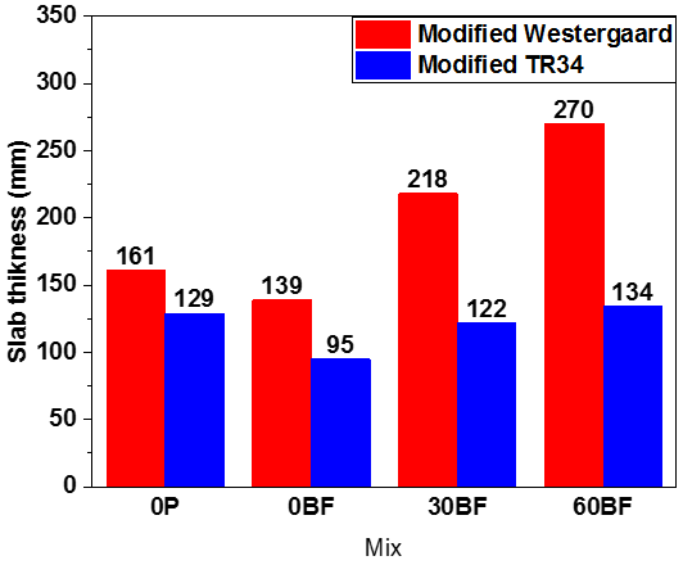

Figure 5.12: Slab thickness comparison for all concrete mixes

The capability of flexible SFRRuC pavements to accommodate subgrade settlements is demonstrated through finite element (FE) analysis in the following section.

5.6 Finite Element Modelling

A two-dimensional (2D) plane strain model of a pavement slab was developed in the FE software ABAQUS® [57]. Recent research [58] has shown that 2D plane strain models provide similar results to 3D models (differences of less than 2%) in the study of transverse profiles of pavements with large longitudinal dimensions. To show the true benefits of flexible SFRRuC, two pavements designed using the modified TR34 approach (Figure 5.12) were modelled: i) a SFRC pavement (*0BF*) of 95 mm depth; ii) a SFRRuC pavement (*60BF*) of 134 mm depth. The pavements were assumed to be on top of a stiff clay subgrade of length=10.0 m and depth=4.0 m, as shown in Figure 5.13a. The length of the pavement was chosen to prevent boundary and edge effects. Previous research has shown that there are no subgrade deformations beyond such depth [59]. Two scenarios were considered: 1) a continuous subgrade (Figure 5.13b), and 2) a subgrade with a gap filled with loose material (length=1 m, depth=0.10 m, see Figure 5.13c). The gap is intended to simulate common defects arising from non-uniform subgrades due to deterioration developing over time, such as settlement due to poor compaction during construction or temperature variations and freeze-thaw.

8-node quadrilateral plane strain reduced integration elements (CPE8R) were used for the analyses. An initial convergence analysis was performed to optimise the characteristics of the mesh. Based on these results, only a fine mesh was selected for the loading area. The total number of nodes and elements was 14962 and 4800, respectively.

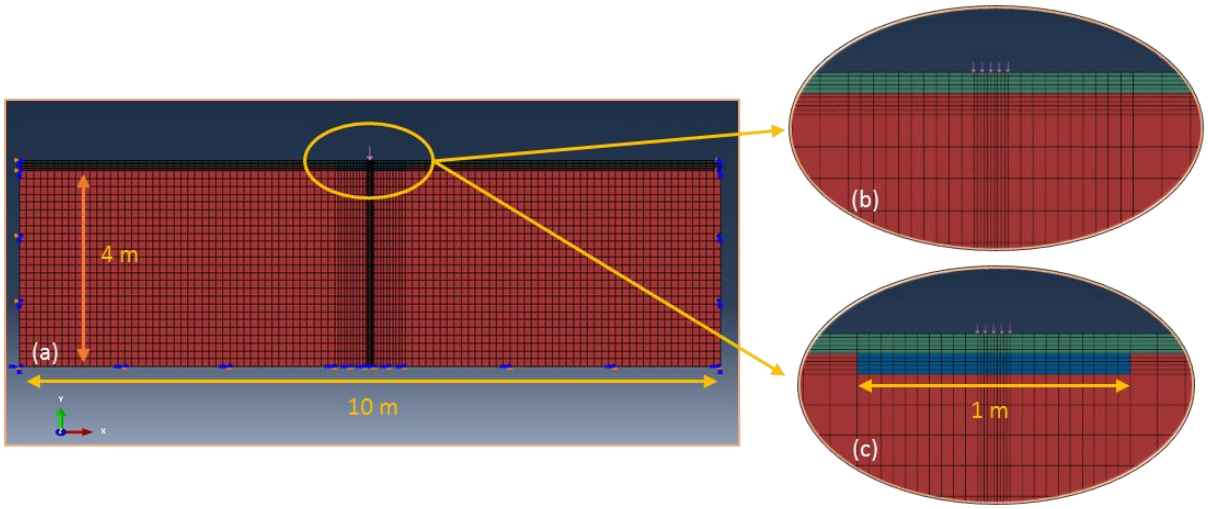

Figure 5.13: Finite element model: a) discretised pavement and subgrade, b) continuous subgrade, c) subgrade with a gap

The bottom edge of the subgrade was fixed to prevent horizontal and vertical movements. The boundary nodes along the pavement edges were constrained horizontally only. A Coulomb

friction law was used to define the surface-to-surface contact interaction between the pavement and subgrade (friction parameter=0.3). The load (standard axle) on the pavement was applied through a static contact pressure of 800 kPa. Previous research has widely adopted the Mohr-Coulomb plasticity criterion for subgrade analysis [60], hence, this criterion is used to model the inelastic behaviour of the subgrade and the filling material in the gap. Table 5.8 summarises the soil properties used in the FE analyses.

Table 5.8 Assumed soil properties used in FE analyses

Soil	Elastic modulus (MPa)	Poisson's ratio, ν	Friction angle, ϕ (º)	Dilation angle ψ (º)	Yield stress (KPa)	Plastic strain
Stiff Clay (subgrade)	80	0.45	0	0	200	0
Loose Sand (hole filling)	10	0.20	28	0	1	0

The concrete was modelled using the concrete damaged plasticity (CDP) constitutive model built-in in ABAQUS®. This model accounts for the inelastic behaviour of concrete in both tension and compression, and can include damage. The model considers two main failure mechanisms in concrete: tensile cracking and compressive crushing. The stress-strain relationship for uniaxial concrete in tension was obtained using section analysis [61, 62]) on the load-deflection curves presented in Figure 5.6b and d. The values for the CDP model (dilation angel=30, eccentricity=0.1, $\frac{F_{b0}}{f_{c0}}$ =1.116, K=0.667 and viscosity=1×10^{-5}) were taken from previous research [61, 63, 64] using SFRC.

Figure 5.14 compares the plastic strain distribution (cracks) for the SFRC pavement (*0BF*) considering the two scenarios. Whilst wide localised cracks develop in both scenarios, the results in Figure 5.14 b indicate that cracks can be up to 5 times wider if a gap develops under the pavement. It is also shown that if the pavement settles, two wide cracks propagate through the pavement towards its top surface within the loaded area. This implies that the pavement would experience significant damage due to multiple wide cracks, thus jeopardising its serviceability requirements.

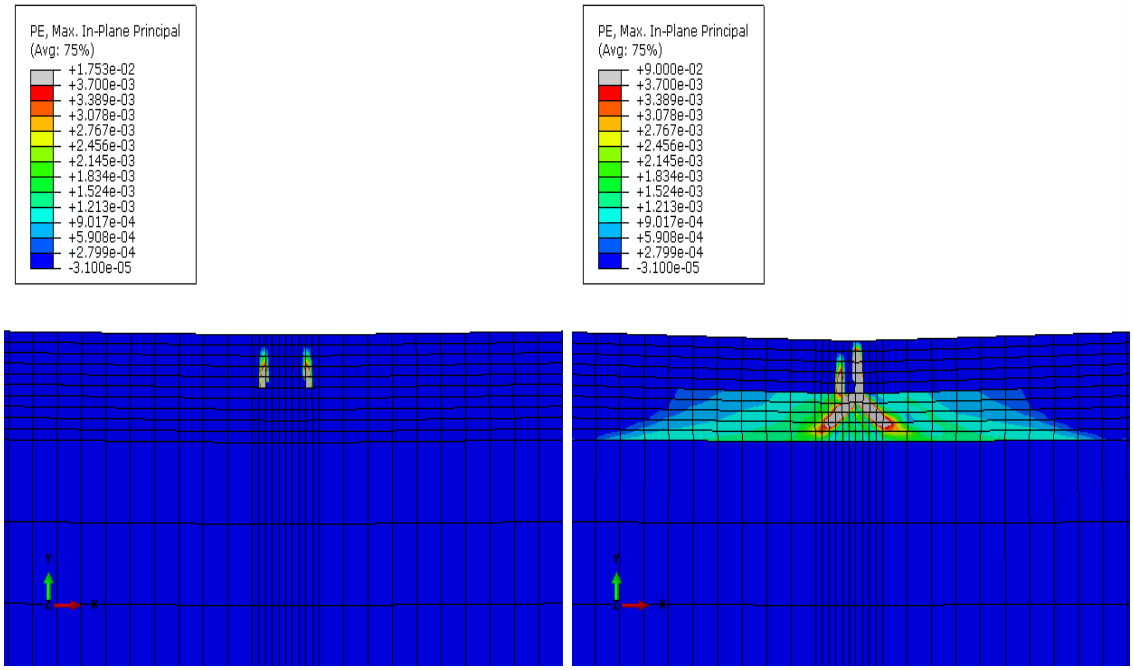

Figure 5.14: Plastic strain model 0BF-95 mm a) without a gap, and b) with 10 cm ×1 m gap

Figure 5.15 compares the plastic strain distribution (cracks) for the SFRRuC pavement (*60BF*) considering both scenarios. Figure 5.15a shows that some minor cracks develop in the pavement on the continuous subgrade. However, these cracks are more spread and up to 7 times narrower compared to the SFRC pavement (see Figure 5.14a). In presence of the gap (Figure 5.15b), the cracks in the SFRRuC pavement are not only more evenly distributed over a larger area, but also significantly narrower (up to 24 times) than those in the SFRC pavement. Even when the same depth of 134 mm is used for the SFRC pavement, the cracks are still 10 times larger than the SFRRuC pavement. This shows that flexible SFRRuC pavements are capable of accommodating subgrade movements and settlements more effectively than their SFRC counterparts.

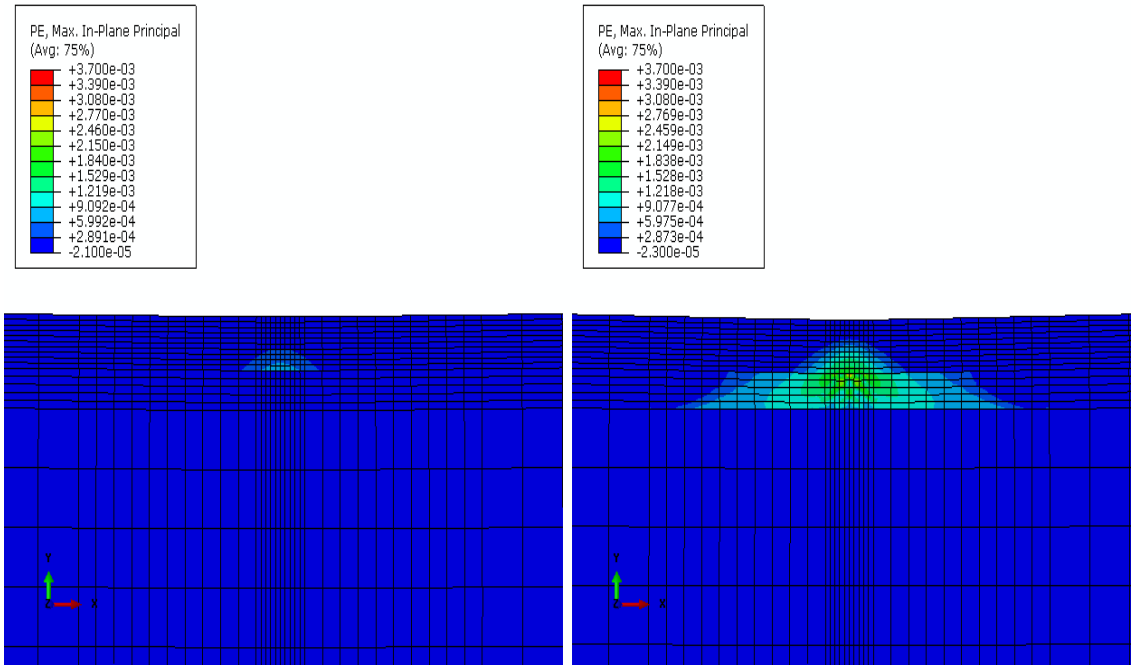

Figure 5.15: Plastic strain for model 60BF-134 mm a) without a gap, and b) with 10 cm ×1 m gap

It should be mentioned that previous research by the authors showed that optimised flexible SFRRuC a) is highly ductile and flexible [8], and b) that such concrete meets the flexural strengths specifications defined in pavement design [28]. The authors have also demonstrated the adequate durability and long term performance of SFRRuC [29, 30]. In this article, the authors prove that (despite its lower fatigue resistance) SFRRuC can accommodate large subgrade movements and settlements. The experimental, analytical and numerical evidence confirm that SFRRuC is a promising solution for building sustainable road pavements, particularly considering that reusing end-of-life tyre materials (WTR and RTSF) in concrete can contribute to reducing stockpiles of discarded tyres. It should be also noted that, due to the limited number of specimens and mixes examined in the above studies, further research is necessary to fully understand the mechanical behaviour and long-term performance of different SFRRuC mixes with other mix proportions and tested with different stress ratios (e.g. 6 specimens tested at each stress level). Current research by the authors is validating the predictions given by the modified TR34 approach against additional experiments so as to provide practical design guidelines.

5.7 Conclusions

This study assesses the mechanical and fatigue performance of steel fibre reinforced rubberised concrete (SFRRuC) using fatigue flexural loads on prisms. Based on the results in this study, the following conclusions are drawn:

- The addition of a blend of steel fibres in concrete enhances its compressive strength by 20%, while the flexural strength and elastic modulus remain roughly the same. On the other hand, the addition of rubber as aggregate decreases significantly the compressive strength, static flexural strength and elastic modulus of SFRRuC. However, the compressive strength of SFRRuC degrades faster than its flexural strength, which shows that the combination of fibres and rubber enhances the tensile capacity of SFRRuC.

- The relationships between probability of failure, stress ratio and fatigue life (P_f-S–N) given by three probabilistic models widely used in pavement design agree reasonably well. They also provide comparable estimates of fatigue stress ratios that can be used for practical design of SFRRuC pavements.

- Steel fibres enhance the flexural fatigue resistance of concrete by controlling the growth of micro-cracks and subsequently the development of macro-cracks. SFRRuC exhibits a relatively lower fatigue resistance due to severe degradation in stiffness.

- The modified Westergaard's approach does not show the benefits of adding blends of steel fibres or rubber to concrete since the post-peak behaviour of concrete is neglected. The use of the modified TR34 design approach proposed in this study leads to thinner slab thickness when compared to the modified Westergaard's model. Consequently, it is recommended to use this approach for the design of SFRRuC flexible pavements.

- FE analyses confirm that flexible SFRRuC pavements can accommodate large subgrade settlements, thus making it an attractive solution for road pavement applications.

Acknowledgements

The authors would also like to thank all of the material suppliers and companies for their in-kind contribution of materials for this research study: Tarmac UK, Sika, Aggregate Industries UK Ltd, Twintech, and Twincon Ltd.

Disclosure

Funding: This study was funded by the European Union Seventh Framework Programme [FP7/2007–2013] under grant agreement no 603722.

5.8 References

[1] A.G. Graeff, K. Pilakoutas, K. Neocleous, and M.V.N. Peres, *Fatigue resistance and cracking mechanism of concrete pavements reinforced with recycled steel fibres recovered from post-consumer tyres*, Engineering Structures 45 (2012) 385-395.

[2] P.C. Perdikaris, A.M. Calomino, and A. Chudnovsky, *Effect of fatigue on fracture toughness of concrete*, Journal of Engineering Mechanics 112 (8) (1986) 776-791.

[3] M. Lee and B. Barr, *An overview of the fatigue behaviour of plain and fibre reinforced concrete*, Cement and Concrete Composites 26 (4) (2004) 299-305.

[4] O.A. Abaza and Z.S. Hussein, *Flexural Behavior of Steel Fiber-Reinforced Rubberized Concrete*, Journal of Materials in Civil Engineering 28 (1) (2015) 04015076.

[5] T. Nguyen, A. Toumi, and A. Turatsinze, *Mechanical properties of steel fibre reinforced and rubberised cement-based mortars*, Materials & Design 31 (1) (2010) 641-647.

[6] A. Grinys, H. Sivilevičius, D. Pupeikis, and E. Ivanauskas, *Fracture of concrete containing crumb rubber*, Journal of Civil Engineering and Management 19 (3) (2013) 447-455.

[7] F. Liu, W. Zheng, L. Li, W. Feng, and G. Ning, *Mechanical and fatigue performance of rubber concrete*, Construction and Building Materials 47 (2013) 711-719.

[8] A. Alsaif, L. Koutas, S.A. Bernal, M. Guadagnini, and K. Pilakoutas, *Mechanical performance of steel fibre reinforced rubberised concrete for flexible concrete pavements*, Construction and Building Materials 172 (2018) 533-543.

[9] S. Raffoul, R. Garcia, D. Escolano-Margarit, M. Guadagnini, I. Hajirasouliha, and K. Pilakoutas, *Behaviour of unconfined and FRP-confined rubberised concrete in axial compression*, Construction and Building Materials 147 (2017) 388-397.

[10] F. Hernández-Olivares, G. Barluenga, M. Bollati, and B. Witoszek, *Static and dynamic behaviour of recycled tyre rubber-filled concrete*, Cement and Concrete Research 32 (10) (2002) 1587-1596.

[11] S. Raffoul, R. Garcia, K. Pilakoutas, M. Guadagnini, and N.F. Medina, *Optimisation of rubberised concrete with high rubber content: An experimental investigation*, Construction and Building Materials 124 (2016) 391-404.

[12] R. Siddique and T.R. Naik, *Properties of concrete containing scrap-tire rubber–an overview*, Waste Management 24 (6) (2004) 563-569.

[13] Z. Khatib and F. Bayomy, *Rubberized portland cement concrete*, Journal of Materials in Civil Engineering 11 (3) (1999) 206-213.

[14] A. El-Dieb, M. Abd El-Wahab, and M. Abdel-Hameed, *Mechanical, Fracture, and Microstructural Investigations of Rubber Concrete*, Journal of Materials in Civil Engineering (10) (2008) 640-649.

[15] A.R. Khaloo, M. Dehestani, and P. Rahmatabadi, *Mechanical properties of concrete containing a high volume of tire–rubber particles*, Waste Management 28 (12) (2008) 2472-2482.

[16] E. Ganjian, M. Khorami, and A.A. Maghsoudi, *Scrap-tyre-rubber replacement for aggregate and filler in concrete*, Construction and Building Materials 23 (5) (2009) 1828-1836.

[17] M.A. Aiello and F. Leuzzi, *Waste tyre rubberized concrete: properties at fresh and hardened state*, Waste Management 30 (8-9) (2010) 1696-704.

[18] C. Wang, Y. Zhang, and A. Ma, *Investigation into the fatigue damage process of rubberized concrete and plain concrete by AE analysis*, Journal of Materials in Civil Engineering 23 (7) (2010) 953-960.

[19] F. Liu, L.-y. Meng, G.-F. Ning, and L.-J. Li, *Fatigue performance of rubber-modified recycled aggregate concrete (RRAC) for pavement*, Construction and Building Materials 95 (2015) 207-217.

[20] N. Ganesan, J.B. Raj, and A. Shashikala, *Flexural fatigue behavior of self compacting rubberized concrete*, Construction and Building Materials 44 (2013) 7-14.

[21] F. Hernández-Olivares, G. Barluenga, B. Parga-Landa, M. Bollati, and B. Witoszek, *Fatigue behaviour of recycled tyre rubber-filled concrete and its implications in the design of rigid pavements*, Construction and Building Materials 21 (10) (2007) 1918-1927.

[22] T. Gupta, A. Tiwari, S. Siddique, R.K. Sharma, and S. Chaudhary, *Response Assessment under Dynamic Loading and Microstructural Investigations of Rubberized Concrete*, Journal of Materials in Civil Engineering 29 (8) (2017) 04017062.

[23] I. Mohammadi, H. Khabbaz, and K. Vessalas, *In-depth assessment of Crumb Rubber Concrete (CRC) prepared by water-soaking treatment method for rigid pavements*, Construction and Building Materials 71 (2014) 456-471.

[24] A. Turatsinze, J.L. Granju, and S. Bonnet, *Positive synergy between steel-fibres and rubber aggregates: Effect on the resistance of cement-based mortars to shrinkage cracking*, Cement and Concrete Research 36 (9) (2006) 1692-1697.

[25] J.-h. Xie, Y.-c. Guo, L.-s. Liu, and Z.-h. Xie, *Compressive and flexural behaviours of a new steel-fibre-reinforced recycled aggregate concrete with crumb rubber*, Construction and Building Materials 79 (2015) 263-272.

[26] N.F. Medina, D.F. Medina, F. Hernández-Olivares, and M. Navacerrada, *Mechanical and thermal properties of concrete incorporating rubber and fibres from tyre recycling*, Construction and Building Materials 144 (2017) 563-573.

[27] A. Turatsinze, S. Bonnet, and J.-L. Granju, *Mechanical characterisation of cement-based mortar incorporating rubber aggregates from recycled worn tyres*, Building and Environment 40 (2) (2005) 221-226.

[28] BSI, EN 13877-1*, Concrete pavements Part 1: Materials,* BSI 389 Chiswick High Road, London W4 4AL UK, 2013.

[29] A. Alsaif, S.A. Bernal, M. Guadagnini, and K. Pilakoutas, *Durability of steel fibre reinforced rubberised concrete exposed to chlorides*, Construction and Building Materials 188 (2018) 130-142.

[30] A. Alsaif, S.A. Bernal, M. Guadagnini, and K. Pilakoutas, *Freeze-thaw resistance of steel fibre reinforced rubberised concrete*, Construction and Building Materials 195 (2019) 450-458.

[31] V. Baroghel-Bouny, *Evaluation and prediction of reinforced concrete durability by means of durability indicators, Part I: new performance-based approach*, in *ConcreteLife'06-International RILEM-JCI Seminar on Concrete Durability and Service Life Planning: Curing, Crack Control, Performance in Harsh Environments*, 2006, RILEM Publications SARL.

[32] M. Alexander, J. Mackechnie, and Y. Ballim, *Guide to the use of durability indexes for achieving durability in concrete structures*, Research monograph 2 (1999).

[33] Swedish standards, SS 13 72 44 ED. 4*, Concrete Testing - Hardened Concrete - Scaling at Freezing,* Standardiserings-Kommissionen I Sverige, 2005.

[34] RILEM, TC 176-IDC, *Internal damage of concrete due to frost action,* Final Recommendation, Prepared by L. Tang and P.-E. Petersson SP Swedish National Testing and Research Institute, Boras, Sweden, Materials and Structures / Mat6riaux et Constructions, Volume 37, 2004, pp 754-759.

[35] ETRA, *The European Tyre Recycling Association*, 2016, Available at: http://www.etra-eu.org [Last accessed: 02/01/2018].

[36] S. Goel, S. Singh, and P. Singh, *Fatigue analysis of plain and fiber-reinforced self-consolidating concrete*, Materials Journal 109 (5) (2012) 573-582.

[37] B.H. Oh, *Fatigue analysis of plain concrete in flexure*, Journal of structural Engineering 112 (2) (1986) 273-288.

[38] H. Hu, P. Papastergiou, H. Angelakopoulos, M. Guadagnini, and K. Pilakoutas, *Mechanical properties of SFRC using blended manufactured and recycled tyre steel fibres*, Construction and Building Materials 163 (2018) 376-389.
[39] ASTM, *C136: Standard test method for sieve analysis of fine and coarse aggregates,* ASTM International, West Conshohocken, PA, doi:10.1520/C0136-06, 2006.
[40] BSI, EN 12390-2, *Testing hardened concrete, Part 2: Making and curing specimens for strength tests,* BSI 389 Chiswick High Road, London W4 4AL, UK, 2009.
[41] BSI, EN 12390-3, *Testing hardened concrete, Part3: Compressive strength of test specimens,* BSI 389 Chiswick High Road, London W4 4AL, UK, 2009.
[42] JSCE, SF-4, *Method of test for flexural strength and flexural toughness of steel fiber reinforced concrete.* Japan Concrete Institute, Tokio, Japan, 1984.
[43] S. Singh and S. Kaushik, *Flexural fatigue life distributions and failure probability of steel fibrous concrete*, Materials Journal 97 (6) (2000) 658-667.
[44] S. Singh, B. Ambedkar, Y. Mohammadi, and S. Kaushik, *Flexural fatigue strength prediction of steel fibre reinforced concrete beams*, Electronic Journal of Structural Engineering 8 (1) (2008) 46-54.
[45] RILEM, *TC 162-TDF, Test and design methods for steel fibre reinforced concrete, Bending test, Final Reccomendation, Materials and Structures 35, 579-582,* 2002.
[46] B. Zhang, D. Phillips, and K. Wu, *Effects of loading frequency and stress reversal on fatigue life of plain concrete*, Magazine of Concrete Research 48 (177) (1996) 361-375.
[47] M. Darter and E. Barenberg, *Design of zero maintenance plain jointed concrete pavement, volume two-design manual,* 1977.
[48] J.R. Roesler, *Fatigue of concrete beams and slabs*. 1998.
[49] S. Singh and S. Kaushik, *Fatigue strength of steel fibre reinforced concrete in flexure*, Cement and Concrete Composites 25 (7) (2003) 779-786.
[50] B.H. Oh, *Fatigue life distributions of concrete for various stress levels*, Materials Journal 88 (2) (1991) 122-128.
[51] Y. Mohammadi and S. Kaushik, *Flexural fatigue-life distributions of plain and fibrous concrete at various stress levels*, Journal of Materials in Civil Engineering 17 (6) (2005) 650-658.
[52] S. Singh, B. Singh, and S. Kaushik, *Probability of fatigue failure of steel fibrous concrete*, Magazine of Concrete Research 57 (2) (2005) 65-72.
[53] J.T. McCall, *Probability of fatigue failure of plain concrete*. in Journal Proceedings, 1958.
[54] H. Westergaard, *Stresses in concrete pavements computed by theoretical analysis*, Public Roads (1926).
[55] G. Garber, *Design and construction of concrete floors*, 2006: CRC Press.
[56] TR34, The Concrete Society, *Concrete industrial ground floors – a guide to design and construction,* 4rd edition Technical Report 34, 2013.
[57] Abaqus, *6.14 Abaqus Theory Manual, USA:Dassault Systemes Simulia Corporation*, 651, 2014.
[58] J. Hua, *Finite element modeling and analysis of accelerated pavement testing devices and rutting phenomenon*, 2000.
[59] I. ARA, ERES Consultants Division, *Guide for Mechanistic–Empirical Design of New and Rehabilitated Pavement Structures*, Final Report, NCHRP Project 1-37A, 2004.
[60] H. Jiang and Y. Xie, *A note on the Mohr–Coulomb and Drucker–Prager strength criteria*, Mechanics Research Communications 38 (4) (2011) 309-314.
[61] N. Jafarifar, K. Pilakoutas, H. Angelakopoulos, and T. Bennett, *Post-cracking tensile behaviour of steel-fibre-reinforced roller-compacted-concrete for FE modelling and design purposes*, 2017.
[62] P. Casanova and P. Rossi, *Analysis and design of steel fiber reinforced concrete beams*, Structural Journal 94 (5) (1997) 595-602.

[63] N. Jafarifar, K. Pilakoutas, and T. Bennett, *Moisture transport and drying shrinkage properties of steel–fibre-reinforced-concrete*, Construction and Building Materials 73 (2014) 41-50.

[64] B. Mobasher, *Mechanics of fiber and textile reinforced cement composites*. 2011: CRC press.

Chapter 6

Conclusions & recommendations for future work

6.1 Conclusions

The aim of this research was to investigate the mechanical, transport/pore-structure related properties and long-term behaviour of Steel Fibre Reinforced Rubberised Concrete (SFRRuC) pavements, as an alternative for flexible pavements. An extensive experimental programme on the fresh, mechanical, transport and durability properties of SFRRuC, was complemented by and an investigation on fatigue and long term properties, including experimental, analytical and numerical work. The thesis comprises four peer-reviewed published journal papers and their main conclusions are described below.

6.1.1 Mechanical Performance of Steel Fibre Reinforced Rubberised Concrete for Flexible Concrete Pavements (Chapter 2)

- The replacement of conventional aggregates with rubber particles in fresh concrete mixes:
  a) reduces workability due to the rough surface texture of the rubber particles and the resulting increase in friction,
  b) reduces unit weight due to the lower relative density of rubber, and
  c) increases air content due to the hydrophobic nature and rough surfaces of rubber particles.

- The addition of steel fibres in RuC further:
  a) lowers workability due to the increased friction between the steel fibres and the concrete constituents,
  b) increases air content due to the large specific surface area of fibres and their tendency to agglomerate, and
  c) results in a marginal increase in the unit weight due to the higher specific gravity of steel fibres.

- Owing to their ability to delay micro-crack coalescence and propagation, the addition of steel fibres (dosages up to 40 kg/m^3) into conventional concrete notably enhances the concrete strength (up to 30% in both compressive strength and flexural strength) and slightly increases the concrete modulus of elasticity.

- Increasing rubber content in RuC causes severe degradation in compressive and flexural strength as well as modulus of elasticity. This can be mainly attributed to the lower

stiffness and higher Poisson's ratio of rubber compared to conventional aggregates, as well as the weak bond between cement paste and rubber.

- The addition of steel fibres into RuC recovers the loss in flexural strength [from 50% to 9.6% loss (for the 40% total rubber replacement)], and improves the compressive strength and modulus of elasticity (up to 12.5% and 28.4%, respectively), compared to conventional concrete. This enhancement is mainly due to the ability of the fibres to:
  a) delay the micro-cracks that develop in the matrix during loading,
  b) control the propagation of wider cracks, and
  c) redistribute stresses.

  Hence, fibres are an important component when RuC is to be used for structural purposes.

- Concrete strain capacity (deflection at peak load) is significantly enhanced when steel fibres are added (from 0.04 mm for conventional concrete to 0.22 mm for SFRC) and further improved by the combination of both fibres and rubber particles (up to 1.32 mm for SFRRuC produced with 60% rubber content and 40 kg/m^3 of blended fibres).

- The replacement of conventional aggregates with rubber particles slightly improves the post-peak energy absorption due to the ability of the rubber particles to undergo large deformation in tension and promote high energy absorption. The addition of steel fibres into RuC substantially enhances the post-peak energy absorption and dissipation due to:
  a) the ability of fibres to bridge cracks and resist their opening, and
  b) increased interlocking and friction at fibre–matrix and fibre-rubber interfaces.

- Free shrinkage strain increases with increasing rubber content (127% increase for 60% RuC compared to conventional concrete at 57 days). This increase in free shrinkage strain is mainly attributed to the lower stiffness of rubber particles compared to conventional aggregates.

- A high performance (class d according to fib 2010 model code [1]) and highly flexible SFRRuC that is suitable for pavement applications can be produced with 60% rubber content and blended fibres (20 kg/m^3 of MSF and 20 kg/m^3 of RTSF).

6.1.2 Durability of Steel Fibre Reinforced Rubberised Concrete Exposed to Chlorides (Chapter 3)

- No visual signs of deterioration or cracks (except superficial rust) were observed on the surface of concrete specimens subjected to 150 or 300 days of accelerated wet-dry chloride exposure. No corrosion was observed on the steel fibres embedded in concrete indicating that the fibres were not affected by the wet-dry chloride exposure. This shows that blended fibres help maintain the integrity of concrete and make a positive contribution to the durability of both conventional concrete and RuC.

- As a consequence of the ongoing hydration of the cementitious materials, a slight general increase in the mechanical properties of all mixes after 150 and 300 days of wet-dry chloride exposure was identified in comparison to the 28-day mechanical properties.

- While VPV and sorptivity generally increase with increased rubber content, the change with respect to plain concrete is minor. After 300 days of mist curing, all mixes exhibit VPV values lower than 6% and sorptivity values lower than 6 mm/h$^{0.5}$, which means that they can be classified as highly durable concrete mixes.

- Due to the compressibility of rubber particles when pressure is applied, the oxygen gas can find its way easier through the specimen and around the rubber particles. Hence, the oxygen permeability test can produce misleading results when assessing RuC mixes with high amounts of rubber.

- The depth of chloride penetration in both conditions (fully-saturated and wet-dry) generally increases with rubber content. At the colour change boundary, 30BF and 60BF specimens record lower chloride concentrations than 0.4% by weight of cement (critical concentration inducing corrosion) and present apparent diffusion coefficients values within the range of highly durable concrete mixes.

6.1.3 Freeze-Thaw Resistance of Steel Fibre Reinforced Rubberised Concrete (Chapter 4)

- After 56 freeze-thaw cycles, all SFRRuC mixes did not show any signs of significant deterioration. The cubes show acceptable scaling resistance according to the Swedish Criteria SS 13 72 44 ED, while the prisms maintain their RDMs values above the threshold value for internal damage (80%) specified in RILEM TC 176-IDC. Hence, as hypothesised by the authors, the inclusion of steel fibres in RuC greatly mitigates the negative effects of large volumes of rubber on freeze-thaw resistance.

- The presence of steel fibres in SFRRuC mixes significantly reduces the rate of reduction in flexural strength due to the addition of large volumes of rubber, compared to that in compressive strength. All SFRRuC mixes show flexural strengths that satisfy the requirement for pavement design according to EN 13877-1.

- Comparable mechanical performance is observed from specimens subjected to freeze-thaw and control specimens cured in the mist room, thus making SFRRuC a potentially sustainable flexible concrete pavement solution capable of adequate freeze-thaw performance.

6.1.4 Fatigue Performance of Steel Fibre Reinforced Rubberised Concrete Proposed for Flexible Concrete Pavements (Chapter 5)

- The relationships between probability of failure, stress ratio and fatigue life (P_f-S–N) given by three probabilistic models widely used in pavement design agree reasonably well. They also provide comparable estimates of fatigue stress ratios that can be used for practical design of SFRRuC pavements (i.e. for a fatigue life of 2×10^6 cycles and Pf=25%, the estimated fatigue stress ratios were 0.61, 0.68, 0.45 and 0.35 for conventional concrete, SFRC, 30% SFRRuC and 60% SFRRuC, respectively).

- Steel fibres enhance the flexural fatigue resistance of concrete by controlling the growth of micro-cracks and subsequently the development of macro-cracks. SFRRuC exhibits relatively lower fatigue resistance due to severe degradation in stiffness.

- The modified Westergaard's approach does not show the benefits of adding blends of steel fibres or rubber to concrete since the post-peak behaviour of concrete is neglected. The use of the modified TR34 design approach proposed in this study leads to thinner slab thickness (e.g. from 270 mm to 134 mm for 60% SFRRuC) when compared to the modified Westergaard's model. Consequently, it is recommended to use this approach for the initial design of SFRRuC flexible pavements.

- FE analyses confirm that flexible SFRRuC pavements can accommodate large subgrade settlements, thus making it an attractive solution for road pavement applications.

6.1.5 Final remarks

This study provides the compelling evidence that the combination of rubber particles, up to 60%, and steel fibres can lead to an innovative flexible SFRRuC concrete with:

1) workability properties and flexural strengths that meet the specifications defined in pavement design [2],
2) high ductility and toughness properties,
3) stiffness values similar to those of flexible asphalt pavements, i.e. around 8 GPa,
4) adequate durability and long term performance as well as good transport characteristics, and
5) the ability to accommodate large subgrade movements and settlements.

This confirms that SFRRuC is a promising solution for building sustainable road pavements, particularly considering that reusing end-of-life tyre materials (WTR and RTSF) in concrete can contribute to reducing stockpiles of discarded tyres.

In practice, the production of ready-mix SFRRuC can follow the conventional procedure described in section 2.2.2.3, by altering/calibrating the mixing times. The integration of both MSF and RTSF can be easily achieved on site by first disposing the fibres into a mechanically rotated perforated drum (for a slow fibre dispersal to avoid agglomeration) and then introducing them into the concrete truck mixer by using a blower. Hence, it is a matter of conducting trial mixes at the batching plant to ensure the right workability can be achieved.

6.2 Recommendations for future work

This section provides recommendations for future research aiming to investigate issues that were not addressed during this study, mainly due to limitations in time and available resources.

6.2.1 Rubber properties improvement

- The physical properties of the coarse rubber particles were obtained following the lightweight course aggregates test procedures, which have led, in some cases, to unexpected results. For example, due to the difficulty in achieving surface dry conditions on course rubber particles, their water absorption was unpredictably high, e.g. up to 8.8% by mass. On the other hand, the physical properties of the fine rubber particles were not evaluated due to difficulties in applying typical lightweight fine aggregate test procedures. For instance, fine rubber particles were found to folate when submerged in

water hindering the ability to measure their particle density and water absorption. Hence, future research should investigate better test procedures/techniques to accurately evaluate the physical properties of both coarse and fine rubber particles.

- To better understand the behaviour of rubber aggregates and efficiently use them in concrete, future research should consider observing their microstructure as well as their chemical composition using special techniques such as Energy Dispersive X-ray Analyser (EDAX) and X-Ray Diffraction (XRD) together with Scanning Electron Microscopy (SEM).

- Future research should study possible chemical or physical pre-treatment techniques of rubber particles to improve their performance in terms of fresh, mechanical and durability properties.

6.2.2 Mix design optimisation

- To allow direct comparisons of different RuC mixes and to create a robust experimental database, the mix design used in this work was adopted from an optimised RuC mix developed by Raffoul et al. [3]. However, the adopted mix design could be further optimised to improve fresh, mechanical and durability properties as well as to reduce its cost. The optimisation can be achieved by using various: 1) water to cement ratios, 2) sizes and amounts of mineral aggregates/rubber aggregates, 3) types, dosages, geometries and blends of steel fibres, 4) pozzolanic additives (e.g. Metakaolin or GGBS), 5) mixing sequences and 6) chemical admixtures.

6.2.3 Mechanical properties of SFRRuC

- During this study, the mechanical properties of SFRRuC showed high variability due to the uneven distribution of rubber particles and fibre orientation; these two factors are heavily affected during mixing, casting and vibrating of fresh concrete mixes. Further research is needed to investigate rubber distribution, fibre orientation (the boundary conditions of the laboratory small sized moulds affect the orientation dramatically), concrete flow and fresh state properties. This could be achieved by casting large SFRRuC slabs and coring specimens (e.g. cylinders, cubes and prisms) at different locations (centre, corners and edges). Specimens could be extracted either perpendicular or parallel to the concrete flow direction and then rubber particles and steel fibres distribution of the cut planes could be investigated using image analysis.

- The weak bond between the cement matrix and rubber particles at the Interfacial Transition Zone (ITZ) appears to be one of the main reasons of the strength and stiffness degradation in SFRRuC. Future research should focus on developing innovative techniques to enhance the bond by using chemical or physical treatments.

- The influence of rubber and steel fibres characteristics, including methods of extraction (e.g. mechanical shredding or cryogenic grinding), contamination, and their shape and surface parameters on the fresh, mechanical and durability properties should be examined in future studies.

- The current study did not consider the effect of restrained shrinkage in SFRRuC. Hence, future work should evaluate the restrained shrinkage behaviour of SFRRuC as it is an important parameter for the design of concrete pavements.

- The current experimental programme consisted of 100x100 mm cubes, 100x200 mm cylinders and 100x100x500 mm prisms. To investigate the size-effect issues, the mechanical properties of SFRRuC should be further investigated using different size of cubes, cylinders and prisms.

- Part of the initial plan of this thesis, was to extract small SFRRuC cylinder cores (25 mm dia×10mm height) to perform microstructure analysis. However, this was not achieved due to the difficulties of extracting such small cores with the presence of both rubber particles and steel fibres. Future research should consider developing better techniques to extract these cores and obtain the microstructure analysis, which could be an essential tool to provide diagnosis of concrete composites.

6.2.4 Transport properties and long term performance

- Due to the limited capacity of the laboratory concrete mixer and the large number of parameters investigated in the parametric study (Chapters 3 and 5), each mix was cast in three batches and only three specimens were assigned for each parameter (one from each batch). Since this caused variability in the findings, a more comprehensive study is required to be performed using ready-mixed concrete and 6 (or more) specimens per parameter.

- The effect of curing on transport properties was planned to be examined on 150x 300 mm SFRRuC cylinders cured in the mist room for a period of 150 days. However, it was not possible to slice the large cylinders into appropriate sample size (150 x 50 mm) as

the rubber particles acted as break pads onto the blade of the circular saw during the slicing process. Future study should consider slicing the SFRRuC cylinders at earlier ages < 28 days of mist curing or trying to find more advanced ways of cutting the specimens.

- The effect of curing conditions and pre-conditioning techniques other than the ones used in this study should be investigated in future research when preparing specimens for transport and permeability tests.

- The transport and pore structure-related properties of SFRRuC should be further investigated using different experimental procedures such as the use of mercury porosimetry, helium pycnometry, electronic microscopy, etc. This would advance the knowledge of SFRRuC on degree of saturation and rate of transport of aggressive agents that directly affect its durability and long-term performance.

- The chloride corrosion effects due to exposure to accelerated marine environment (intermittent wet-dry cycles in 3% NaCl solution) should be further investigated to understand how the accelerated method is comparable to real environments. This could be achieved numerically by modelling the ingress of chloride into SFRRuC at a splash zone where there is diffusion and absorption effects. In addition, alternative techniques should be investigated to assess the effect of NaCl at different temperatures and wet-dry periods. The chloride corrosion resistance of cracked SFRRuC should be also assessed. Furthermore, the impact of other accelerated chloride exposure methods (e.g. the salt-spray chamber) on SFRRuC specimens should be investigated too.

- Future studies should consider investigating other deterioration processes such as corrosion due to carbonation, sulphate attack, creep, shrinkage stresses, abrasion and wearing of SFRRuC.

- The effect of coupled mechanical and environmental exposure on the performance of, SFRRuC slab pavements should be examined (e.g. wet-dry and stress).

- The Service Life Design (SLD) method based on probabilistic analysis should be considered to predict the service life behaviour of SFRRuC pavements. The SLD of SFRRuC pavements may be evaluated in terms of environmental influences such as corrosion and freeze-thaw.

- Due to the limited number of specimens and mixes used to examine the flexural fatigue resistance of SFRRuC in this study, future work should consider using a larger number of specimens cast with several optimised mix proportions and tested with different load frequencies and stress ratios.

- To better understand the mechanism of fatigue failure, it was planned to investigate the toughness and fracture behaviours of SFRRuC specimens during fatigue cyclic loads. However, technical issues during the test experiments hindered the accurate recording of load-displacement data of most of the specimens. Future research should focus on improving the qualities of deformation measurements during fatigue loading.

- The accuracy of the proposed modified TR34 approach at predicting the thickness of flexible SFRRuC pavements, should be validated against other experimental databases when/if available.

- The Life Cycle Assessment (LCA) and Life Cycle Cost Analysis (LCCA) of SFRRuC are necessary to be conducted to further evaluate its feasibility as alternative flexible concrete pavement.

6.3 References

[1] fib, *Model Code for Concrete Structures 2010,* Federal Institute of Technology Lausanne–EPFL, Section Génie Civil, Swizerland, 2010, p. 978-3.

[2] *BSI, EN 13877-1, Concrete pavements Part 1: Materials,* BSI 389 Chiswick High Road, London W4 4AL, UK, 2013.

[3] S. Raffoul, R. Garcia, K. Pilakoutas, M. Guadagnini, and N.F. Medina, *Optimisation of rubberised concrete with high rubber content: An experimental investigation,* Construction and Building Materials 124 (2016) 391-404.